

Chapter 4: Results and discussion

Part – I

4.1 Gas metal arc welding of ferritic stainless steel

4.1.1 Introduction

The GMAW of the ferritic stainless steel AISI 409L was performed at 18 different combinations of welding parameters. To perform this welding operation successfully, the selection of the base metal, electrode wire and backing plate was carried out carefully. The range of welding process parameters (welding voltage, welding current, welding speed, shielding gas flow rate, root gap, nozzle to plate distance) in which the welding operation can be carried out successfully, were obtained after carrying out several trial runs. After the final run, the samples for different characterisations were extracted from the welded plates. The characterisation of the welded plates consists of the metallographic study, hardness testing, tensile testing and Charpy impact testing. The different regions of the welded plate S7 have also been characterised using the MBN and MHL analysis, which is non-destructive testing.

In this section, the results of the various characterisations of the welded plates have been described. The quality of the welded plate was checked by using visual examination and X-ray radiography. The chemical composition of the WMZ has been calculated with the help of percentage dilution. The variation of the percentage dilution with the welding process parameters (welding current, welding voltage, welding speed and welding heat input) have been described. The metallographic study, XRD analysis, hardness testing, tensile testing, Charpy impact testing and residual stress testing have been described. Also, the variations in the MBN and MHL analysis results of different regions of the sample S7 at different values of magnetic field intensity and magnetising frequency have been analysed and described in this section.

4.1.2 Visual examination of the weld

Visual inspection is one type of non-destructive testing technique to test the weld quality by viewing the surface of the weld. Although a simple test, it can be used for checking the surface discontinuities. However, it cannot tell anything about the internal flaws present within the material. This technique is widely used in the welding industry since it is an inexpensive and quick method. Fillet weld gauge and a magnifying glass are used as the equipment in this technique. However, this technique requires a well-trained inspector with good eyesight to identify accurately any surface discontinuities.

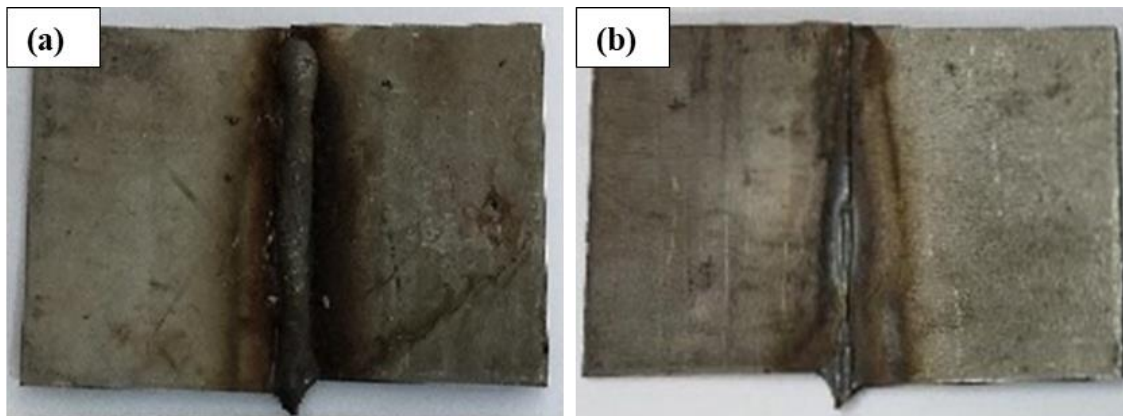


Figure 4.1 Image of the trial run weld sample: (a) top surface, and (b) bottom surface.

Figure 4.1 shows the image of the weld produced during the trial run. In this figure, on visual inspection of the weld by the naked eye, it was found that more deposition of filler metal has occurred on the top surface of the weld, which results in more height of upper reinforcement, while the bottom surface does not show any joining at various locations. It was due to the restriction in the flow of filler metal up to the bottom of the weld joint due to incorrect joint design along with the insufficient amount of heat produced (due to incorrect process parameters) to melt the base metal up to the

bottom of the weld. However, there was no sign of any porosities present at the surfaces of the weld.

All the welded plates welded as per the design of experiment was carefully examined during visual inspection. On inspecting the final run, as shown in Figure 4.2 visually, a weld joint with proper penetration was observed. Also, no gas porosity was found to be present on the surface of the weld.

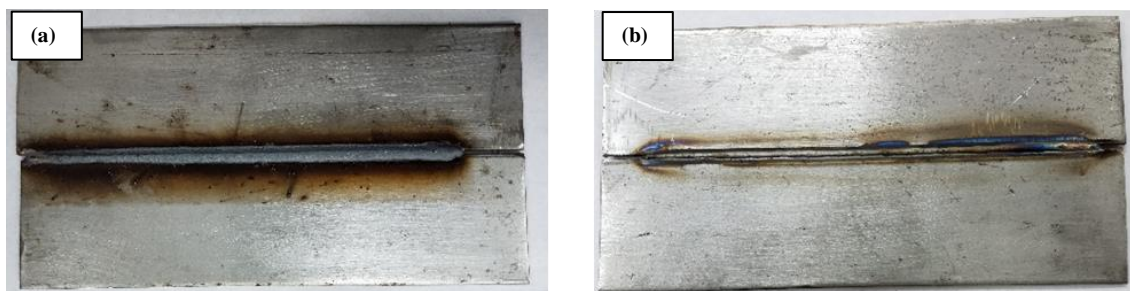


Figure 4.2 Image of the final weld sample: (a) top surface, and (b) bottom surface.

Only a few spatters were observed in all weld samples of the final run during the visual examination and were far too few to be a cause of any concern. Therefore, all the samples that were tested visually, were of acceptable quality.

4.1.3 X-ray radiography of the welds

GMAW process, if not carried out properly, can lead to the formation of defects in the weld. Since subsurface defects such as slag inclusion, gas porosity cannot be detected by visual inspection; therefore, to confirm the soundness of the welded joint, further inspection of the weld joint is necessary. In this study, radiography has been used to inspect the weld for any defect. Among gamma ray radiography and X-ray radiography, the latter has been chosen since X-rays possess larger wavelength than gamma rays but can easily penetrate the welded plate of thickness 3 mm thickness. Gamma rays can be used for plates with thickness greater than 6 mm, but they give poor

contrast on a 3 mm thick plate. X-ray radiography provides the image of the internal defects if present inside the structure of the material in dark and white contrast.

Figure 4.3 presents the scanned image of the X-ray film of one such weld plate, which was produced after the final experimentation.

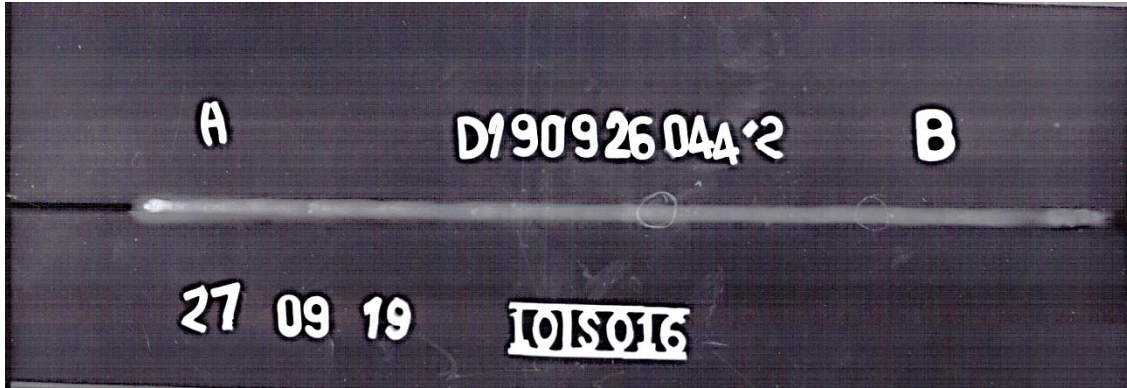


Figure 4.3 X-ray radiography of welded plate.

In this image, the weld and the base metal are clearly distinguishable. No defects were observed in the weld metal. Therefore, the weld sample was found to be of acceptable quality. Similarly, all the welded plates have been radiographed, and the results of each testing are given in Table 4.1.

Table 4.1 Results of the radiographic testing.

Sample	Results	Acceptability
S1	No defect	Acceptable
S2	No defect	Acceptable
S3	No defect	Acceptable
S4	Crater crack at the end of the weld	Acceptable
S5	No defect	Acceptable
S6	No defect	Acceptable
S7	No defect	Acceptable
S8	No defect	Acceptable
S9	No defect	Acceptable
S10	No defect	Acceptable
S11	No defect	Acceptable
S12	No defect	Acceptable
S13	No defect	Acceptable
S14	No defect	Acceptable
S15	No defect	Acceptable
S16	Crater crack at the end of the weld	Acceptable
S17	No defect	Acceptable
S18	No defect	Acceptable

It was observed from the results given in the above table that all the welded plates possess acceptable weld quality.

4.1.4 Calculation of percentage dilution

Percentage dilution is the ratio of the volume of base metal fused to that of the total volume of metal in the fusion zone [12]. Fusion zone metal consists of both the base metal and filler metal. Percentage dilution highly affects the chemical composition of

weld metals which in turn is affected by the welding parameters. Percentage dilution is related to the weld bead shape. The shape of the weld bead geometry is decided by the welding parameters like welding current, welding speed, etc. Percentage dilution has been calculated by using equation (3.2) and equation (3.3), and the results are given in Table 4.2.

Table 4.2 Percentage dilution calculated for welds produced using GMAW

Sample	Welding current (A)	Welding Voltage (V)	Weld speed (mm/min)	Net heat input (J/mm)	Area of fused based metal (A_{FBM}) (mm^2)	Area of total weld deposit (A_{TWD}) (mm^2)	%Dilution (PD)
S1	120	21	400	302.40	10.77	34.74	31
S2	150	21	400	378.00	13.60	35.79	38
S3	180	21	400	453.60	17.00	36.17	47
S4	120	24	400	345.60	11.60	35.15	33
S5	150	24	400	432.00	16.20	36.00	45
S6	180	24	400	518.40	19.00	38.00	50
S7	120	26	400	374.40	13.30	35.95	37
S8	150	26	400	468.00	18.00	37.50	48
S9	180	26	400	561.60	20.00	39.22	51
S10	120	21	500	241.92	8.00	28.57	28
S11	150	21	500	302.40	10.70	33.44	32
S12	180	21	500	362.88	12.00	33.33	36
S13	120	24	500	276.48	9.00	30.00	30
S14	150	24	500	345.60	11.00	32.35	34
S15	180	24	500	414.72	14.00	32.56	43
S16	120	26	500	299.52	10.50	33.87	31
S17	150	26	500	374.40	12.50	32.89	38
S18	180	26	500	449.28	16.40	35.65	46

4.1.5 Relation between heat input and percentage dilution

Heat input during welding depends upon welding speed, welding current, voltage and arc efficiency. Variation in any one or more parameters will lead to change in heat input. Percentage dilution depends more on the distribution of heat input between the base metal and filler wire rather than total heat input. The distribution of heat input depends on the welding parameters, melting enthalpies of base metal, and filler wire and the arc efficiency. The distribution of heat input between the base metal and filler wire can be considered in such a way that out of the total heat energy generated, a portion of the energy is required for melting of filler wire. The rest of the energy is available to melt the base metal. The results of the percentage dilution of weld metal corresponding to different heat inputs are given in Table 4.2 and shown in Figure 4.4. Three readings of percentage dilution at each heat input have been taken to determine the error bar.

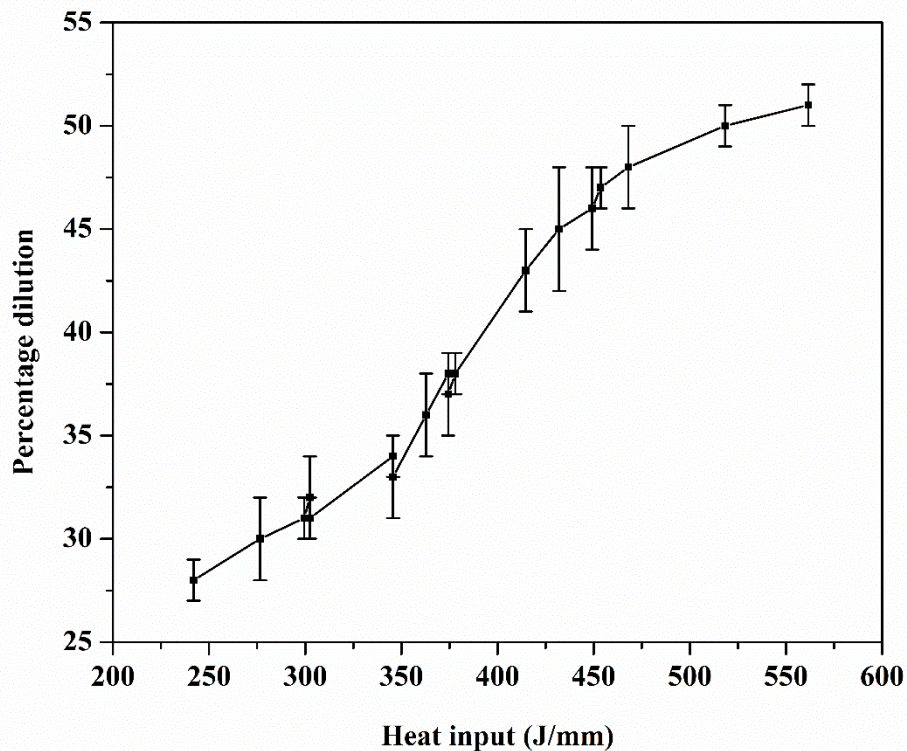


Figure 4.4 Variation of percentage dilution at different heat input.

As seen in Figure 4.4, the percentage dilution increases with the heat input. However, the effect of different welding parameters on the percentage dilution may be different. Since the heat input is a cumulative effect of welding parameters, therefore it can be concluded from Figure 4.4 that the overall effect of increasing welding current, increasing welding voltage and decreasing welding speed is an increase in the percentage dilution. On increasing the heat input, more melting of the base metal occurred than the total weld deposition, resulting in the increase of percentage dilution with the heat input. However, the effect of individual process parameters on dilution has been discussed in more detail in the following sections.

4.1.6 Variation of percentage dilution with the welding current

Percentage dilution of different samples at different combinations of constant welding voltage and variable welding current is shown in Figure 4.5.

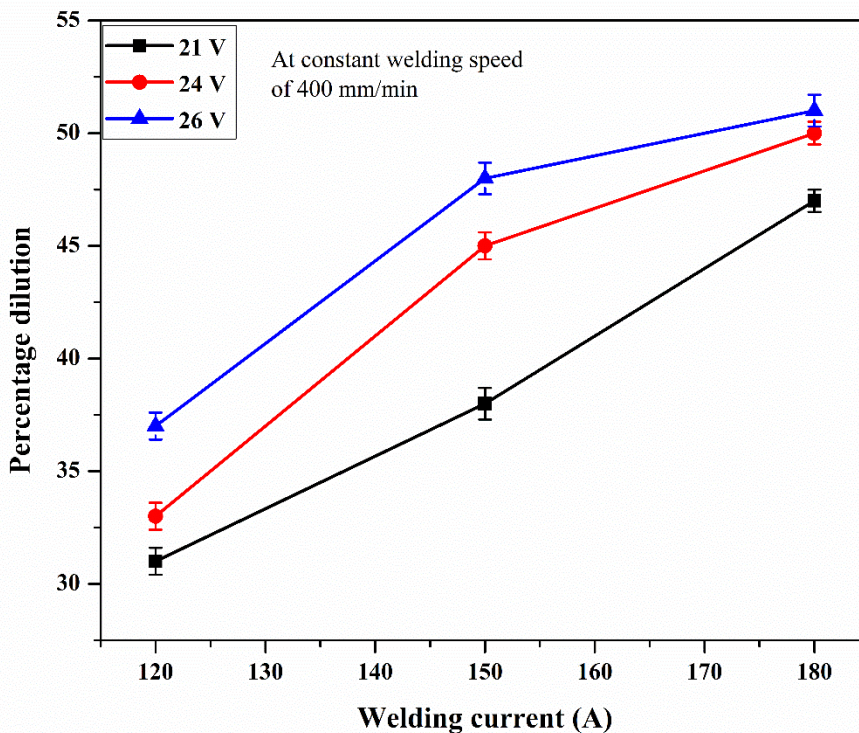


Figure 4.5 Plot of percentage dilution versus welding current at different values of welding speed.

From Figure 4.5, it can be seen that at any constant value of welding voltage and welding speed, the percentage dilution is increasing with the welding current.

Since the wire feed rate controls the welding current, i.e., increasing the wire feed rate, the welding current also increases. When the welding current is increasing, the area of the fused base metal increases due to the more heat input to the base metal. Along with that, the area of total weld deposit also increases due to the increased wire feed rate. Therefore, on increasing the welding current, both areas of fused base metal and total weld deposit are increasing. The volume of the fused base metal is more than the total weld deposit. That results in the increase in percentage dilution on increasing the heat input.

4.1.7 Variation of percentage dilution with the welding voltage

Percentage dilution calculated from weld bead profile were plotted against different values of welding voltage. Figure 4.6 presents the percentage dilution obtained in different samples at different combination of constant welding current and variable welding voltage.

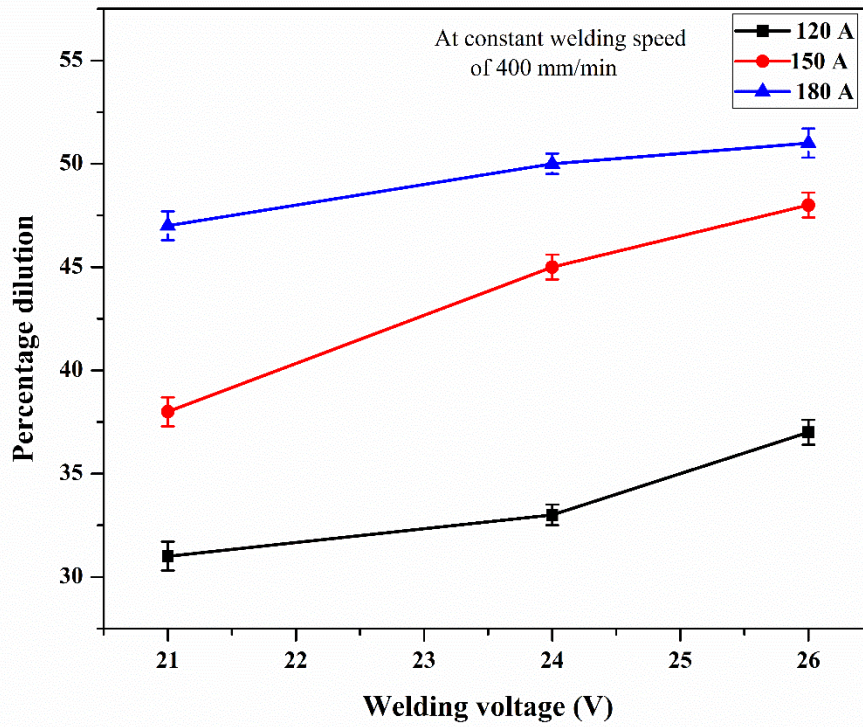


Figure 4.6 Plot of percentage dilution versus welding voltage at different values of welding speed.

As shown in Figure 4.6, at any constant welding current and welding speed, the percentage dilution is increasing with the welding current. As expected, the percentage dilution is higher for higher values of welding current. According to ohm's law, the voltage is proportional to the resistance at given value of current. On increasing the resistance to the flow of electricity, the generation of heat is increasing, which is transferred to the base metal and the electrode wire. That is why on increasing the welding voltage, the area of fused metal increases, as well as the area of total weld deposit, also increases.

The distribution of heat takes place between the electrode wire and the base metal. Some part of the heat that is required for melting of the electrode wire, the remaining heat goes to the base metal. The heat is distributed so that on increasing the welding voltage, the area of the fused base metal is much affected than the area of the

total weld deposit, which resulted in the increase in the value of percentage dilution with the welding voltage.

4.1.8 Variation of percentage dilution with the welding speed

At the different combination of constant welding current and variable welding speed, the percentage dilution of different samples is shown in Figure 4.7.

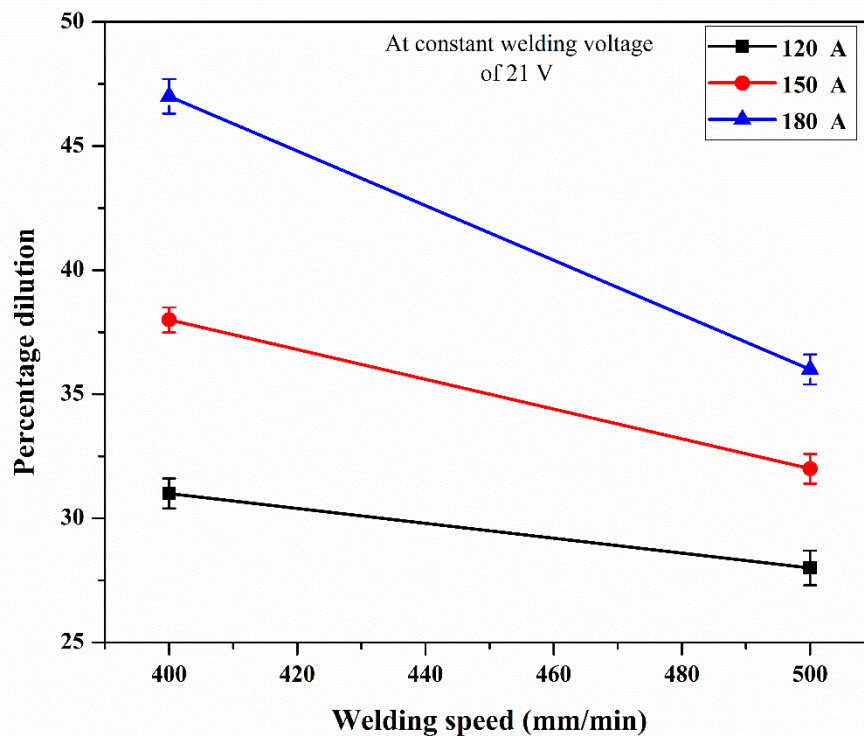


Figure 4.7 Plot of percentage dilution versus welding speed at different values of welding voltage

Since the heat input per unit length also depends upon the welding speed. The higher the welding speed, the lower will be heat input per unit length. Lower heat input tends to reduce the area of the fused base metal as well as also tends to reduce the area of the total weld deposit. But the effect of increasing the welding speed on the reduction of area of total weld deposit is more pronounced than the reduction in the area of the fused base metal that results in the increase in percentage dilution.

4.1.9 Chemical composition of welds

Based on the percentage dilution, the composition of the base material and the composition of the filler material, the chemical composition of weld metal was predicted using equation (3.4). The value of percentage dilution was taken from Table 4.2. The result of weld metal composition is tabulated in Table 4.3.

In this table, WM(x) represents the chemical composition of the WMZ of welded sample S(x), where x varies from 1 to 18. For example, WM1 shows the chemical composition of the WMZ of sample S1. Similarly, WM2, WM3, etc., shows the chemical composition of the WMZ of sample S2, S3, respectively and so on.

The corresponding values of nickel equivalent and chromium equivalent have been mentioned in the last two rows of the tables. In this table, the equivalent of chromium and nickel has also been tabulated. It was calculated by equation (4.1) and equation (4.2), respectively.

$$\text{Cr equivalent} = \text{Cr}\% + \text{Mo}\% + 1.5 \times \text{Si}\% + 0.5 \times \text{Nb}\% \quad (4.1)$$

$$\text{Ni equivalent} = \text{Ni}\% + 30 \times \text{C}\% + 0.5 \times \text{Mn}\% \quad (4.2)$$

Table 4.3 Chemical composition (weight %) of WMZ.

Element	BM	ER304L	WM1	WM2	WM3	WM4	WM5
C	0.024	0.015	0.018	0.018	0.019	0.018	0.019
Mn	0.263	1.650	1.220	1.123	0.998	1.192	1.026
Si	0.517	0.243	0.328	0.347	0.372	0.333	0.366
S	0.001	0.013	0.009	0.008	0.007	0.009	0.008
P	0.023	0.031	0.029	0.028	0.027	0.028	0.027
Cr	11.240	18.460	16.222	15.716	15.067	16.077	15.211
Ni	0.066	8.140	5.637	5.072	4.345	5.476	4.507
Cu	0.010	0.434	0.303	0.273	0.235	0.294	0.243
Mo	0.006	0.352	0.245	0.221	0.189	0.238	0.196
Nb	0.040	0.050	0.047	0.046	0.045	0.047	0.046
Ti	0.324	0.008	0.106	0.128	0.157	0.112	0.150
N	0.027	0.220	0.160	0.147	0.129	0.156	0.133
Creq			16.982	16.481	15.836	16.839	15.980
Nieq			6.781	6.186	5.421	6.611	5.591
Creq/Nieq ratio			2.504	2.664	2.921	2.547	2.858

Table 4.3 (continued....)

Element	WM6	WM7	WM8	WM9	WM10	WM11	WM12
C	0.020	0.018	0.019	0.020	0.018	0.018	0.018
Mn	0.957	1.137	0.984	0.943	1.262	1.206	1.151
Si	0.380	0.344	0.375	0.383	0.320	0.331	0.342
S	0.007	0.009	0.007	0.007	0.010	0.009	0.009
P	0.027	0.028	0.027	0.027	0.029	0.028	0.028
Cr	14.850	15.789	14.994	14.778	16.438	16.150	15.861
Ni	4.103	5.153	4.264	4.022	5.879	5.556	5.233
Cu	0.222	0.277	0.230	0.218	0.315	0.298	0.281
Mo	0.179	0.224	0.186	0.176	0.255	0.241	0.227
Nb	0.045	0.046	0.045	0.045	0.047	0.047	0.046
Ti	0.166	0.125	0.160	0.169	0.096	0.109	0.122
N	0.124	0.149	0.127	0.122	0.166	0.158	0.151
Cr _{eq}	15.622	16.552	15.765	15.550	17.197	16.910	16.624
Ni _{eq}	5.166	6.271	5.336	5.081	7.036	6.696	6.356
Cr _{eq} /Ni _{eq} ratio	3.024	2.640	2.954	3.060	2.444	2.526	2.616

Table 4.3 (continued....)

Element	WM13	WM14	WM15	WM16	WM17	WM18
C	0.018	0.018	0.019	0.018	0.018	0.019
Mn	1.234	1.178	1.054	1.220	1.123	1.012
Si	0.325	0.336	0.361	0.328	0.347	0.369
S	0.009	0.009	0.008	0.009	0.008	0.007
P	0.029	0.028	0.028	0.029	0.028	0.027
Cr	16.294	16.005	15.355	16.222	15.716	15.139
Ni	5.718	5.395	4.668	5.637	5.072	4.426
Cu	0.307	0.290	0.252	0.303	0.273	0.239
Mo	0.248	0.234	0.203	0.245	0.221	0.193
Nb	0.047	0.047	0.046	0.047	0.046	0.045
Ti	0.103	0.115	0.144	0.106	0.128	0.153
N	0.162	0.154	0.137	0.160	0.147	0.131
Cr _{eq}	17.054	16.767	16.123	16.982	16.481	15.908
Ni _{eq}	6.866	6.526	5.761	6.781	6.186	5.506
Cr _{eq} /Ni _{eq} ratio	2.484	2.569	2.799	2.504	2.664	2.889

It was observed from the Table that the value of chromium equivalent lies between 15.55 and 17.197, while the nickel equivalent lies between 5.081 and 7.036. The ratio of the chromium equivalent to nickel equivalent lies between 2.444 and 3.060.

The variation of the ratio of the chromium equivalent to nickel equivalent with the heat input is shown in Figure 4.8.

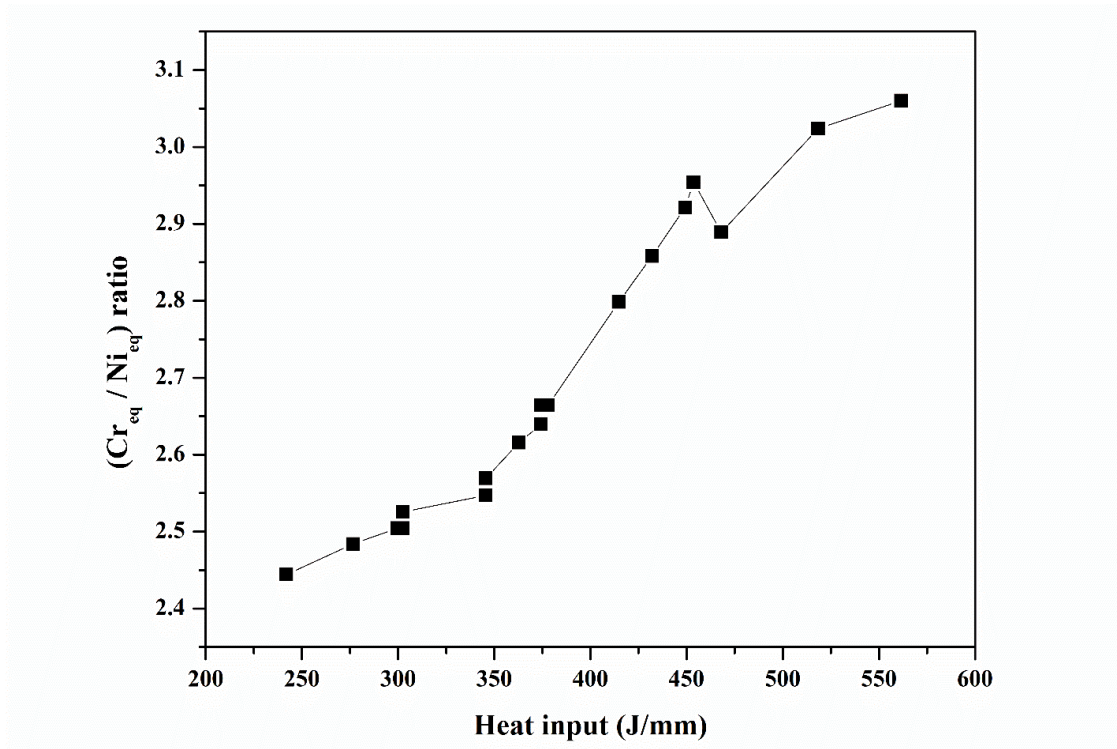


Figure 4.8 Variation of (Cr_{eq}/Ni_{eq}) ratio with the heat input.

It was observed from the above Figure 4.8 that on increasing the heat input from 241.92 J/mm to 561.60 J/mm, the chromium equivalent to nickel equivalent ratio is also increasing from 2.444 to 3.060.

It was observed from Figure 4.4 that on increasing the heat input, the percentage dilution is increased, which indicates the more melting of the base metal (which is dominant with the ferrite phase) in comparison to the total weld deposition. Since the base material is ferritic stainless steel, therefore, on increasing the melting of the base metal, the ferrite stabilising elements' contribution is increased compared to the austenite stabilising elements. That is why, the chromium equivalent to nickel equivalent ratio is increased by increasing the heat input.

4.1.10 Metallography study

The welded plate consists of different regions such as the BMZ, HAZ and WMZ. These regions possess different microstructures due to the difference in the cooling rate as well as chemical compositions.

4.1.10.1 Microstructures of different regions

The metallographic study has been carried out to understand the microstructures of the BMZ, HAZ, and WMZ. For microstructural examination, optical microscopy has been used.

The scanned image of the weld sample in the etched condition is shown in Figure 4.9.

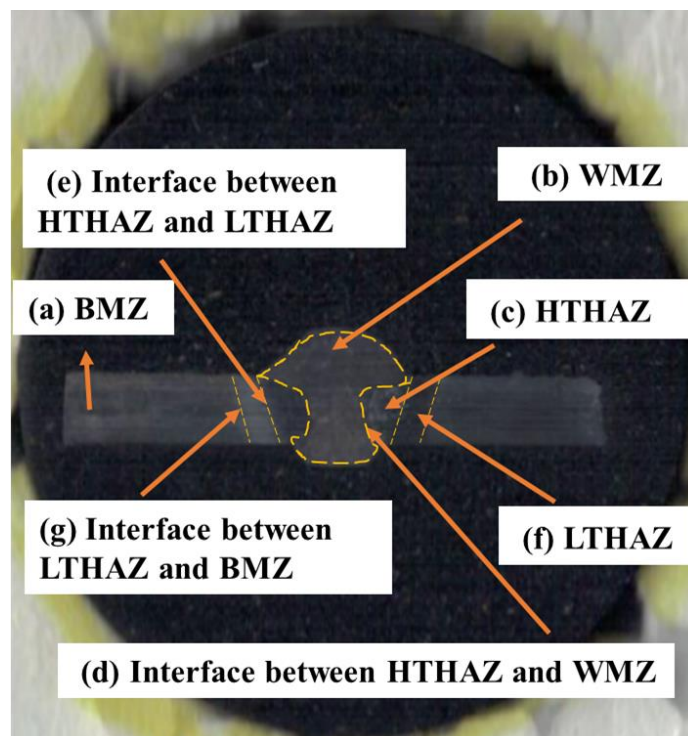


Figure 4.9 Macrograph of the weld sample.

In this Figure 4.9, the different regions are clearly distinguishable and indicated by the arrows. As indicated in this figure, HAZ of two types is clearly distinguishable.

One is closer to the WMZ, and another is closer to the BMZ. These two regions are known as the high temperature HAZ (HTHAZ) and low temperature HAZ (LTHAZ), respectively. The microstructures of these different regions (from a to g) were also taken and shown in Figure 4.10.

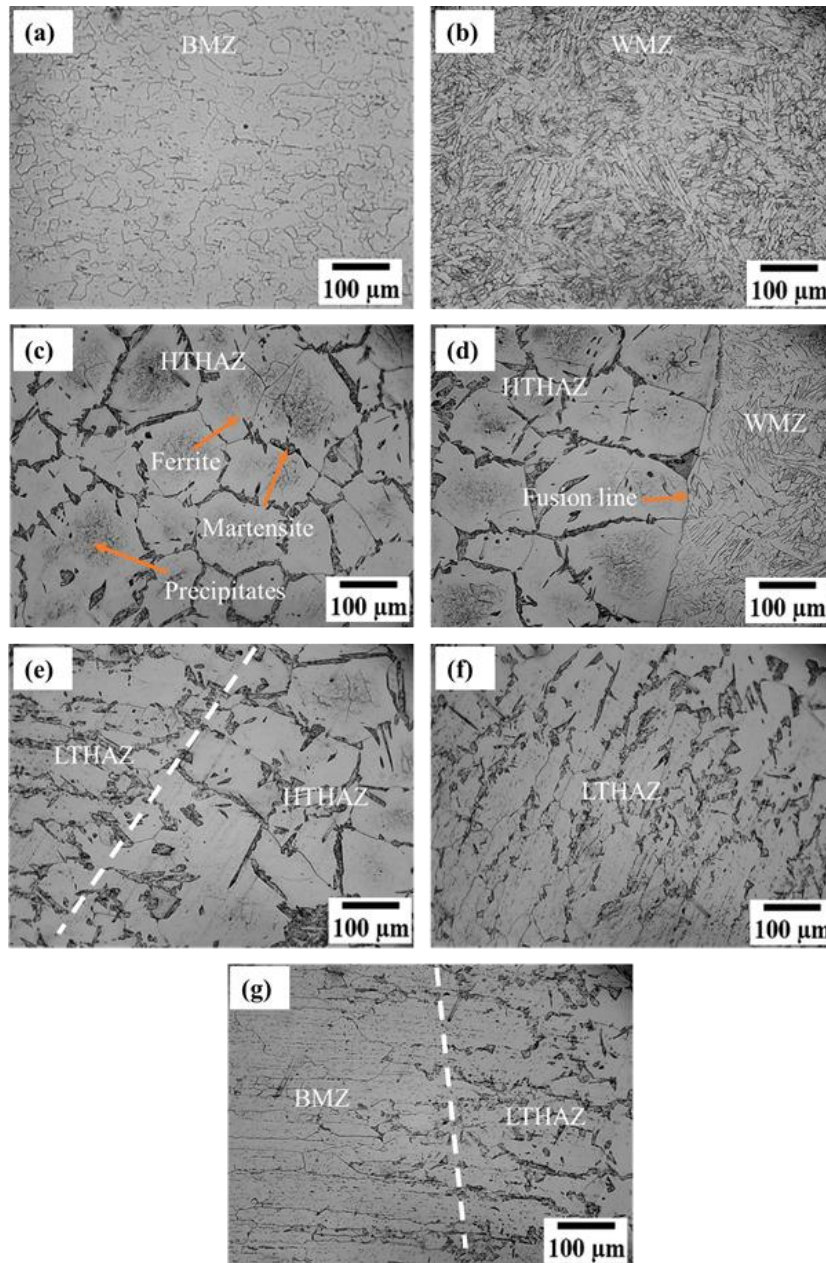


Figure 4.10 Microstructure of different regions: (a)BMZ, (b) WMZ, (c) HTHAZ, (d) interface between HTHAZ nd WMZ, (e) interface between LTHAZ and HTHAZ, (f) LTHAZ, and (g) interface between LTHAZ and BMZ.

Different regions are labelled in each microstructure (from a to g). Also, the fusion boundary was shown by the dotted white line. In Figure 4.10 (c), different phases formed in the HTHAZ are also shown.

The mechanism of the development of microstructure within the WMZ and the HAZ is different and explained in details below.

4.1.10.2 Development of microstructure within the weld metal

The microstructure of any region of the weldment is controlled by its chemical composition and temperature history. The alloying elements in the stainless steel can be divided into two categories, one, which promotes the formation of the ferrite phase and another, which promotes the austenite phase. Ferrite promoting elements are chromium, molybdenum, silicon, niobium, titanium, aluminium, vanadium and tungsten whereas, the austenite promoting elements are nickel, manganese, carbon, nitrogen, copper and cobalt. Any austenite that forms during welding of ferritic stainless steel will ultimately transform into martensite on cooling since the cooling rate is fast in welding and the amount of alloying elements is high. The formation of the martensite phase, therefore, depends upon the formation of the austenite phase at elevated temperature. Without forming the austenite phase at elevated temperature, the formation of the martensite phase at a lower temperature is impossible. The phases of austenite or ferrite that forms at elevated temperature are primarily governed by the amount of alloying elements present. So, the microstructure of the interested region in the stainless steel can be controlled by balancing the present alloying elements. The control of the amount of alloying elements in weld metal can be easily done by changing the composition of the filler material and the extent of dilution. However, the chemical composition of the HAZ remains the same as the composition of the base material being welded.

Researchers have carried out various investigations to predict the weld metal microstructure. In this reference, the Schaeffler diagram was first diagram developed by Anton Schaeffler in the year 1947 [1]. In this diagram, the ferrite promoting elements are included in the chromium equivalent, whereas austenite promoting elements are included in the nickel equivalent. Anton Schaeffler has developed several diagrams over a period of time by rectifying the problem associated with the previously developed diagrams, and the final version of the Schaeffler diagram was proposed in 1949, as shown in Figure 4.11 [1]. Chromium equivalent and nickel equivalent can be calculated by using the equation (4.1) and equation (4.2) and shown in Table 4.3.

From Figure 4.10, it can be seen that the WMZ consists of different phases depending on the percentage dilution obtained at various process parameters. The phase primarily present is the ferrite phase. In this study, the upper and lower values of chromium equivalent and nickel equivalent of all weld metals at different values of heat inputs are shown by red lines.

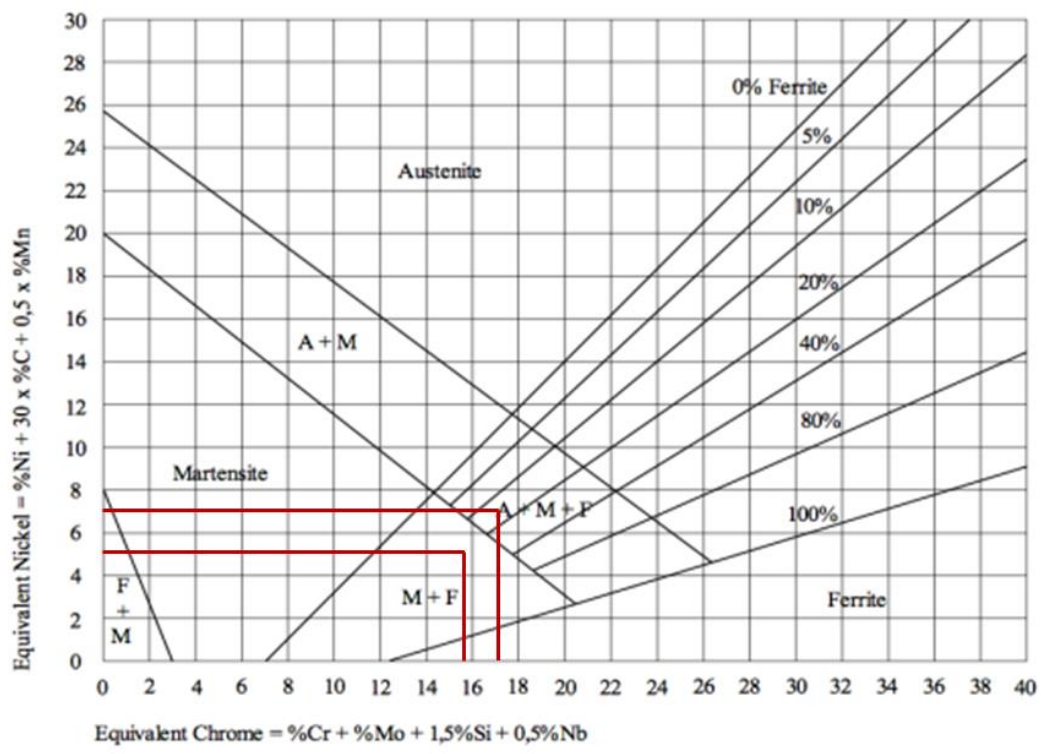


Figure 4.11 Schaeffler diagram.

It was observed from Figure 4.8 that on increasing the heat input, the ratio of Cr equivalent to Ni equivalent increases. The lowest ratio of the Cr equivalent to Ni equivalent has been obtained at the highest value of chromium equivalent as well as nickel equivalent, as can be seen from Table 4.3. On the contrary, the highest ratio of the Cr equivalent to Ni equivalent has been obtained at the lowest value of chromium as well as nickel. When the lowest ratio was plotted on the Schaeffler diagram (Figure 4.11), this ratio was observed to fall into the (A+M+F) region, which tells that the WMZ corresponding to this ratio consists of the ferrite phase along with the martensite and austenite phase. But, when the highest ratio was plotted, it lies in the (M+F) region, which means that the WMZ possess a ferrite phase along with the martensite phase. It has happened because the chromium is a ferrite stabilising element, and on increasing the ratio of the chromium equivalent to the nickel equivalent, the presence of ferrite phase is dominating while the remaining austenite has been converted into the martensite phase due to the dominating effect of the ferrite phase over the austenite phase. On the contrary, when this ratio was decreased, the dominating effect of ferrite phase tends to decrease and the formation of stable austenite has also occurred. Some unstable austenite still gets converted into the martensite phase.

Thus, it can be concluded from the above discussion that weld metal possessed either combination of martensite and ferrite or a combination of austenite, martensite and ferrite phases. The use of austenitic filler wire and ferritic base metal resulted in the formation of mixed phases of ferrite, austenite and martensite in the weld metal. The ratio of different phases varies with the heat input, which in turn is affected by the process parameters.

4.1.10.3 Formation of phases within the heat affected zone

The microstructures of HAZ are shown in Figure 4.10 (c-g). Martensite formation was clearly observed at the grain boundaries in both types (i.e. LTHAZ and HTHAZ) of HAZ. The growth of martensite from the grain boundaries to inside the grains was also observed. Precipitates of carbides or nitrides were observed to be dispersed within the ferrite phase.

The formation of different phases can also be predicted by using a phase diagram. In this case, to find out the possible microstructure within the HAZ, a 13 % Cr pseudobinary phase diagram has been used, which is shown in Figure 4.12 [1].

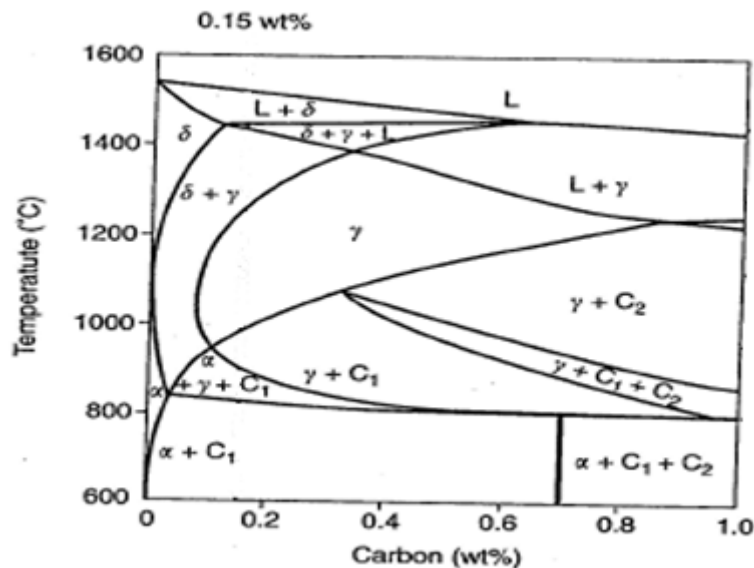


Figure 4.12 13% Cr pseudobinary phase diagram.

On increasing the temperature during welding, the formation of δ ferrite occurred in both types of HAZ. In the HTHAZ region, upon cooling, δ ferrite phase is partially transformed into the austenite phase. On further cooling, the formation of α ferrite, martensite (after conversion of austenite) and precipitates occurred. This martensite is

present mainly on the grain boundaries of α ferrites while some amount of martensite is also present within the grains, which can be clearly observed from Figure 4.10.

In the LTHAZ region, since this region possessed a higher cooling rate than the HTHAZ region due to its position near the base material, the amount of transformation of the δ ferrite phase into the austenite phase is lesser than the HTHAZ region. That is why on further cooling, the amount of martensite phase is also lesser than in the HTHAZ region, which can be clearly observed in Figure 4.10.

When the ferrite is supersaturated with carbon and nitrogen at high temperatures, the formation of precipitates also takes place. These precipitates are mostly carbides and nitrides of titanium. The formation of precipitates in the interior of grains occurs when the cooling rate is high. The chromium, which is available at grain boundaries, migrate toward the inner side of grain to form chromium carbide or nitride by combining with the carbon or nitrogen. All precipitates are formed far away from the grain boundaries. Thus a zone around grain boundaries up to some distance (about 20 micron to 50 micron) are free from precipitates, and these zones are known as precipitate free zone (PFZ) [1].

Since the austenite acts as a sink of carbon and martensite is formed from this austenite, therefore, the amount of carbon is high in the martensite that forms from austenite. More martensite formation will reduce the availability of carbon to react with the chromium to form chromium carbides. That is why more formation of martensite causes almost no precipitate formation in the HAZ. Thus, the amount of martensite formation is inversely proportional to the amount of precipitates formation.

4.1.10.4 Grain size of weld metal zone and heat affected zone

The average grain size of base metal has been found 27 μ m. Figure 4.13 shows the variation in the grain size of HAZ and WMZ with the heat input.

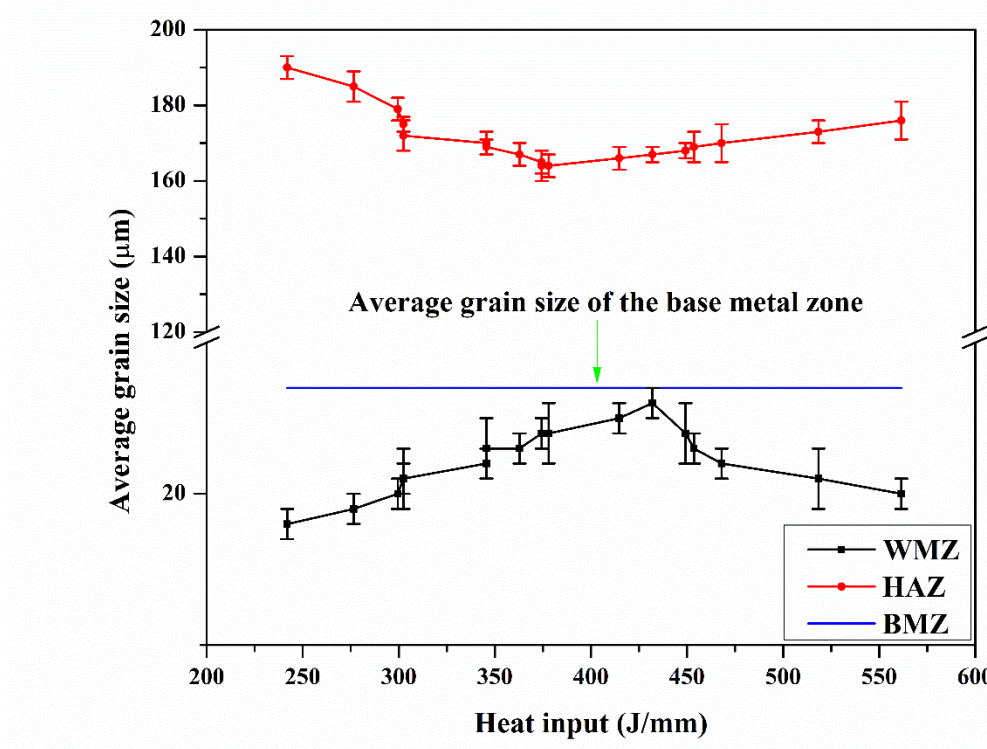


Figure 4.13 Variation in the grain size of HAZ and WMZ with the heat input.

It was observed from Figure 4.13 that the grain size of WMZ is first increasing and then decreasing on increasing the heat input. As the heat input increases, the ratio of the chromium equivalent to the nickel equivalent is also increasing. Since the chromium is a ferrite stabilising element, therefore, more formation of ferrite phases occurred as compared to the austenite and martensite phases. Due to the formation of ferrite phases in more amount, the grain size of the ferrite phase was increased up to 432 J/mm of heat input. But on further increasing the heat input, when the ratio of Cr to Ni increases and falls into the M+F region, as observed in Figure 4.11, the grain size of WMZ decreases. It was due to the strong restriction of grain growth of ferrite phases by the martensite. It can be visualized from Figure 4.13 that the grain size of HAZ is first decreasing with the heat input and then increases with further increase in the heat input. Two contrary effects were produced on increasing the heat input (cooling rate and grain growth time). One effect is responsible for reducing the grain size, and another effect is for increasing

the grain size. The dominance of one effect over the other decides the trend of variation of grain size with the heat input.

The first effect is that on increasing the heat input, the cooling rate of the HAZ was decreased, which allowed more transformation of δ ferrite into the austenite phases, and thus, more martensite formation occurred. Due to the presence of the martensite phase, the growth of the ferrite phases were hindered which resulted in the reduction of the grain size of HAZ.

The second effect is that on further increasing the heat input, due to the lower cooling rate, the time was sufficient to grow the ferrite phases which resulted in the grain growth of the ferrite phases.

Therefore, the grain size of the HAZ first decreasing with the heat input due to the dominance of the first effect and then increases with a further increase in the heat input due to the dominance of the second effect.

The grain size of base metal lies between the HAZ (coarser grains) and WMZ (finest grains).

4.1.11 X-ray diffraction analysis

To investigate the different phases formed within the WMZ and HAZ, X-ray diffraction (XRD) analysis of the weld metal has been carried out, as shown in Figure 4.14. Working voltage and current of 40 kV and 15 mA respectively have been used with the step width of 0.02 degree. The range of scan lies between 10° to 90° with the scan speed of 10 degree/min. X'Pert High Score Plus software was used to analyse the peaks of different intensities.

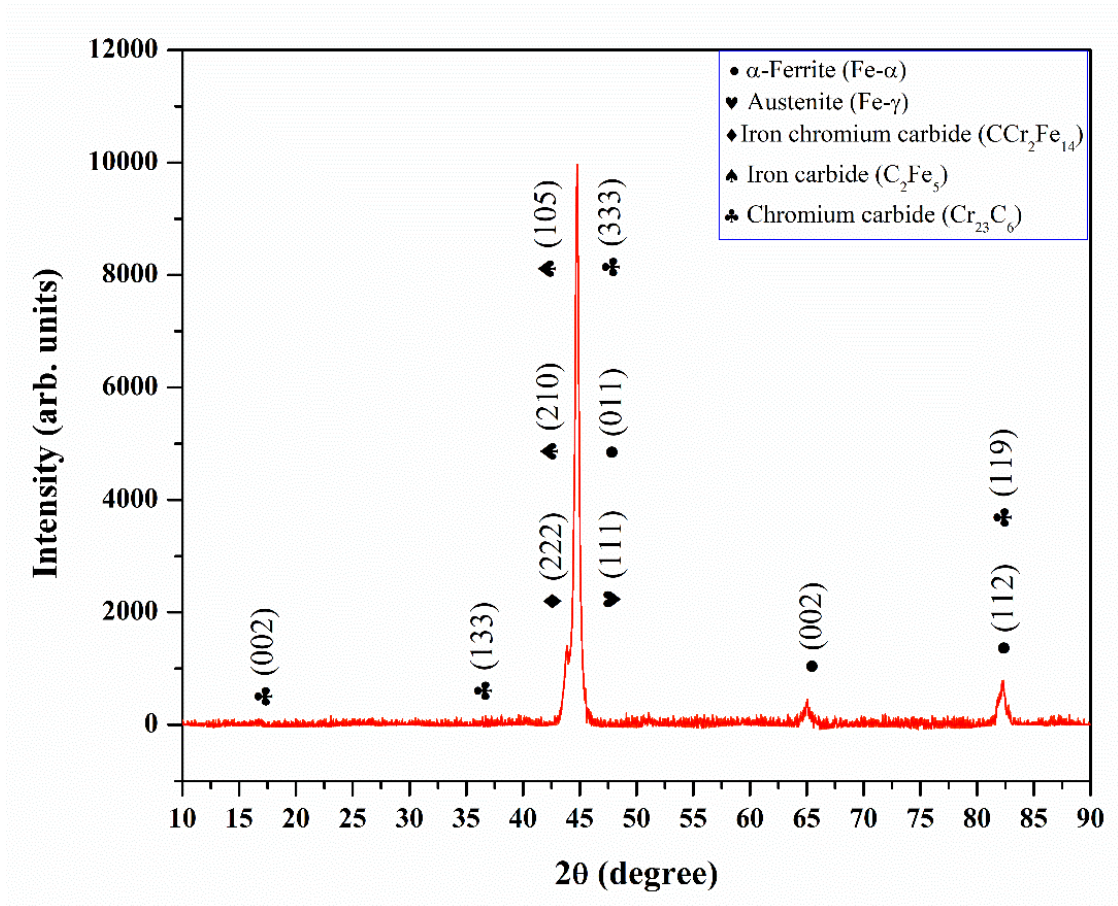


Figure 4.14 XRD analysis of weld metal.

Major peaks of alpha ferrite are found at 44.68 °, 65.03° and 82. 34° and are matching with the ICSD file number 98-005-3451. Major peaks of austenite are found at 44.26 °. While major peaks of chromium carbide are found at 16.63°, 36.75°, 44.15° and 82.44° and are matching with the ICSD file number 98-000-2837. Also, other carbides like iron chromium carbide and iron carbide are also found with the file number 98-007-6800 and 98-024-5334, respectively.

4.1.12 Hardness of weld metal zone and heat affected zone

The hardness of base metal was found 210 HV. The hardness variation of HAZ and WMZ with the heat input has been shown in Figure 4.15.

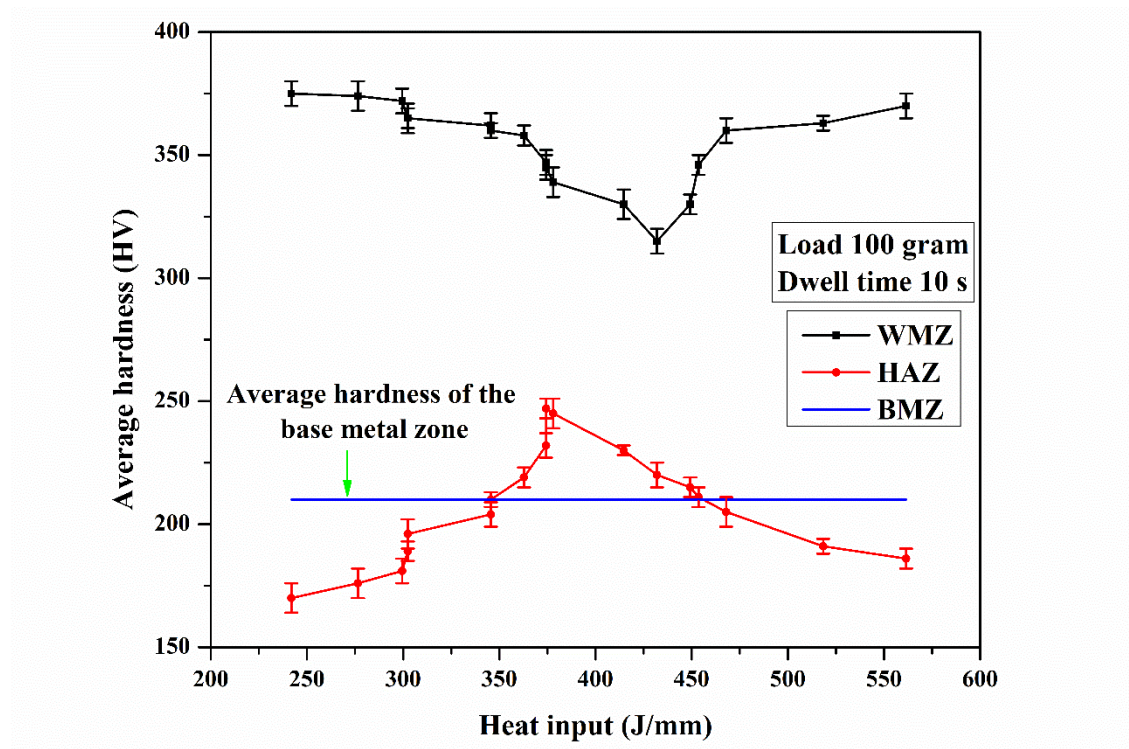


Figure 4.15 Variation of the average hardness of WMZ and HAZ at different heat input.

It can be observed from Figure 4.15 that the hardness of the WMZ is firstly decreasing with the heat input, but after 432 J/mm heat input, the hardness of WMZ tends to increase. The material's property to resist the localized deformation on applying mechanical load or by abrasion is known as hardness. The hardness of the material is strongly dependent on its grain size and the type of phases present within the grain.

The relation between grain size and microhardness can be described by the Hall-Petch equation below (4.3) [183].

$$\sigma_y = \sigma_0 + \frac{k_y}{\sqrt{d}} \quad (4.3)$$

Where, σ_y is the yield stress

σ_0 is the materials constant

k_y is the strengthening coefficient, and

d is the average grain diameter.

According to the Hall-Petch equation, the yield strength is inversely proportional to grain size. The empirical relation between yield strength and microhardness shows a linear relationship between these two properties. Less grain size results in more number of grains and grain boundaries. On applying the load, the dislocations are generated, and these dislocations tend to move under the action of the applied load. The movement of dislocations is essential for causing plastic deformation. The grain boundaries, as well as different phases, act as a barrier for the movement of dislocations. To move the dislocations further, more forces are required, and thus, microhardness is increased. Hence, microhardness and grain size are inversely proportional to each other, and the effect can be observed in Figure 4.15. Therefore, the hardness of the HAZ and the grain size possessed opposite trend, i.e. hardness is firstly increasing with the heat input, but after 374 J/mm heat input, the hardness of HAZ tends to decrease. As observed from Figure 4.13 that on increasing the heat input up to 374 J/mm, the grain size of HAZ decreases with the heat input. According to the Hall-Petch equation, as explained earlier, the hardness must be increased by decreasing the grain size. On further increasing the heat input, the grain size of HAZ was increased, and according to the Hall-Petch equation, the hardness has been decreased.

From Figure 4.15, it was also observed that WMZ possessed more hardness while HAZ possessed lower hardness. It is due to the fact that the grain size of WMZ is more refined than the grain size of HAZ.

4.1.13 Tensile testing

Two types of tensile samples have been prepared, one is a transverse tensile sample, and another is a reduced section tensile sample. The transverse tensile sample is used to find the weakest region in the welded plate, whereas a reduced section tensile sample is used to find the tensile strength of the welded plate.

4.1.13.1 Transverse tensile testing

To find the location of the fracture, the tensile testing of the transverse tensile sample has been carried out. The fractured samples of both base metal, as well as welded plate after performing tensile testing, are shown in Figure 4.16.



Figure 4.16 Transverse tensile test specimen after testing: (a) base metal, and (b) welded plate.

All the welded samples fractured in the HAZ, as shown in Figure 4.16, which indicates that the HAZ is the weakest zone in all three zones (BMZ, HAZ and WMZ). In the case of tensile testing of base metal, the fracture occurred in the centre of the gauge length. The fracture always occurs in the weakest region and in the welded plate, the weakest region is HAZ due to its coarser grain size than the other regions of the

weldment. Since the fracture occurred in the HAZ, that is why, the corresponding tensile properties of the welded plate reflect the properties of HAZ.

The stress strain curves for parent material and S7 joint are shown in Figure 4.17.

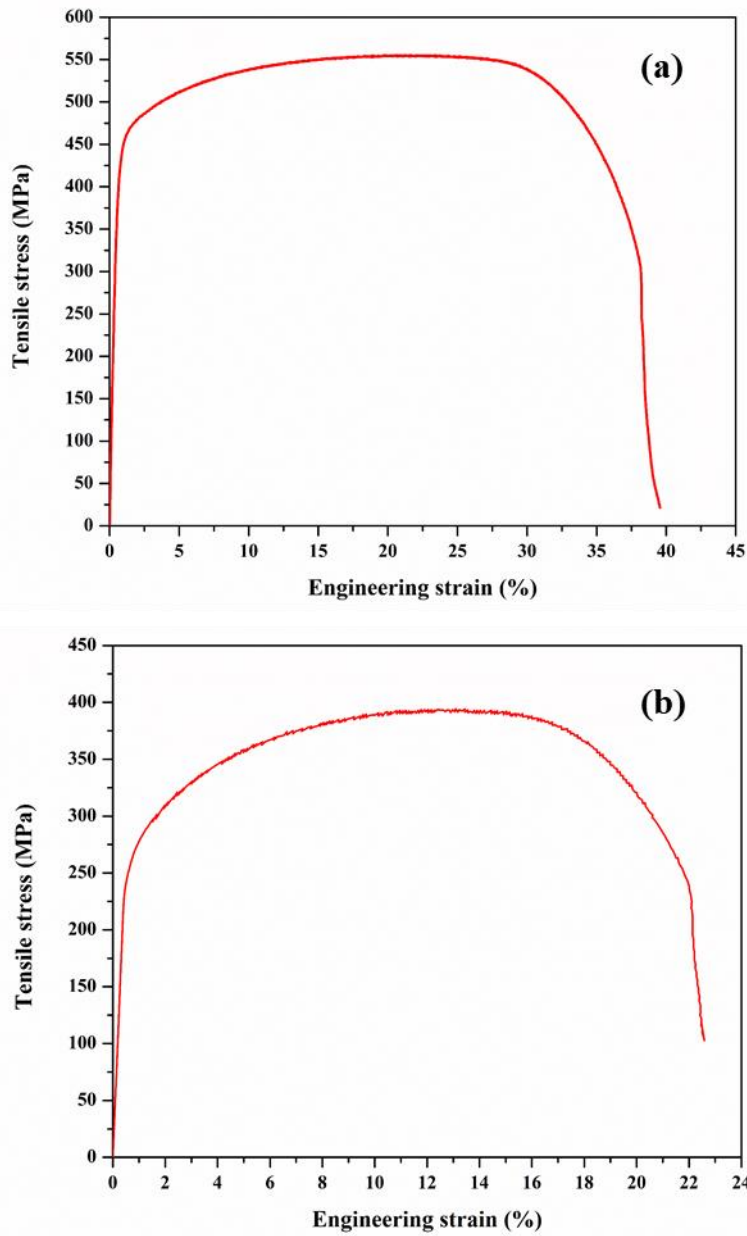


Figure 4.17 Tensile stress-strain curve for (a) base metal SS409L, and (b) welded plate S7.

From Figure 4.17, it can be found that the tensile properties of the weldment S7 is lower than that of the base metal. It was occurred due to the larger grain size in the weakest region of the weldment (i.e. HAZ) of plate S7.

The tensile testing of all the welded plates were performed. It was found that the values of ultimate tensile strength of the weldment lies in the range of 350 to 399 MPa. The range of yield strength was found to lie between 241 to 260 MPa. The percentage elongation lies between 22% to 27%. Sample S7 possessed the best tensile properties (ultimate tensile strength of 399 MPa, yield strength of 260 MPa and percentage elongation of 22 %).

Transverse tensile fractography has also been performed to find out the mode of fracture. Fractographic surfaces of transverse tensile specimens of base metal and sample S7 are shown in Figure 4.18.

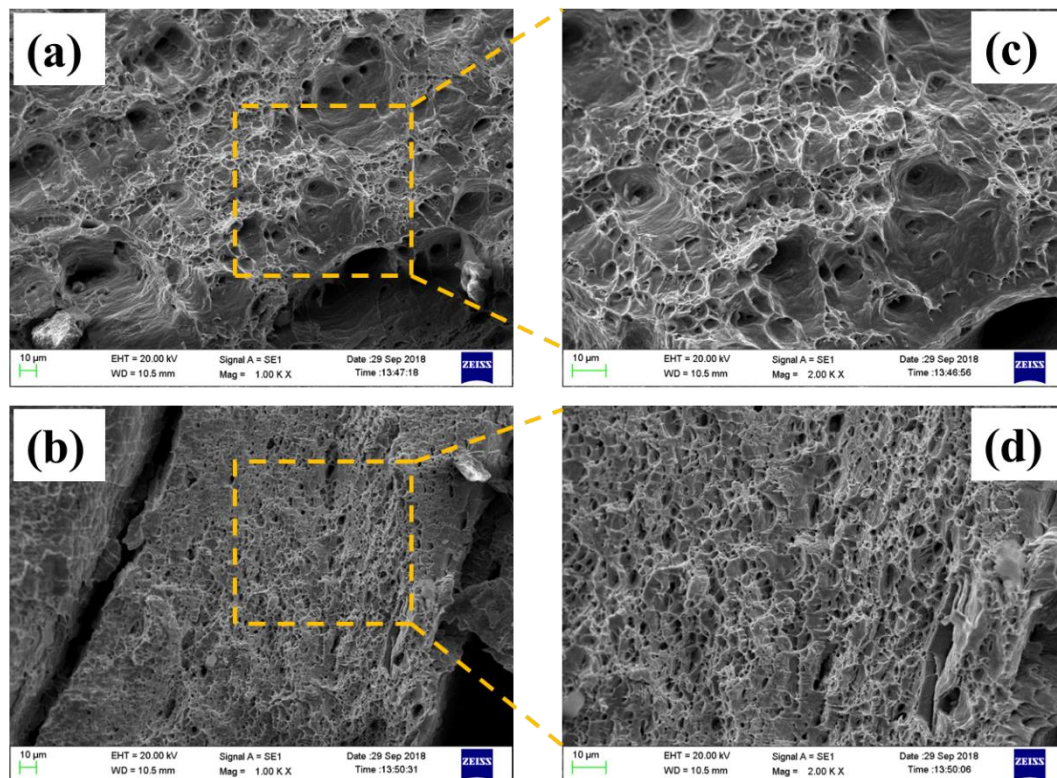


Figure 4.18 Fractographic surfaces of the transverse tensile sample of (a,b) base metal and (c,d) welded plate S7.

In Figure 4.18, it was revealed that both base metal and welded metal possessed dimpled ruptures, indicating that the fracture of both samples occurred in the ductile mode. The mode of fracture (i.e. ductile fracture) can be easily inferred by observing the dimples of various sizes on the fractured surfaces. Ductile mode of fracture shows a dimpled structure, whereas brittle mode of fracture shows cleavage facets. Ductile fracture is the more preferable mode of fracture than brittle fractures under operating conditions because it is not catastrophic [184]. Ductile fracture is also called as dimpled, fibrous, or plastic fracture.

The formation of dimples during the ductile fracture, occurs in three stages [185]. First is the nucleation of internal voids during plastic flow, second is the growth of these voids with continued deformation, and eventually coalesce to form larger voids. Finally, the separation of these voids at the fracture surface occurs which leads to a characteristic dimpled texture. Various factors affect these three stages which vary widely in different material systems. Therefore, fractographic appearance of the final fracture surface is influenced by these same factors. Grain size is one of the most important factor which decides the appearance of the fractographic surfaces. According to Hall-Petch equation, smaller grain size possess more yield strength, i.e. more energy is required to cause fracture of the surfaces. Therefore, in the case of smaller grain size, dimples become more elongated in the tensile direction and therefore deep dimples are obtained. Whereas, for larger grain size, the dimples are shallow due to lower value of yield strength [186].

From the above figure, it can be easily observed that the base metal possessed deeper dimples compared to the welded plate S7, which represents smaller grain size of the base metal than that of the sample S7. Thus, the results obtained from the fractographic analysis, support the results obtained from the tensile testing.

4.1.13.2 Reduced section tensile testing

It was found from the tensile testing of transverse samples that HAZ is the weakest region present in the welded plate. Since sample S7 represents the best tensile properties of the HAZ, therefore sample S7 was selected for comparison of tensile properties of the welded sample and base metal.

To find out the weld strength of welded plate and base plate, reduced section tensile testing has been carried out, and the results are given in Table 4.4.

Table 4.4 Reduced section tensile properties

Material	UTS (MPa)	YS (MPa)	% EL
Base metal	583	450	25
Sample S7	620	503	20

In the reduced section tensile testing, the tensile properties differ considerably from the tensile properties obtained in the case of transverse tensile testing. It was happened due to the stress concentration in the WMZ. During the tensile testing, the stress produced leads to strain hardening, which increased tensile load for further deformation, and thus strength increased. The sample S7 has been fractured in the WMZ, which reflects the weld metal strength of the welded plate.

Figure 4.19 shows the fractographic surfaces of reduced section tensile specimens of base metal and sample S7.

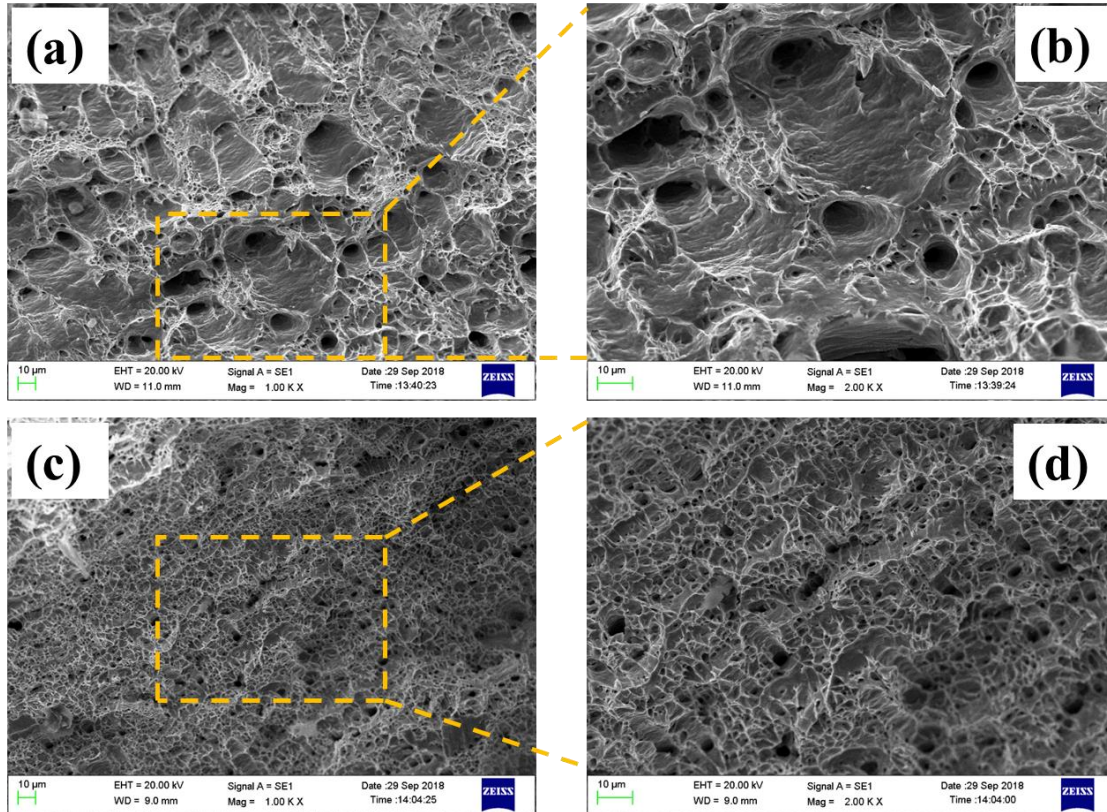


Figure 4.19 Fractographic surfaces of reduced section tensile sample of (a,b) base metal and (c,d) welded plate S7.

Dimple ruptures are clearly visualized in the fractography of both tensile samples. There is a difference in the size of the dimple ruptures of the base metal and the welded plate tensile samples, as shown in Figure 4.19. Large size dimples have been observed in the base metal as compared to the welded sample, which means that base metal possessed a larger percentage elongation and lower tensile strength than the welded plate.

4.1.14 Charpy impact testing

To find the toughness of BMZ, WMZ and HAZ, the Charpy impact testing has been carried out. The broken samples after this testing are shown in Figure 4.20.



Figure 4.20 Charpy impact toughness test specimen after testing.

The toughness of base metal was found 29J. The toughness variation of HAZ and WMZ with the heat input has been shown in Figure 4.21.

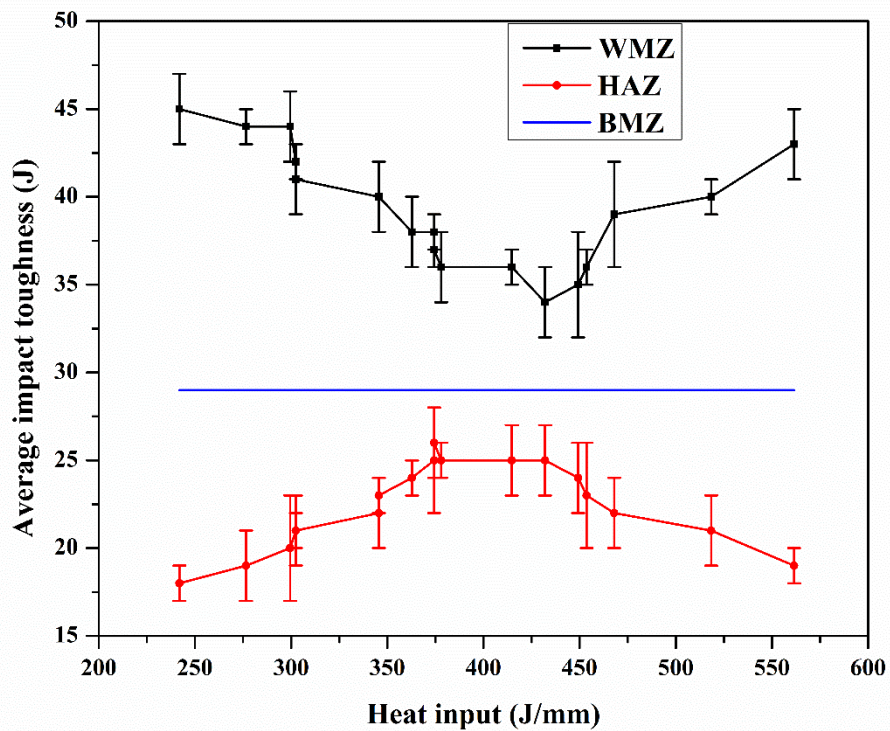


Figure 4.21 Variation of Impact toughness of WMZ and HAZ at different heat input.

Average Impact toughness of base metal has been found 29 J. As shown in Figure 4.21, the toughness of the WMZ is firstly decreasing with the heat input, but after 432 J/mm heat input, the toughness of WMZ tends to increase.

Toughness is the energy absorbing capacity of material without fracturing. Toughness depends upon the grain size. When an impact load is applied to the material, the formation of dislocations happened, and these dislocations tend to move. The grain boundaries create hurdles in their movement. To move dislocations further, more force is required, and thus, energy is consumed to move dislocations before fracture. This energy absorbed by the material before fracture is known as toughness. However, the amount of energy absorbed depends upon the grain size. In the case of finer grains, more restriction happened in the motion of dislocations which result in more absorption of energy and hence more toughness value. As observed from Figure 4.13 that the grain size of WMZ is increasing with the heat input up to 432 J/mm; that is why, the toughness is decreasing correspondingly.

The toughness of HAZ was observed to be increased on increasing the heat input up to 374 J/mm, but after that, it starts to decrease. This variation of toughness with the heat input is related to grain size variation with the heat input. As observed from Figure 4.13, on increasing the heat input, the grain size of HAZ decreases up to 374 J/mm; after that, it starts to increase. As explained earlier that toughness is inversely related to grain size. That is why, finer grains possessed better toughness property than coarser grains.

4.1.15 Residual stress measurement of the welded plate

The variation of the longitudinal residual stress at different locations of the welded plate S7 along the width of the plate is shown in Figure 4.22.

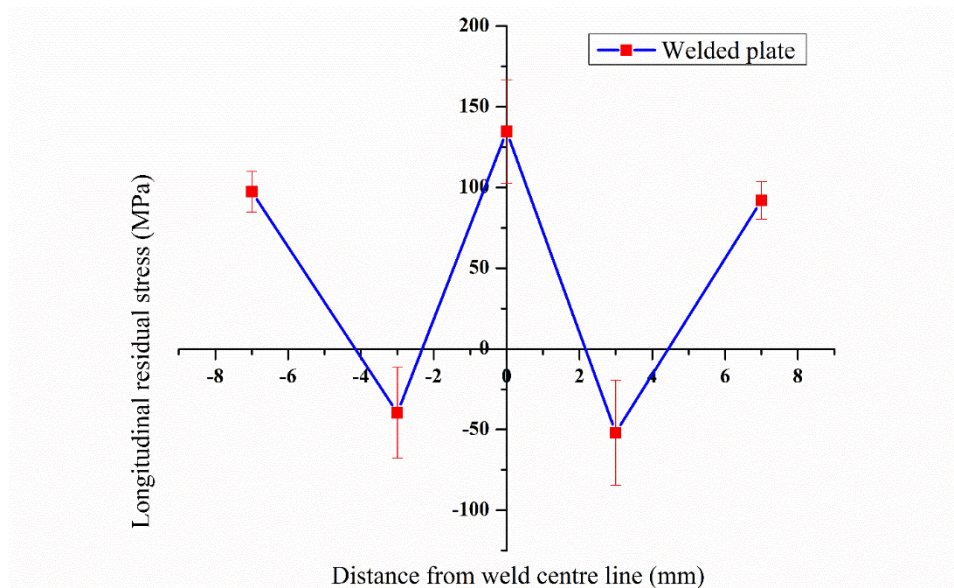


Figure 4.22 Longitudinal residual stress measurements in the welded plate.

The above figure shows that the BMZ and WMZ possess tensile residual stress; however, its magnitude in the BMZ is not much, while the residual stress in the HAZ possess is compressive.

Residual stress is that stress which remains present inside the material, even when no external load is applied to the material [187]. This stress remains stationary and at equilibrium with its surroundings [188]. It may be of tensile or compressive nature. Thermal variations, phase transformations and mechanical processing are three main reasons to generate the residual stress in any material [189]. Generally, thermal variations and phase transformations are two major factors responsible for the generation of residual stress in the welding process [190, 191]. During welding, localized heating and non-uniform cooling are experienced at each point, accompanied by steep thermal gradients,

leading to residual stresses in the welded plate [192-199]. The residual stress is also produced due to phase transformation that occurred in the weld metal and adjacent heat-affected zone (HAZ) owing to the difference in the volume of the newly formed phases with that of the initial phases. In some welding processes involving plastic deformations of the material, such as FSW, residual stress is produced due to non-uniform plastic deformation of the material through the cross-section of an object.

The mechanical properties of the material are strongly affected by the presence of residual stresses [200-202]. The tensile residual stresses deteriorate the mechanical properties such as hardness, tensile strength, fatigue strength, etc., whereas the compressive residual stresses improve them [203]. Therefore, compressive residual stress is more beneficial than tensile residual stress.

Hydrogen induced cracking and stress corrosion cracking are major problems that can be occurred in the weld metal due to the presence of residual stresses [204].

In the case of the welded plate, when the molten weld pool cools and tends to solidify, then contraction occurs in WMZ much more than the surrounding regions (HAZ and BMZ) due to the density difference between the liquid and solid. But, these surrounding regions tend to restrict this contraction of the weld pool, which creates tensile residual stresses in the WMZ and compressive residual stresses in the HAZ [205].

Tensile residual stresses were observed in the BMZ. It was occurred due to the clamping of the base metal to be welded during the welding process.

4.1.16 Micro-magnetic characterisation of welds

Micro-magnetic characterisation of different zones of sample S7 has been performed by using MBN and MHL techniques. The grain size and microhardness of different zones of sample S7 are already known. In the MBN technique, the response is in terms of V_{rms} , V_{peak} and number of pulses, while in the MHL technique, the responses

is in terms of average permeability, coercivity, AMFD, remanence and coreloss. The MBN analyzer software provides the value of response parameters, and no need to calculate manually.

4.1.16.1 Magnetic hysteresis loop testing

At different zones (BMZ, HAZ and WMZ) of the sample S7, the micro-magnetic testing using the magnetic hysteresis loop (MHL) technique has been performed at different values of MFI and magnetising frequency. The values of MFI was varied from 250 Oe to 1000 Oe at a constant value of magnetising frequency of 0.1 Hz. The values of magnetising frequency were varied from 0.05 Hz to 0.25 Hz in the low frequency range and 1.0 Hz to 4.0 Hz in the high-frequency range at a constant value of MFI (800 Oe).

The effect of variation of MFI and magnetizing frequency on the hysteresis loop characteristics such as AMFD, coreloss, average permeability, coercivity and remanence has been investigated.

(a) Average maximum flux density

Ferromagnetic material consists of magnetic domains, and each domain is separated from each other by domain walls [206]. In the absence of an external magnetic field, the magnetic moment of each magnetic domain lies in a certain direction, and this direction of magnetic moment is different for different magnetic domains such that the net magnetic moment of the ferromagnetic material becomes zero. The direction of the magnetisation of a particular magnetic domain depends upon the balance between the several competing energies such as exchange energy, magneto-crystalline anisotropy, and magnetostatic energy. Along with these internal mechanisms, the magnetisation is also influenced by the external magnetic field, which favors the direction of the magnetisation in the direction of the applied magnetic field. When an external magnetic

field is applied and varies with time, the energy balance of the domain is destroyed. To attain the stable position again, the rearrangements of the domain structure occur, and this rearrangement is done by the motion of domain walls. In this rearrangement of domains, due to the motion of domain walls, growth of those domains occurred whose direction of the magnetic moment is already much closer to the direction of the applied magnetic field and hence the shrinkage, and ultimately elimination of all other domains occurred depending upon the magnitude of the applied magnetic field, whose direction of the magnetic moment is not in the direction of the applied magnetic field. Thus the magnetisation is increased on increasing the MFI by the alignment of energetically favoured domains as well as shrinkage or elimination of less energetically favoured domains. The magnetisation of the material is increased with the MFI, but beyond a particular value of MFI, the magnetisation is not increased on further increasing the MFI. It is due to the existence of only one domain in the ferromagnetic material, and this stage is known as the saturation stage. This stage can only be obtained at a higher value of MFI [207].

The relationship between magnetisation (M) and applied MFI (H) is shown in equation (4.4).

$$M = \chi H \quad (4.4)$$

Where, χ represents the magnetic susceptibility.

The magnetisation (M) and magnetic flux density (B) is directly related to each other, as shown in equation (4.5) [208].

$$B = \mu_0 (H+M) \quad (4.5)$$

Where μ_0 represents the magnetic permeability of free space. In the case of the B-H hysteresis loop, the maximum value of B corresponding to the maximum value of H is known as maximum flux density.

In one B-H hysteresis loop, the external magnetic field is applied in the positive as well as in the negative directions. Therefore, two values of maximum flux density are associated with one hysteresis loop corresponding to the maximum value of the magnetic field applied in each direction. The values of both maximum magnetic flux density are slightly different from each other. The average of both values of maximum magnetic flux densities is known as average maximum flux density.

The value of maximum flux density depends upon various factors such as magnetizing frequency, MFI and pinning sites.

(a.1) Effect of magnetic field intensity on average maximum flux density

Figure 4.23 presents the variation of AMFD of each zone of weldment with the variation of MFI at a constant magnetizing frequency of 0.1 Hz.

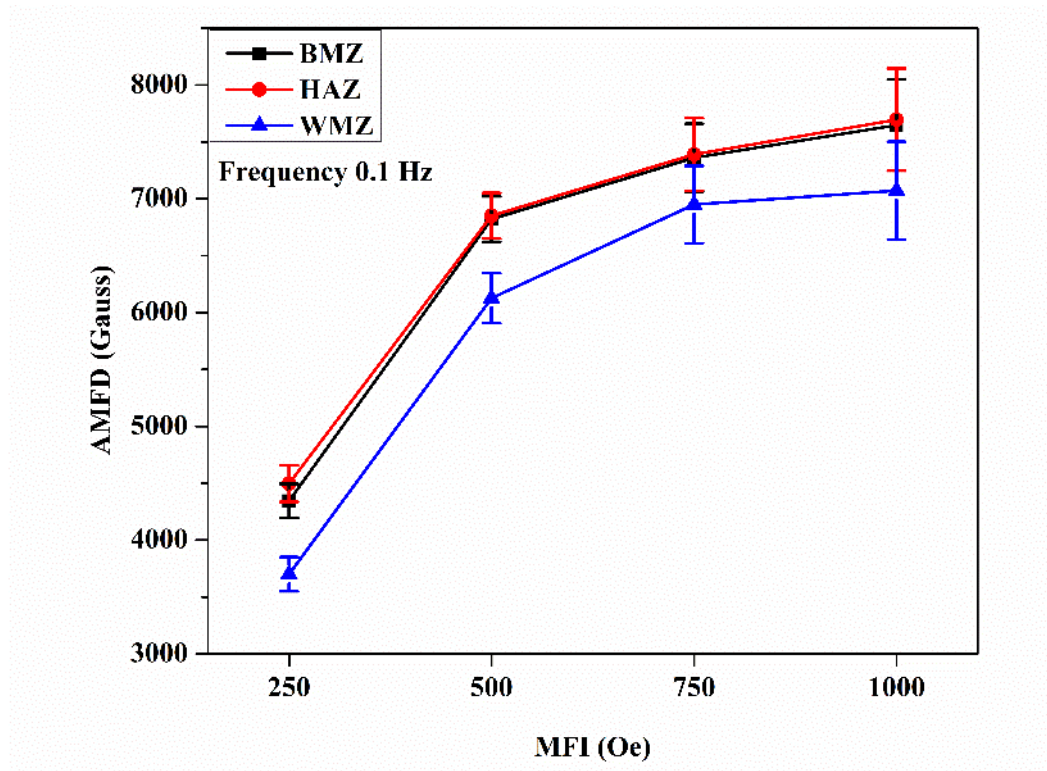


Figure 4.23 Variation of AMFD.

From the above figure, it was observed that the value of AMFD of each zone is increased with the increase of MFI.

As discussed above, when a ferromagnetic material is placed under the varying magnetic field, the magnetic domains tend to orient themselves by the movement of domain walls in the direction of the applied magnetic field and, hence, increases the magnetization. Since the MFI acts like a force to align the magnetic domains, therefore, the magnitude of the magnetic field decides the extent up to which a magnetic domain can align itself in the direction of the applied magnetic field [209]. The higher the magnitude of the applied magnetic field, the higher will be the alignment of domains in the direction of the applied magnetic field, which result in the higher value of maximum flux density and hence AMFD.

This figure also presents the variation in the value of AMFD of each zone at each value of MFI. It was observed that the HAZ possessed a higher value of AMFD while WMZ possessed a lower value. Different zones possessed different value of AMFD for the same value of MFI. It was due to the difference in the motion of the domain walls because each zone possessed a different grain size. The motion of the domain walls is restricted by various pinning sites such as grain boundaries, precipitates, dislocations, etc.[46, 47]. The restriction in the motion of domain walls cause the problem in the alignment of domains in the direction of the applied magnetic field which results in the reduction of magnetisation of the material and hence the value of AMFD. The WMZ possessed lesser grain size and hence more grain boundaries which restrict the motion of the domain walls more than the other zones; therefore WMZ possessed a lesser value of AMFD. While HAZ possessed coarser grains, therefore, it possessed more value of AMFD.

(a.2) Effect of magnetizing frequency on average maximum flux density during the magnetization process

The effect of change in frequency in both frequencies ranges on AMFD of BMZ, HAZ and WMZ at a constant MFI of 800 Oe are shown in Figure 4.24 (a) and (b).

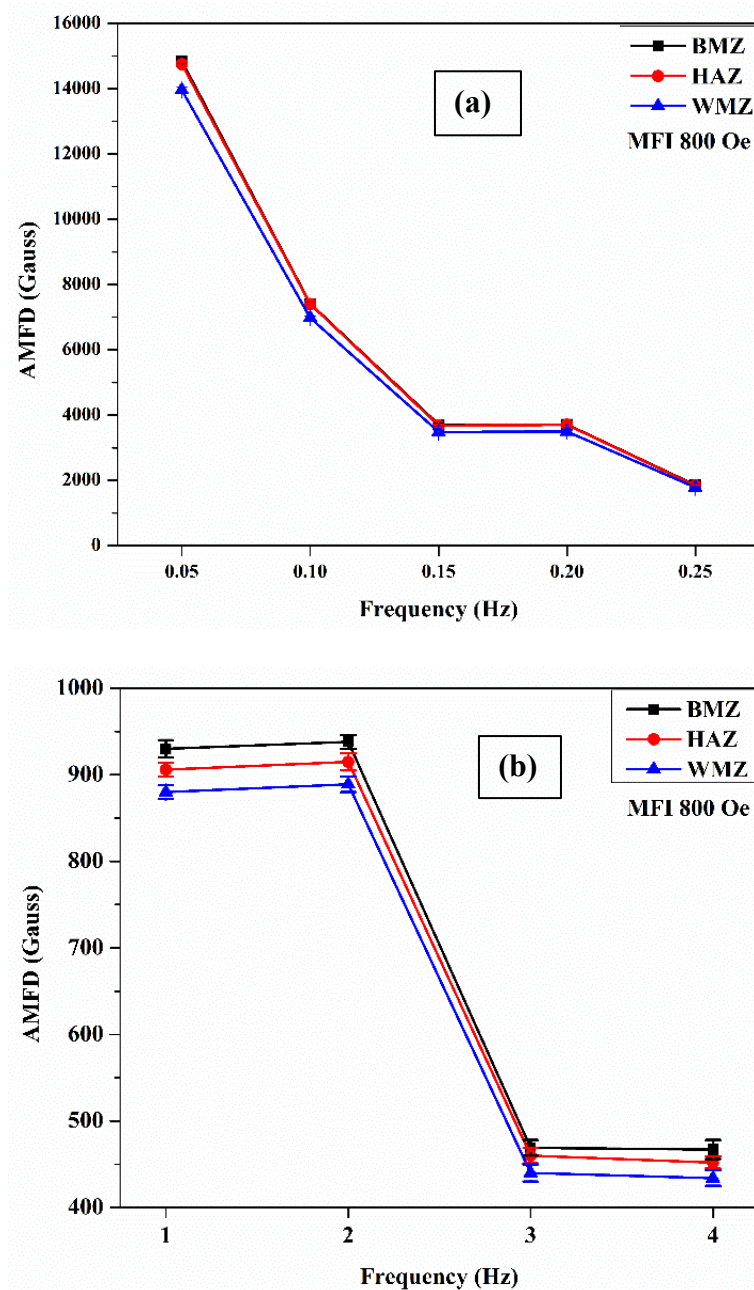


Figure 4.24 Variation of AMFD in (a) low frequency range, and (b) high frequency range.

It was observed that in both frequency ranges, AMFD is decreased with the increase in frequency except at 0.20 Hz and 2.0 Hz. The variation of AMFD with the increase in the magnetising frequency can be described by first understanding the role of eddy current and pinning sites in this hysteresis loop parameter variation.

On applying the external field, the system tends to attain the new energy position by the motion of domain walls. In this process, the domain walls move as well as jump depending upon the restriction in their path. During the jump or motion of domain walls, the change in magnetisation takes place. Localized eddy current is produced around the jumping and moving domain walls due to the changes in the magnetization. According to Lenz's law, these localized eddy currents tend to reduce the cause by which it is produced, i.e. magnetization changes. More the jumping or motion of domain walls create more eddy current, which tends to reduce the magnetisation.

Also, when a varying magnetic field is applied to a conductor, eddy currents are produced within the conductor in the form of loops according to Faraday's law of induction. The magnitude of the eddy current in a given loop is directly proportional to the strength of the MFI, magnetizing frequency, area of the loop, and rate of change of flux and inversely proportional to the material's resistivity. According to Lenz's law, this eddy current generates a magnetic field that opposes the applied magnetic field, which is produced by the alternating current. This opposition is strongest at the centre of the conductor, that is why, the magnitude of the alternating current (and hence applied magnetic field) is reduced to the lowest value at the centre of the conductor, while at the surface of the conductor, the current density is most significant, and hence, magnitude of the magnetic field is most significant at the surface of the conductor. This decline in the value of current density and hence magnetic field from the surface to the centre of the conductor is known as the 'skin effect'. The depth below the surface of the conductor up

to which the current density is decreased to $(1/e)$, i.e. 37 percent of the surface current density, is known as skin depth which is related to some parameters as shown in equation (4.6).

$$\delta = \frac{1}{\sqrt{\pi f \sigma \mu}} \quad (4.6)$$

Where, - δ represents skin depth (m)

- σ represents the conductivity of the conductor (S/m)

- f represents the frequency of the current (Hz)

- μ represents the permeability of the conductor (H/m)

From the above equation, it can be clearly seen that the skin depth is inversely proportional to the magnetising frequency. On increasing the magnetising frequency, the skin depth will be reduced. On reducing the skin depth, the magnetisation is concentrated in a smaller zone; therefore, the amount of magnetic domains taking participation in the magnetisation process is reduced, which tends to reduce the magnetisation. But since the magnetisation is concentrated in a smaller zone; therefore, the moving or jumping domain walls will face lesser pinning sites that tend to increase the magnetisation.

Thus the trend of variation of AMFD with the magnetising frequency depends upon the amount of domain walls and pinning sites in the effective area of magnetisation as well as eddy currents generated around the moving and jumping domain walls.

As described above, on increasing the magnetising frequency, the variation of AMFD is decided by two factors. First is that on increasing the magnetising frequency, more eddy current is produced, reducing the skin depth and motion of jumping and moving domain walls that tend to reduce the magnetisation. The second is that, on reducing the skin depth with the increasing magnetising frequency, jumping and moving domain walls will be restricted by the lesser amount of pinning sites which tend to increase the magnetisation. The dominating factor decides the trend of variation of

AMFD with the magnetising frequency. Figure 4.24 (a) and (b) show that the AMFD of all zones is decreased with the increase in frequency except at 0.20 Hz and 2.0 Hz. It is due to the dominance of the first factor over the other at all values of magnetising frequencies except at 0.20 Hz and 2.0 Hz.

It was observed from Figure 4.24 (a), and (b) that in both frequency ranges, the highest values of AMFD is possessed by the BM followed by HAZ and WM. It was also observed that the difference between the AMFD of HAZ and BMZ is not much; however, the difference between the amount of pinning sites in the form of grain boundaries in the HAZ and BMZ is considerably significant. Since the HAZ consists of coarser grains, domain walls move and jump more easily than the other zones, leading to more significant change in the magnetisation. But the motion and jumping of domain walls also depend upon the types of pinning sites, such as the martensite phase, which the HAZ possesses, acts as a stronger inhibitor than the other phases, which results in the greater reduction to the motion and jumping of domain walls and hence tending to decrease the magnetisation. Thus the dominating factor between these two opposite behaviours decides the value of AMFD. In the HAZ, the reduction in the magnetisation due to the pinning sites is dominant over the increase in the magnetisation due to the coarser grain size of the HAZ, and the reduction in the magnetisation due to the pinning sites occurred at such a level that the difference between the value of AMFD of HAZ and BMZ becomes negligible. In the WMZ, the amount of pinning sites in the form of grain boundaries is more which results in more reduction of motion and jumping of domain walls; thus, this zone possessed the lowest value of AMFD in both frequency ranges.

(b) Coreloss

The amount of energy transformed into heat during one magnetization cycle is known as coreloss, which is equal to the hysteresis loop area. This energy loss is

primarily due to the generation of eddy currents. The total energy loss (coreloss) due to the generation of eddy currents can be decomposed into the sum of three energy losses, known as hysteresis loss, classical loss and excess loss. But along with this, energy loss is also occurred due to the restriction in the motion of magnetic domain walls by pinning sites.

The magnetization curve of the hysteresis loop is looking smooth, but it is not so. On magnifying the tiny portion, as shown in Figure 4.25, it is stepwise rather than smooth.

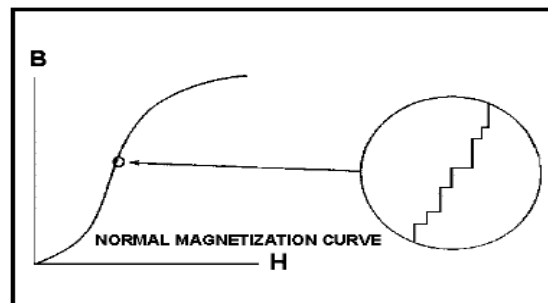


Figure 4.25 Magnetisation curve at the magnified view.

This step-wise change in the magnetisation occurs due to the jumping of domain walls, which leads to the changes in the magnetization, and thus, eddy current is produced as described earlier. This eddy current tends to oppose the jumping of the domain walls. This opposition to the change in magnetisation by the eddy current result in the loss of energy in the form of heat, known as hysteresis loss.

As described earlier, on applying the magnetic field to a conductor, the eddy current is produced within the conductor, and this eddy current opposes the applied magnetic field. In this process of opposition, some energy has been lost in the form of heat, which is known as classical loss.

The losses associated with the eddy current produced due to the motion of domain walls are known as excess loss.

Pinning sites tend to restrict the motion of domain walls. To cross these pinning sites, more energy is required, and that energy is lost in the form of heat.

The coreloss, or, in other words, area of the hysteresis loop, is influenced by many parameters such as magnetising frequency, MFI and pinning sites in the form of grain boundaries, precipitates.

(b.1) Effect of magnetic field intensity on coreloss

The variation of coreloss in different zones of the welded plate at the constant magnetising frequency with the MFI is shown in Figure 4.26.

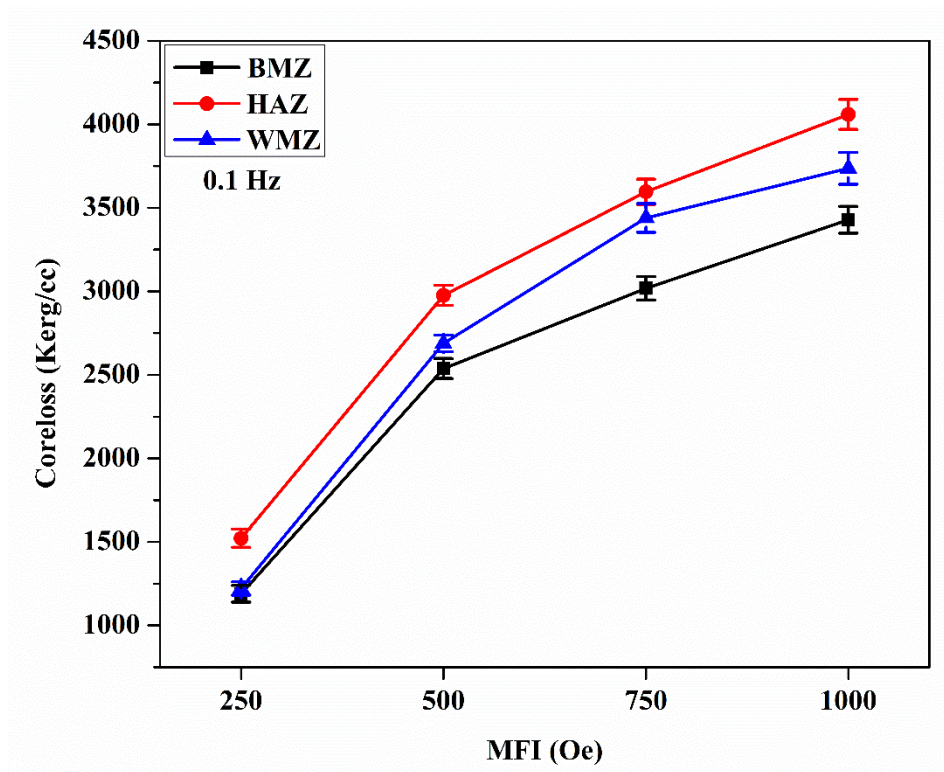


Figure 4.26 Variation of coreloss.

It was observed from Figure 4.26 that on increasing the MFI, the coreloss of each zone increases. As described previously that on applying the MFI, the jumping of domain walls, as well as motion of domain walls, takes place, which is the origin of hysteresis loss and excess loss. Since the MFI acts like a force; therefore, the jumping and motion

of domain walls are increased on increasing the MFI. Hence, hysteresis loss and excess loss is increased on increasing the MFI. Also, when the MFI is increased, more eddy current is produced within the conductor; therefore, classical loss is increased. Due to the enhancement of all three losses with the MFI, the coreloss of each zone was observed increasing with the MFI.

The motion of domain walls is restricted by various pinning sites such as grain boundary and precipitates. The energy is required to cross these pinning sites. The more the amount of pinning sites, the more energy is required, which results in more loss of energy. Along with this, the coreloss also depends upon the motion of domain walls which is reflected as the maximum flux density. The motion of domain walls is directly related to excess loss.

Since the HAZ possessed coarser grain size, this zone possessed lesser pinning sites in the form of grain boundaries, resulting in a lesser restriction to the motion of domain walls. Therefore the lesser energy is required to cross these pinning sites; hence, the energy loss is lesser due to the presence of lesser pinning sites, and thus, the contribution in the core loss due to the pinning sites is lesser. But the motion of domain walls in the coarser grains becomes easier, resulting in more generation of eddy currents around the moving domain walls. More eddy currents will result in more excess loss. Also, the jumping of domain walls is much easier due to the lesser pinning sites, resulting in a more eddy current generation around the jumping domain walls that will increase the hysteresis loss. Since all energy losses are more in the HAZ, this zone possessed more value of coreloss than the other zones.

On the other hand, WMZ possessed finer grains, or, in other words, this zone possessed more pinning sites. To cross these pinning sites by domain walls, more energy is required, which is lost in the form of heat. The jumping, as well as motion of domain

walls, is much restricted; therefore, the hysteresis loss, and excess loss is much lower than the other zones. The loss associated with the pinning sites is much more, whereas the hysteresis loss and excess loss is much lower. The summation of all these losses is such that the WMZ possessed lesser core loss than the HAZ but more than the BMZ.

(b.2) Effect of magnetizing frequency on core loss

As already explained that when the magnetic field is increased, domain walls tend to align themselves in the direction of an applied magnetic field and magnetic flux density increases non-linearly with the magnetic field. However, in this process, the motion of the domain walls is restricted by various pinning sites, and to pass these pinning sites, some amount of energy has been spent, which is irreversible. Restriction to the motion of domain walls happen during magnetization as well as demagnetization process. Due to this energy loss, the path followed by the value of magnetization on removing the magnetic field is not the same as the path followed during the application of magnetic field, which results in the generation of hysteresis loop during the one complete cycle of magnetization and demagnetization. This energy loss in the generation of the hysteresis loop is known as hysteresis loss, whose amount is equal to the area of the hysteresis loop.

The flow of eddy current in circular loops is associated with some energy loss, known as eddy current loss, increasing eddy current. The eddy current loss also increases with fewer magnetic domain walls, by which the domain walls move faster [210]. The summation of hysteresis loss and eddy current loss is known as coreless.

The variation in the core loss versus magnetising frequency has been plotted at low frequency range and high frequency range in the Figure 4.27 (a), and Figure 4.27 (b) respectively.

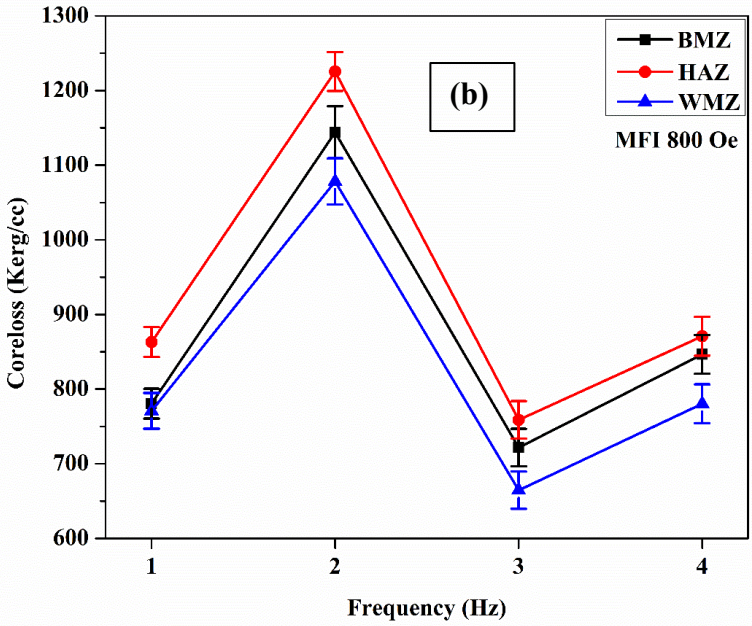
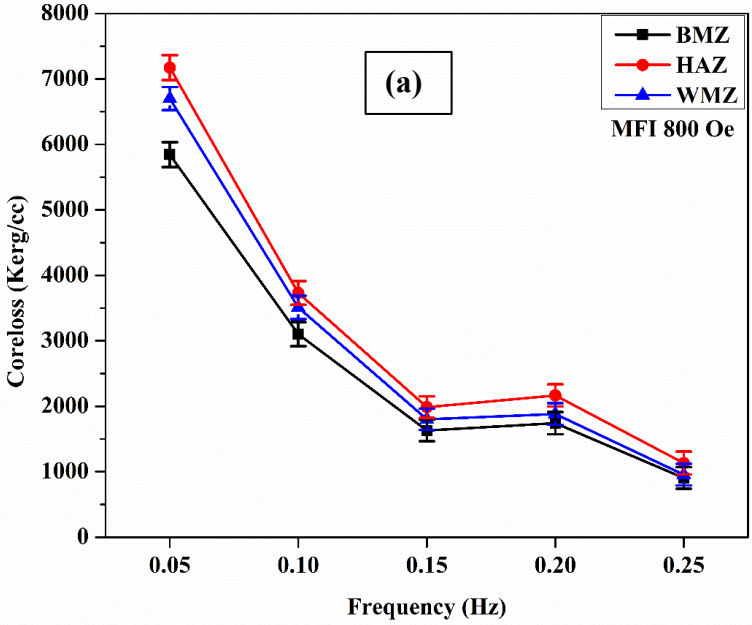


Figure 4.27 Variation of core loss in (a) low-frequency range, and (b) high-frequency range.

As it is well known that on increasing the magnetising frequency, the eddy current in the conductor is increased, which results in the reduction of the skin depth due to the classical loss. Higher the magnetising frequency, higher will be eddy current and hence higher will be classical loss. But due to the reduced skin depth on increasing the magnetising frequency, the amount of domain walls (jumping as well as moving) passed through that zone is reduced. Since the hysteresis loss and excess loss is related to the jumping and moving domain walls, respectively, therefore on reducing the amount of domain walls, the hysteresis loss and excess loss is reduced. Thus the competition between the classical loss, which is increased with the magnetising frequency, and sum of hysteresis loss and excess loss, which is decreased with the magnetising frequency, decides the trend of variation of coreloss with the magnetising frequency. As shown in Figure 4.27 (a) that the core loss is decreased with the magnetising frequency except at 0.20 Hz in the lower frequency range. It was due to the dominance of the sum of hysteresis loss and excess loss over the classical loss except at 0.20 Hz.

From Figure 4.27 (b), it was observed that in the higher frequency range, there is no trend of variation of coreloss with the magnetising frequency. As already described that the coreloss at any value of magnetising frequency is decided by the competition between the classical loss and sum of hysteresis loss and excess loss. Therefore the trend of variation of coreloss is highly fluctuating with the magnetising frequency.

The coreloss is also affected by the pinning sites in the form of grain boundaries, precipitates, and phases. Different zones of the welded plate possessed different grain sizes and phases. The variation of coreloss of all zones with the magnetising frequency is shown in Figure 4.27 (a) and (b). In both frequency ranges, the HAZ possessed a higher value of coreloss while BMZ and WMZ possessed lower coreloss in the low frequency range and high frequency range, respectively. Since the HAZ possessed coarser grains in

which the motion and jumping of domain walls are easy, that increases the excess loss and hysteresis loss, respectively than the other zones. Due to coarser grains, the energy loss to cross these pinning sites by the domain walls is lesser, contributing a very small part to the coreloss. Thus the summation of excess loss and hysteresis loss contribute a larger part of the coreloss while the pinning sites contribute a very smaller part. The value of coreloss of any zone is the result of competition between the summation of eddy current losses (hysteresis loss, excess loss and classic loss) and the energy loss due to the pinning sites. Since the HAZ possessed more eddy current losses than the energy loss due to the pinning sites due to its coarser grain size. On the contrary, the WMZ possessed finer grains in which the motion and jumping of domain walls are reduced; therefore, the excess loss and hysteresis loss is reduced, but more energy is lost to cross these pinning sites in the form of grain boundaries. As it is known that on increasing the magnetising frequency, the skin depth is decreased, which reduces the amount of jumping and moving domain walls and hence the excess loss and hysteresis loss is much reduced in the high frequency range, as shown in Figure 4.27 (b) such that it possessed lower value of coreloss in the high frequency range. The excess loss and hysteresis loss is not much reduced in the low frequency range, as shown in Figure 4.27 (a); therefore the WMZ possessed coreloss in between the HAZ and BMZ.

(c) Average permeability

Permeability is a measure of magnetisation of a conductor on applying the external magnetic field, which is equal to the maximum ratio of B and H. Easier magnetisation will lead to more permeability.

(c.1) Effect of magnetic field intensity on average permeability

Figure 4.28 shows the trend of variation of average permeability of each zone with the MFI at a constant magnetizing frequency.

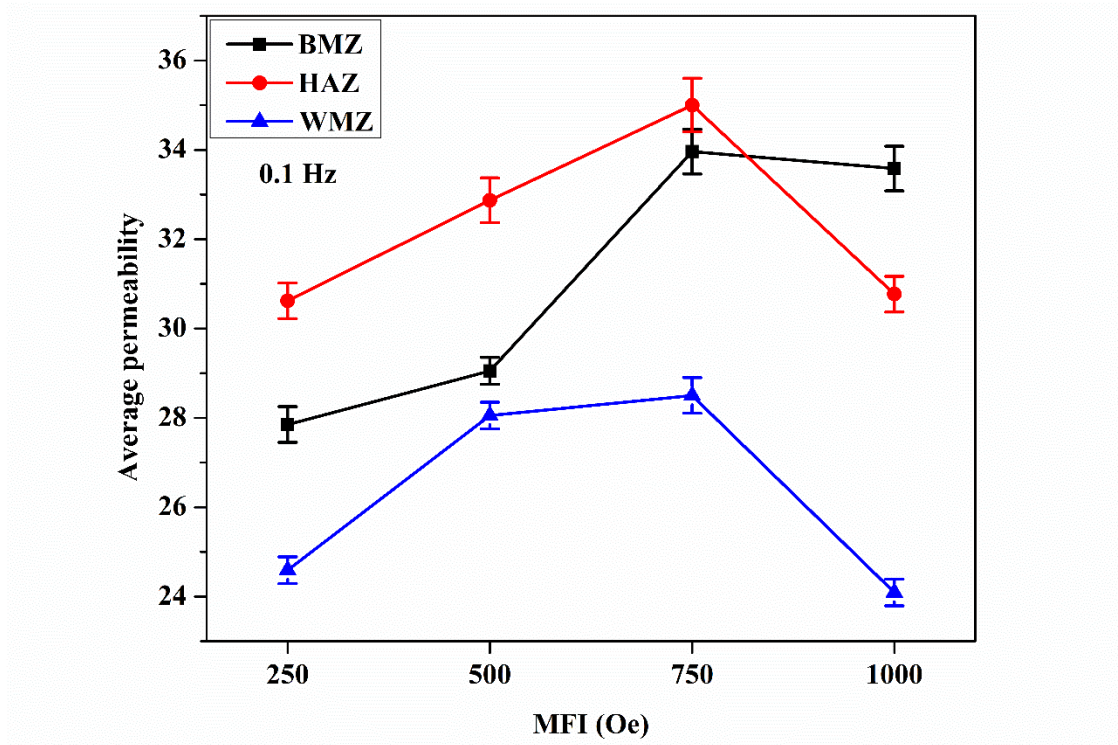


Figure 4.28 Variation of average permeability.

It was observed that when the MFI is increased from 250 Oe to 750 Oe, the permeability of each zone increases. But on further increasing the MFI, the permeability tends to decrease. As described earlier that the permeability refers to the ease of magnetisation on applying the external magnetic field. Since the MFI acts as a force; therefore, it activates more domain walls, that are pinned at various locations to take part in the magnetisation process resulting in more magnetisation on increasing the MFI. The movement or jumping of the domain walls is also increased on increasing the MFI, resulting in more magnetisation. But at the same time, on increasing the MFI, eddy current produced due to the motion and jumping of domain walls as well as due to the

magnetisation of the magnetic material is also increased as described earlier. According to Lenz's law, these eddy currents tend to reduce the causes by which it is produced, resulting in the reduction of magnetisation on increasing the applied magnetic field. As the eddy current effect is increasing with the MFI, therefore the change in the magnetisation is reduced for the exact change in the value of MFI at lower values (from 250 Oe to 750 Oe), but still, the maximum ratio of magnetic flux density to the applied magnetic field (i.e. permeability) is increased with the MFI. As the MFI is increased beyond 750 Oe, the eddy current effect is more dominating, reducing the magnetic flux density to such a level that the maximum ratio of magnetic flux density to the applied magnetic field (i.e. permeability) is decreased.

It was observed from Figure 4.28 that within the range of 250 Oe to 750 Oe, HAZ possessed the highest permeability, followed by the BM and WMZ. But after this range, the permeability of the HAZ becomes lower than the BM while the permeability of the WMZ is still at its minimum value. As described earlier that the HAZ is easily magnetized than the other zones due to the coarser grain size of this zone. Therefore the permeability of this zone is higher than the other zones within the range of 250 Oe to 750 Oe. But it is also known that the more eddy current is produced in the coarser grains due to the motion and jumping of the domain walls with lesser restrictions in their path of movement. These eddy currents tend to reduce magnetisation. These eddy currents are also increased with the MFI; therefore, as the MFI is increased from 750 Oe to 1000 Oe, the eddy current effect is more dominating due to the combination of coarser grain and high value of MFI, which causes the reduction of permeability of the HAZ than the BMZ. The permeability of the WMZ is lower than the other zones at all values of MFI due to the finer grain size because magnetisation of zones having finer grains is difficult.

(c.2) Effect of magnetizing frequency on average permeability

The variation of average permeability at a constant MFI of 800 Oe within low and high magnetizing frequency range is shown in Figure 4.29 (a) and (b), respectively.

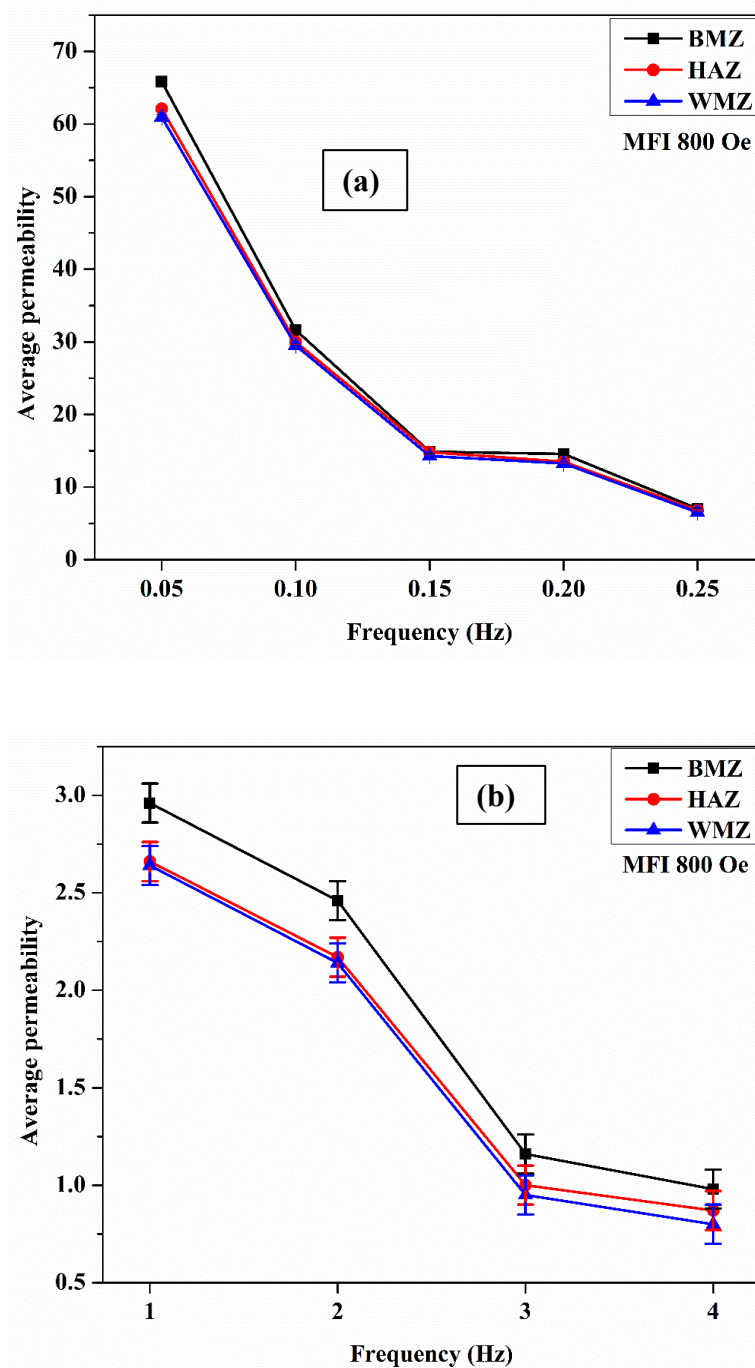


Figure 4.29 Variation of average permeability in (a) low-frequency range, and (b) high-frequency range.

It was observed from both figures that permeability is reducing with the increase in magnetizing frequency. As it is well known that on increasing the magnetising frequency, the eddy current is decreased, which tends to reduce the magnetisation. Since the permeability is the ratio of magnetic flux density to the applied magnetic field; therefore, at a constant magnetic field of 800 Oe, the permeability is decreased on reducing the magnetisation (magnetic flux density).

It was also observed that the value of permeability is much lesser in the high frequency range than in the low frequency range. It was due to the fact that on increasing the magnetising frequency, the eddy current is increased which tends to reduce the magnetisation and hence permeability. More the magnetising frequency, more will be eddy current and hence lesser will be permeability.

In both the frequency ranges, the BM possessed a higher permeability value while the WMZ possessed lower permeability. The magnetisation is also affected by the pinning sites as well as the eddy current. The HAZ possessed coarser grains in which the motion and jumping of domain walls become easier that tends to increase the magnetisation and hence permeability, but simultaneously the eddy current is also increased due to the easier movement and jumping of domain walls that tend to reduce the magnetisation and hence permeability. The competition between these two factors decides the value of permeability of each zone at all values of magnetising frequency. Thus the permeability of the HAZ lies in between the BMZ and WMZ. Similarly, the WMZ possessed finer grains than the other zones that tend to reduce the magnetisation due to the pinning effects, but the eddy current produced due to the motion and jumping of domain walls is also reduced that tend to increase the magnetisation. In this competition, the magnetisation reduction due to the pinning sites is more dominant. Therefore the permeability of the WMZ is lesser than the other zones.

(d) Remanence

When the MFI is reduced from its maximum value to zero, the corresponding magnetic flux density is not reduced to zero, instead of that, some magnetisation remains within the material. This retained magnetisation is known as remanence.

(d.1) Effect of magnetic field intensity on remanence

The trend of variation of remanence of each zone with MFI at the constant magnetizing frequency is shown in Figure 4.30.

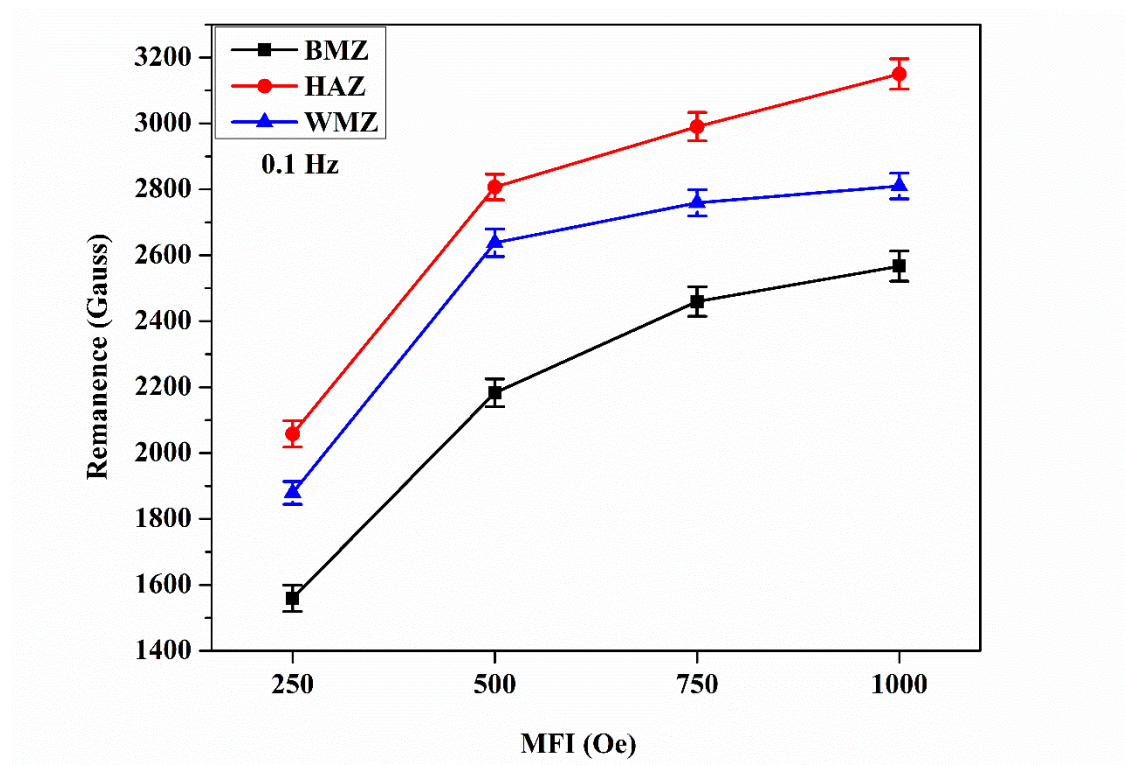


Figure 4.30 Variation of remanence.

It was observed from above figure that all the zones show the incremental behaviour of remanence with the MFI at all values.

Since the magnetic field act as a force to align the magnetic domains in the direction of the applied magnetic field by the movement of domain walls and also the magnetic domains whose direction of magnetic moment is already in the direction of the

applied magnetic field tends to grow at the expense of other magnetic domains. Therefore, as the applied magnetic field is increased (as it is well known that in one hysteresis loop, the magnitude of the applied magnetic field is gradually increased from zero to the maximum value and then again reduced to zero and then again increases the magnitude of the applied magnetic field in the negative direction, and finally the magnetic field is reduced to zero), the number of magnetic domains is reduced, and at the maximum value of the magnetic field, the number of remaining magnetic domains is minimum. But as the applied magnetic field is reduced from its maximum value, the force required to maintain the alignment of the magnetic domains is reduced; hence, the system tends to regain its initial number of magnetic domains. Therefore, the nucleation of magnetic domains (domain walls) at different pinning sites such as grain boundaries, martensite phase, precipitates, and pre-existing domains occurs. Since the change in magnetisation is occurred through the motion of domain walls and rotation of magnetisation in the direction of the applied magnetic field. Therefore, on decreasing the magnetic field, the existing and nucleated domain walls start to move in such a way that the magnetisation is reduced with the magnetic field. Also, the rotation of magnetisation took place, which results in the reduction of magnetisation. Due to various losses generated from the eddy current effect and pinning effect as described earlier, the magnetisation is not completely reduced to zero after removing the applied magnetic field. The eddy current and pinning sites create hurdles to the movement of domain walls and rotation of magnetisation on decreasing the applied field, therefore the magnetisation is not completely reduced to zero after removing the applied magnetic field, and some magnetisation is retained. This remaining magnetisation is known as remanence. The value of remanence is decided by the maximum flux density as well as eddy current and pinning sites at constant process parameters; all these factors tend to increase the

remanence. Maximum flux density, as well as eddy current, depends upon the presence of pinning sites and process parameters such as MFI and magnetising frequency.

As the MFI is increased from 250 Oe to 1000 Oe, the magnetic flux density of all zones is increased, as shown in Figure 4.23, due to the alignment of more magnetic domains in the direction of the applied magnetic field. As it is described earlier that remanence depends upon the magnetic flux density and pinning sites. As the MFI is increased in any zone, the magnetic flux density will be increased, which tends to increase the remanence. Each zone possessed a different amount of pinning sites which hinders the movement of domain walls that will affect the remanence. A higher amount of pinning sites result in more remanence. Since the WMZ possessed finer grains than the other zones, therefore the remanence becomes increased than the BMZ; however, the WMZ possessed lower value of AMFD. It was occurred due to the dominance of pinning sites in the form of grain boundaries over the value of AMFD in determining the remanence. However, HAZ possessed higher value of remanence than the other zones due to its coarser grain size than the other zones. In the HAZ, the pinning sites are lesser; therefore the role of pinning sites in this zone to determine the remanence become lesser than the role played by the value of AMFD. Since the HAZ possessed higher value of AMFD, therefore it possessed higher value of remanence than the other zones.

The remanence of each zone was found to increase with the MFI. As it is already described that remanence depends upon the value of AMFD. Since the AMFD increases with the MFI, as observed from Figure 4.23, that is why, remanence is increased with the MFI.

(d.2) Effect of magnetizing frequency on remanence

The effect of magnetising frequency in low and high magnetizing frequency range on the remanence of different zones of weldment (BMZ, HAZ and WMZ) at constant MFI of 800 Oe is shown in Figure 4.31 (a) and (b), respectively.

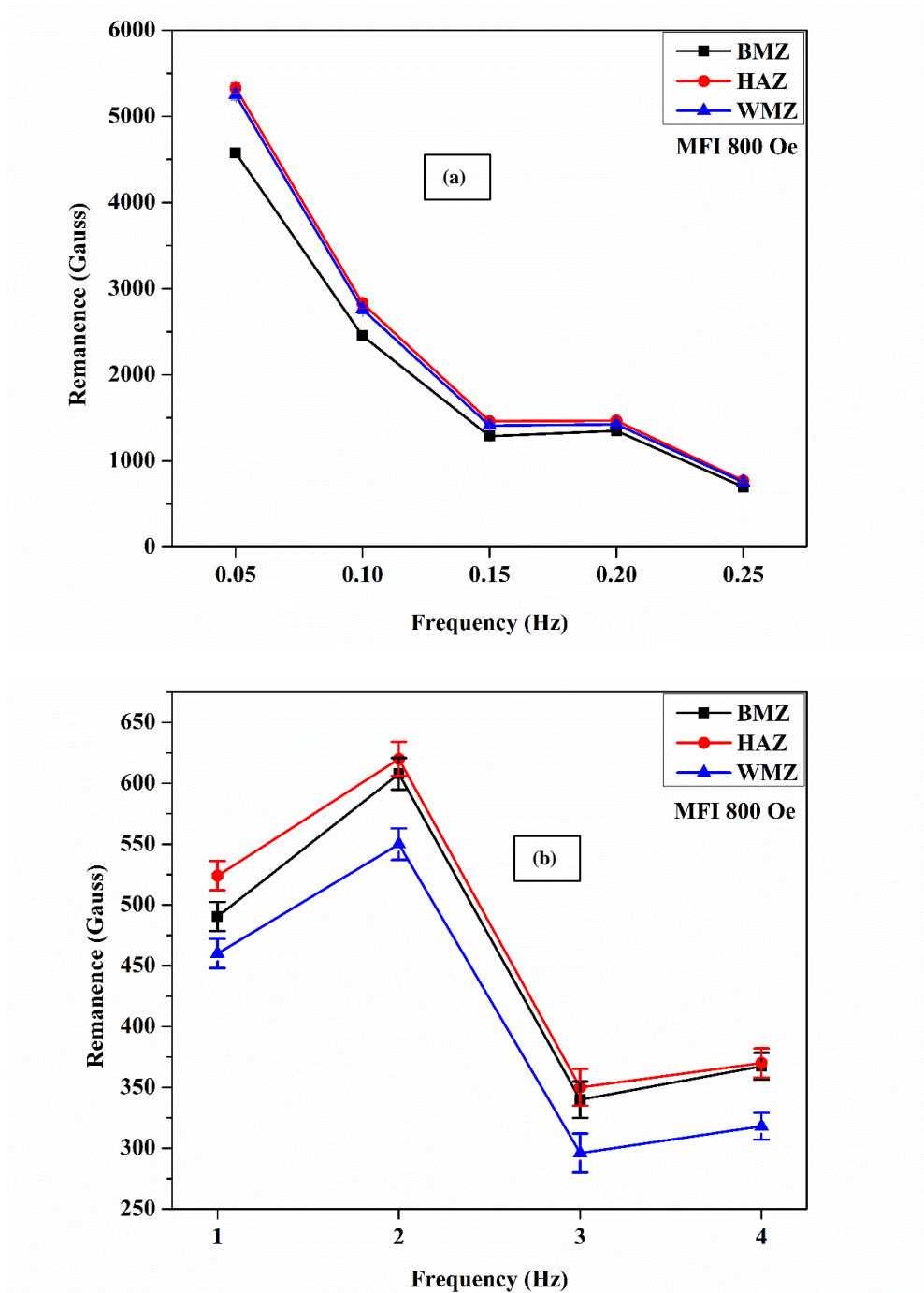


Figure 4.31 Variation of remanence in (a) low-frequency range, and (b) high-frequency range.

It was observed from Figure 4.31 (a) that the remanence of each zone is decreasing on increasing the magnetising frequency except at 0.20 Hz. It is described earlier that the remanence strongly depends upon the AMFD, therefore, the variation of remanence with the magnetising frequency should be in the same manner as the variation of AMFD with the magnetising frequency. Since the AMFD is reduced on increasing the magnetising frequency except at 0.20 Hz, that is why, the remanence is also reduced on increasing the magnetising frequency except at 0.20 Hz in the low frequency range.

But the variation of remanence with the magnetising frequency in the high frequency range is frequently changing, as observed from Figure 4.31 (b). Since remanence's value is also dependent upon the eddy current and pinning sites along with the AMFD at constant process parameters. All these factors tend to increase the remanence. The increase in the remanence has occurred at 2.0 Hz and 4.0 Hz. The value of AMFD of all zones at 2.0 Hz and 4.0 Hz can be found in Figure 4.24 (b). It was found that on increasing the magnetising frequency from 1.0 Hz to 2.0 Hz and from 3.0 Hz to 4.0 Hz, the change in the values of AMFD is almost negligible. Therefore at 2.0 Hz and 4.0 Hz, the role of AMFD to decide the trend of variation of remanence with the magnetising frequency is significantly reduced. In this case, the trend is decided by other factors. Since on increasing the magnetising frequency, the eddy current is increased, which restricts the motion of domain walls resulting in more magnetisation retained, and thus, remanence is increased at 2.0 Hz and 4.0 Hz. At all values of magnetising frequency, the remanence is decreased due to the dominance of AMFD over the eddy current effect.

The remanence value of each zone is different for the same process parameters due to the difference in the grain size and other pinning sites such as different phases and precipitates. Two main factors decide the trend of variation of remanence with the

magnetising frequency: the value of AMFD and the eddy current. The HAZ possessed higher value of remanence than the other zones in both frequency ranges as observed from Figure 4.31 (a) and (b), while the AMFD of this zone lies between the other two zones as observed from Figure 4.24 (a) and (b), which means that in this zone, the AMFD is not dominant to decide the trend of variation of remanence with the magnetising frequency, instead of that eddy current effect is more dominant due to the coarser grains in which the domain walls can easily jump or move. The remanence of BMZ in the low frequency range, as observed from Figure 4.31 (a), is lower than the other zones while it possessed higher value of AMFD in the low frequency range, which indicates the dominance of the eddy current effect over the other factors. In the high frequency range, the remanence of WMZ, as observed from Figure 4.31 (b), is lower than the other zones, and it also possessed lower value in the high frequency range, as observed in Figure 4.31 (b), which indicates the dominance of AMFD over the eddy current effect in the determination of the trend of variation of remanence with the magnetising frequency.

(e) Coercivity

To reduce the remanent magnetisation completely, the magnetic field is applied in the opposite direction, and this amount of applied magnetic field is known as coercivity.

(e.1) Effect of magnetic field intensity on coercivity

The variation of coercivity of each zone with the MFI at a constant magnetizing frequency is shown in Figure 4.32.

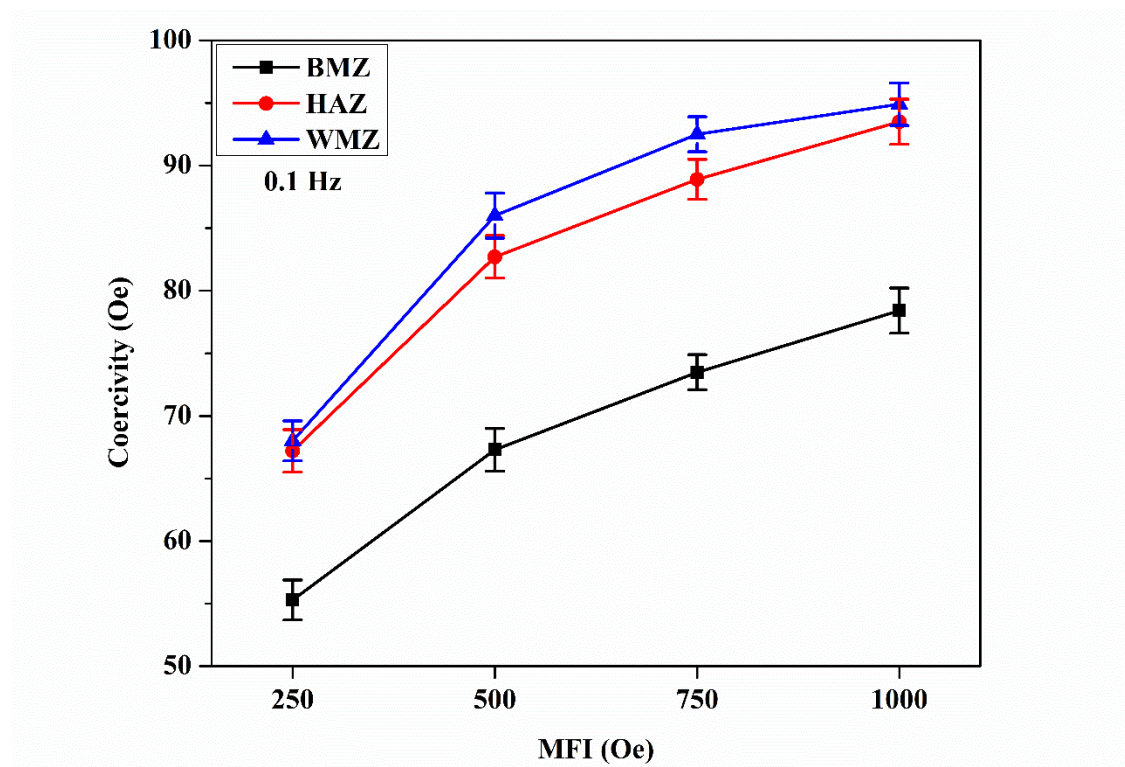


Figure 4.32 Variation of coercivity.

It was depicted from this figure that WMZ possessed higher value of coercivity, followed by the HAZ and BMZ. Since coercivity is the magnitude of the applied magnetic field to reduce the remanent magnetisation; therefore, coercivity depends upon the remanence. Higher the remanent magnetisation of any zone may cause higher value of coercivity, but along with this, the coercivity is also depended on the pinning sites, which resist the motion of domain walls; therefore, more magnetic field is required to

demagnetize the material completely, hence more pinning sites may also cause an increment in the coercivity. Therefore the coercivity of any zone depends upon the remanence as well as pinning sites. The WMZ possessed higher value of coercivity due to the presence of more pinning sites than the other zones in the form of grain boundaries; however, the remanence of the WMZ is lower than the HAZ. Therefore in the case of WMZ, the pinning sites play a major role to decide the coercivity. In the HAZ and BMZ, the pinning sites are in lesser quantity; therefore, the remanence decides the coercivity. Since the HAZ possessed higher value of remanence than the BMZ; therefore, the coercivity of the HAZ is more than the BMZ.

It was observed from Figure 4.32 that the coercivity of each zone is increasing with the MFI. Since the coercivity depends upon the remanence as described earlier, therefore the variation of remanence of each zone with the MFI will decide the variation of coercivity of each zone with the MFI. As observed from Figure 4.32, the remanence is increasing with the MFI, therefore coercivity of each zone was also found to increase with the MFI.

(e.2) Effect of magnetizing frequency on coercivity

The effect of variation of magnetising frequency in the low and high range on coercivity of different zones of the weldment is shown in Figure 4.33 (a) and (b), respectively, at a constant MFI of 800 Oe.

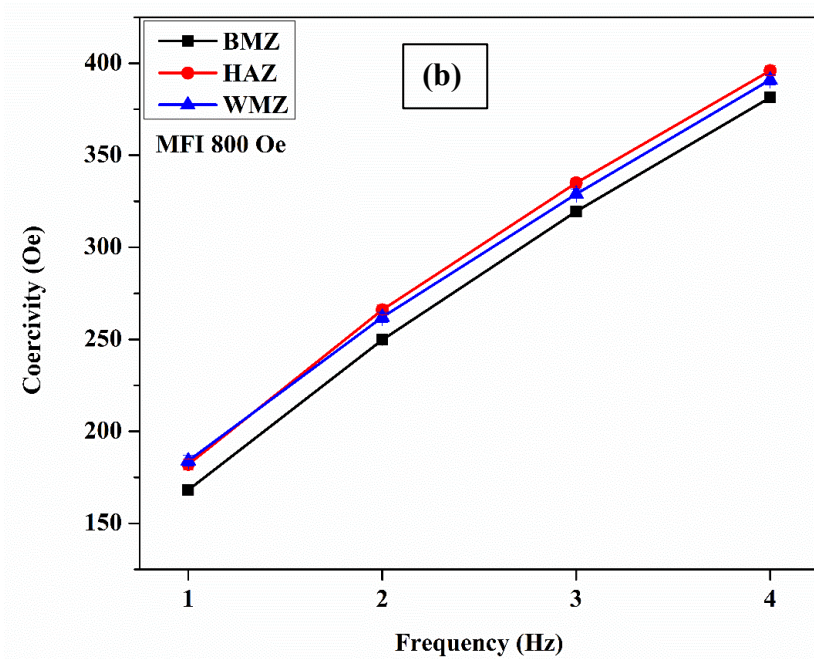
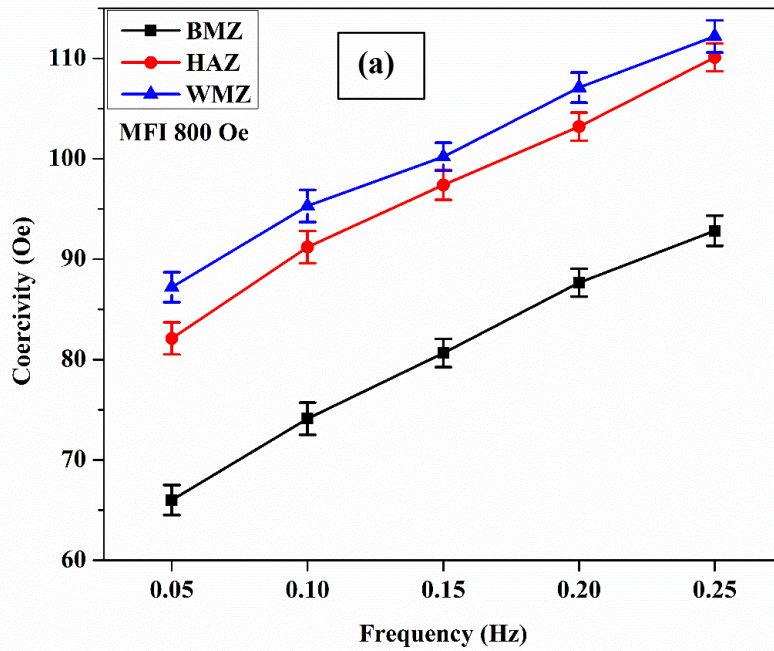


Figure 4.33 Variation of coercivity in (a) low-frequency range, and (b) high-frequency range.

It was observed from both figures that the coercivity of each zone is increasing with the magnetising frequency. It is well known that on increasing the magnetising frequency, the eddy current is increased, which tends to reduce the demagnetization process and hence, the more magnetic field is required to demagnetize the material completely; thus the coercivity is increased on increasing the magnetising frequency.

It was observed from Figure 4.33 (a) that the WMZ possessed higher value of coercivity than the other zones in the low frequency range. It can also be observed from Figure 4.33 (a) that the WMZ possessed remanence value in between the other two zones. It is well known that coercivity depends upon the remanence, eddy current as well as pinning sites. Since the WMZ have finer grains than the other zones and therefore more grain boundaries in the form of pinning sites which tends to restrict the demagnetization process and hence increase in the coercivity. The role of pinning sites is such that the coercivity of the WMZ becomes higher than the other zones. The role of remanence was observed in the other zones to decide the coercivity, which leads to lower value of coercivity.

At higher values of magnetising frequency, the difference in the coercivity of HAZ and WMZ is almost negligible. The WMZ possessed lower remanence value, but it possessed finer grains that increased its coercivity to high value. While the HAZ already possessed higher remanence, which plays a vital role to increase the coercivity. Due to the dominancy of the pinning site effect in the WMZ and remanence in the HAZ, the coercivity is increased at such a level that the difference in the coercivity of these two zones is almost negligible.

4.1.16.2 Magnetic Barkhausen noise testing

Magnetic Barkhausen noise (MBN) testing has been carried out at different zone of the sample S7 by varying the MFI from 250 Oe to 1250 Oe at a constant value of

magnetising frequency of 25 Hz and also by varying the magnetising frequency from 10 Hz to 40 Hz at a constant value of MFI of 800 Oe.

The MBN measurement of different zones of the welded plate has been done at different magnetizing frequency and MFI. The results are given in Table 4.5 and Table 4.6.

Table 4.5 MBN response of different zones with different MFI at the constant magnetizing frequency (25 Hz)

BMZ			HAZ		WMZ	
MFI (Oe)	RMS (mV)	Number of pulses	RMS (mV)	Number of pulses	RMS (mV)	Number of pulses
250	0.018	2	0.025	3	0.012	2
500	0.052	3	0.053	4	0.026	3
750	0.071	5	0.073	11	0.038	4
1000	0.082	27	0.092	65	0.047	5
1250	0.089	44	0.105	130	0.052	8

Table 4.6 MBN response of different zones with different magnetizing frequency at constant MFI (800 Oe)

BM			HAZ		WM	
Frequency	RMS (mV)	Number of pulses	RMS (mV)	Number of pulses	RMS (mV)	Number of pulses
10	0.051	7	0.070	11	0.031	5
20	0.068	10	0.081	15	0.036	6
30	0.080	15	0.089	27	0.042	9
40	0.088	17	0.095	48	0.048	10

Magnetic Barkhausen noise signal

The material (macroscopic magnetic system) consists of various types of structural disorders such as lattice deformations, fluctuation of compositions, inclusions, phase separation, grain boundaries, dislocations, precipitations, and so on. The magnetisation is coupled to these sources of structural disorders through exchange,

anisotropy and magnetostatic interactions. Due to the presence of these structural disorders, the system exhibits an extremely complicated structure of energy landscape with a huge number of local minima and saddle points that reflect the presence of structural disorder. In the stable condition, the domain structure remains in the local minima. The magnetisation is also coupled to the external magnetic field, which continuously alters the system energy balance as the applied magnetic field is varied with time. This variation in the applied field sooner or later destroys the stability of a given domain structure. The energy required to jump from one local minima to another local minima depends upon various factors such as waveform (sine or triangular), magnetising frequency, MFI and pinning action of the structural disorder. By keeping all other process parameters constant, the magnetisation depends upon the pinning action of the structural disorders. The lesser the pinning action of the structural disorders, the lesser will be energy required to cross the energy hills between two local minima, and the magnetisation becomes easier. But when the pinning action of the structural disorders is higher such as grain boundaries, more energy will be required that tends to reduce the magnetisation. On applying the varying magnetic field, the local energy minimum is transformed into a saddle point which causes the domain structure to unstable and spontaneously evolves toward some new configuration. This rearrangement may be quite localized in space, with a small domain wall segment jumping to a neighboring stable position, or may involve the whole domain structure in substantial parts of the body, as may occur, for instance, when new domains of reversed magnetisation are nucleated. This fundamental mechanism is known as the Barkhausen effect, after H. Barkhausen, who, in 1919, gave for the first time experimental evidence of these magnetic instabilities [211]. Due to this jumping of the domain structure from one local energy minimum to another, the voltage is induced in the secondary coil in the form of pulses in which the

values of induced voltages is changing abruptly, i.e. jumps in the values of induced voltages and this jump is known as Barkhausen jumps [212-214]. This jump indicates the presence of structural disorders within the material. These voltage pulses are known as Magnetic Barkhausen noise (MBN) signal characterized by the number of pulses and RMS value.

(a) Relation between number of pulses, magnetizing frequency, and magnetic field intensity

The MBN signal is characterized by the number of pulses, which is dependent upon various factors such as process parameters, the grain size of the material, hardness of the material and various other factors. To investigate the effect of any process parameter, all other factors should be constant.

(a.1) Effect of magnetizing frequency on the number of pulses

The trend of variation of the number of pulses corresponding to various zones with the variation of magnetizing frequency at constant value of MFI of 800 Oe is shown in Figure 4.34.

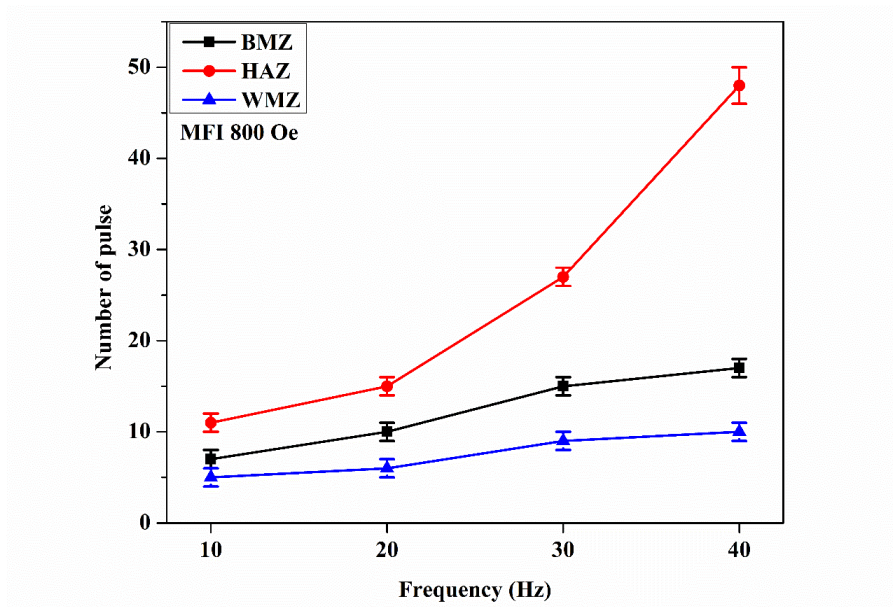


Figure 4.34 Variation of the number of pulses with magnetizing frequency.

It was observed from Figure 4.34 that the number of pulses in each zone is increased by increasing the magnetising frequency. It is well known that on increasing the magnetising frequency, the eddy current is increased and hence skin depth is decreased. Due to the less skin depth, the lesser area is available for movement of domain walls, and hence interaction of domain walls in each zone with the pinning sites having higher pinning action (grain boundaries) was decreased. Thus the domain walls move much easier at higher magnetising frequencies, which results in more response of MBN in terms of the number of pulses. Note that in the following discussion regarding the MBN effect, the pinning site will refer to only the structural disorder having higher pinning action (grain boundaries).

It was also observed from Figure 4.34 that HAZ possessed the highest MBN response in terms of the number of pulses followed by the BM and WM. Since the HAZ possessed coarser grain size in which domain walls move easily that tend to increase the MBN response, whereas, in contrast to this, WMZ possessed finer grains and thus more grain boundaries which act as pinning sites to the motion of domain walls, resulting in lesser MBN response in terms of the number of pulses. It can be seen that the MBN response depends upon the grain size. The coarser grains result in more MBN response, whereas finer grains tends to decrease the MBN response. Since the grain size of BMZ lies between the other two zones, therefore the MBN response in terms of the number of pulses also lies between the other two zones.

(a.2) Variation of the number of pulses with magnetic field intensity at the constant magnetizing frequency

The trend of variation of the number of pulses of each zone with the MFI at a constant magnetizing frequency of 25 Hz is shown in Figure 4.35.

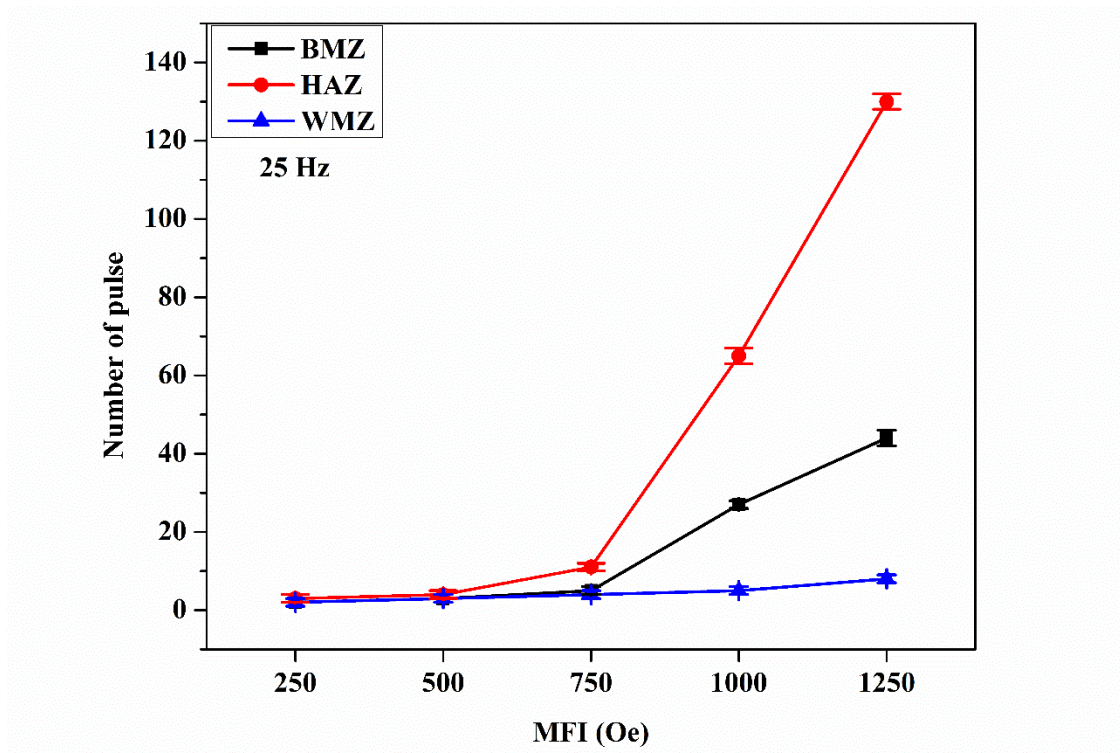


Figure 4.35 Variation of the number of pulses with MFI.

It was observed from Figure 4.35 that on increasing the MFI, the number of pulses of each zone is increased. Since the MFI acts as a force to move the domain walls and also activate more domain walls which are pinned at various locations of structural disorders, therefore MBN response in terms of the number of pulses of each zone is increased on increasing the MFI.

From Figure 4.35, it was also observed that at all values of MFI, the HAZ possessed higher MBN response in terms of the number of pulses, followed by BM and

WM. The reason for this response is the same as described earlier in the case of the effect of magnetising frequency on the MBN response in terms of the number of pulses.

(b) Relation between root mean square value, magnetizing frequency, and magnetic field intensity

As it is already described that the induced voltages are in the form of pulses, i.e. it consists of spikes having different amplitudes. The analysis of this form of voltages is difficult; therefore, to make it easy; a smooth profile curve is fitted onto the spikes, known as the MBN signal profile. Various parameters are used to characterize the profile like amplitude or peak, peak position on X-axis, FWHM (full width at half maximum), and RMS value. Among these parameters, RMS value is the well-established parameter to characterize the MBN response.

(b.1) Variation of root mean square value with magnetizing frequency at a constant magnetic field intensity

The variation of the RMS value of induced voltages during MBN with the magnetising frequency is shown in Figure 4.36.

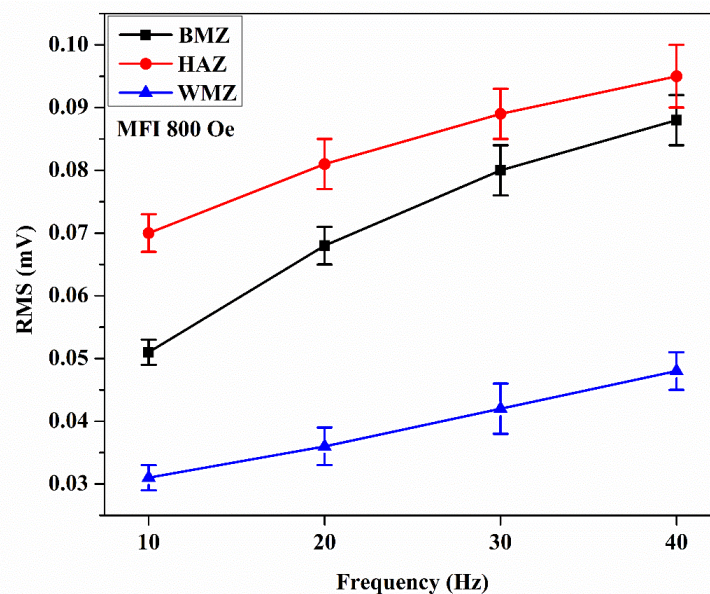


Figure 4.36 Variation of the RMS value with magnetizing frequency.

From Figure 4.36, it was observed that the MBN response in terms of RMS value is increasing with the magnetising frequency. As it is well known that on increasing magnetising frequency, the skin depth is decreased, which tends to reduce the number of active domain walls taking participation in the magnetisation process. In this situation, the number of active domain walls decreases, but along with that, the pinning sites in the form of grain boundaries also decrease. On the one hand, the magnetisation tends to decrease on reducing the number of active domain walls but on the other hand; magnetisation tends to increase on reducing the pinning sites in the path of domain walls due to the reduced skin depth. Change in MBN response leads to change in amplitude of the BN signal profile, which leads to change in RMS value of the BN signal. The competition between these two factors will decide the variation trend of RMS value with the magnetising frequency. The trend of variation of RMS value with the magnetising frequency, as shown in Figure 4.36, is the result of dominating factor of reduction of pinning sites in the path of domain walls over the reducing number of domain walls.

From Figure 4.36, it can also be observed that the HAZ possessed higher MBN response in terms of RMS value at all values of magnetising frequency followed by BM and WM. Since the grain size of HAZ is higher, therefore, the number of pinning sites in the form of grain boundaries to restrict the motion and jumping of domain walls at any fixed value of magnetising frequency is minimum than the other zones. Therefore the HAZ possessed higher MBN response in terms of RMS value than the other zones. Similarly, the WMZ possessed finer grains, or in other words, it possessed more pinning sites than the other zones. Therefore WMZ possessed lesser RMS value than the other zones.

(b.2) Variation of root mean square value with magnetic field intensity at the constant magnetizing frequency

The variation of the RMS value of induced voltages during MBN with the MFI at a constant magnetising frequency of 25 Hz is shown in Figure 4.37.

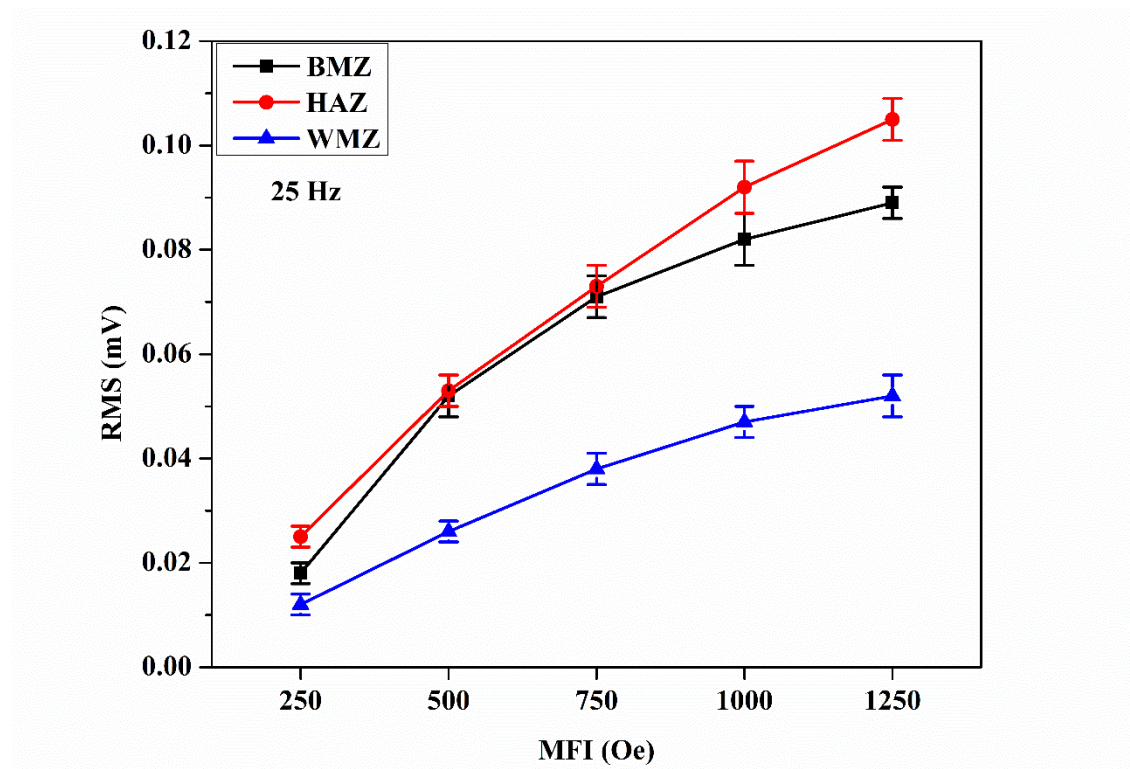


Figure 4.37 Variation of the RMS value with the MFI.

To move or jump of the magnetic domain walls between the local minima, energy is required, and this energy is provided to the domain walls by applying the external magnetic field. On increasing the MFI, more energy is imparted to domain walls by which the domain walls can easily cross the pinning sites resulting in the easy movement of domain walls and thus, MBN response in terms of RMS value is increased, as shown in Figure 4.37.

HAZ exhibited higher RMS value on increasing the MFI at the constant magnetizing frequency in comparison to other zones, while the WMZ possessed lower

RMS value, as depicted in Figure 4.37. Due to coarser grains of the HAZ, the restriction to the movement of domain walls is lesser that tends to increase the RMS value. In contrast to this, the WMZ possessed finer grains; that is why, it possessed lesser RMS value compared to other zones at all values of MFI.

Part – II

4.2 Friction stir processing of gas metal arc welded ferritic stainless steel

4.2.1 Introduction

Out of 18 samples, only one sample (S7) was selected due to its good combination of mechanical properties for carrying out FSP upon them. After finding the range of the FSP parameters, the experimentation was carried out at two different SDs (15 mm and 20 mm) and three different ratios of the RS to the PS (6, 9 and 12 revolution per mm). The different characterisation samples (metallographic study, XRD analysis, hardness testing, tensile testing, Charpy impact testing and residual stress testing) were extracted from the processed plates.

In this section, the results obtained after the characterisation of the processed plates are discussed. To check the quality of friction stir processed plates, first, the visual examination was performed and then X-ray radiography. The metallographic study and microhardness testing of different regions of the processed plates were carried out. The tensile testing and Charpy impact testing were also carried out. The variation in the results of these testing is also analysed with the variation in the SD and the ratio of RS to the PS. The results obtained from the MBN and MHL analysis of the PR of sample A at constant values of MFI of 800 Oe and magnetising frequency of 0.05 Hz have also been discussed. The results obtained from the MBN and MHL analysis of the PR of sample A at these parameters was compared with that of the BMZ, HAZ and WMZ of sample S7.

4.2.2 Visual examination of the processed plate

The friction stir processed plates were thoroughly examined visually, through unaided eyes and with a magnifying glass. A few such processed plates have been shown in Figure 4.38.

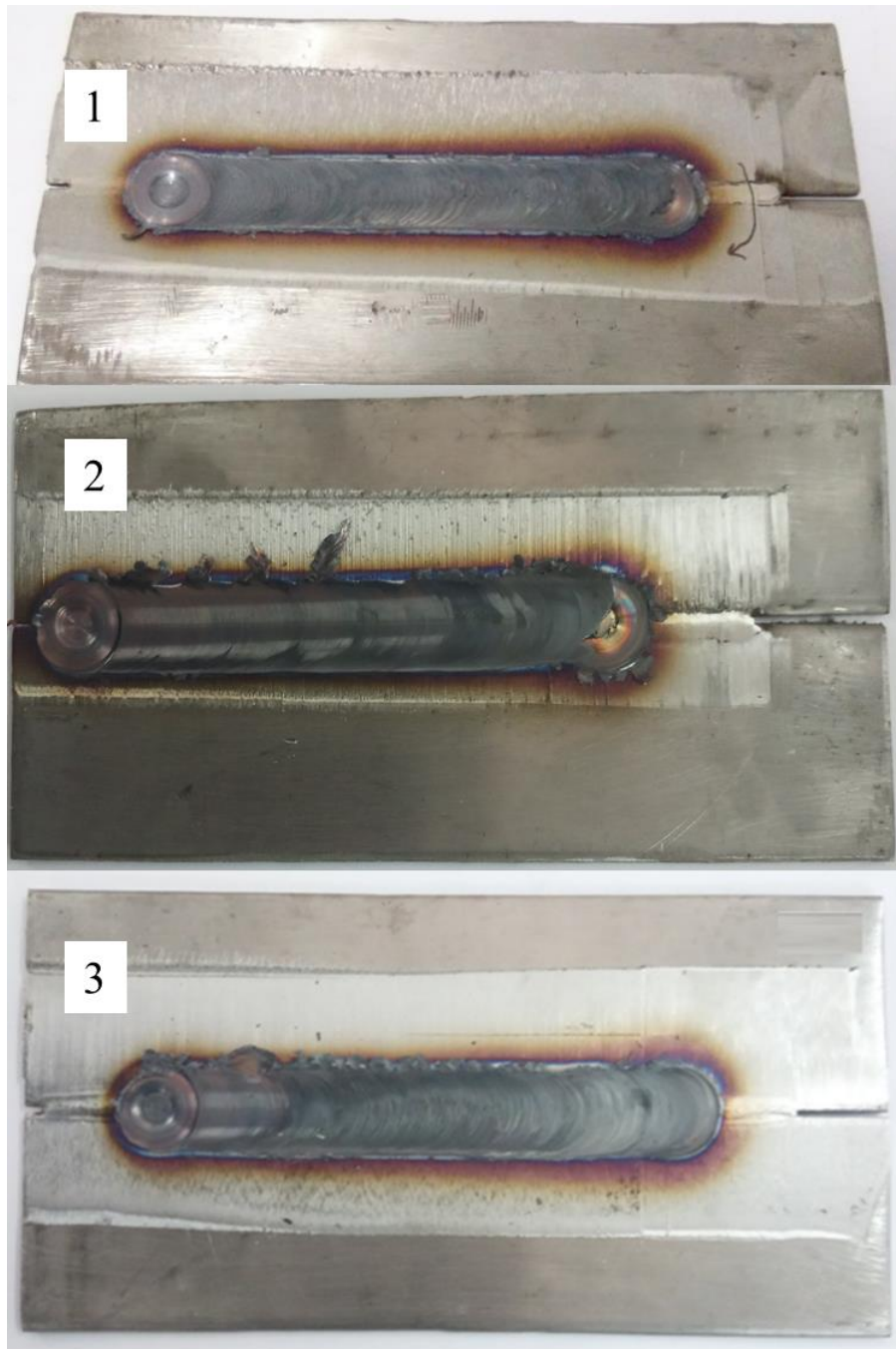


Figure 4.38 Photographs of some of the processed plates.

No visible defects were found in any of the plates, and also, the plates were found to be free of any significant distortion. The ripples have been found on the surface of the processed plate, that are produced due to the rotational as well as translational motion of the tool. Some flash has been found on the retreating side at a few process parameters; however, the flash, in any case, was not significant.

4.2.3 X-ray radiography of the processed plates

The most reliable non-destructive test that can reveal even sub-surface defect is X-ray radiography, and all the plates after processing were subjected to 100% X-ray radiography. The radiographs were compared with typical radiographs of defects, particularly defects like tungsten inclusion and discontinuity in the material. The X-ray radiograph revealed no surface or subsurface defects. The scanned copy of one such X-ray film has been shown in Figure 4.39.

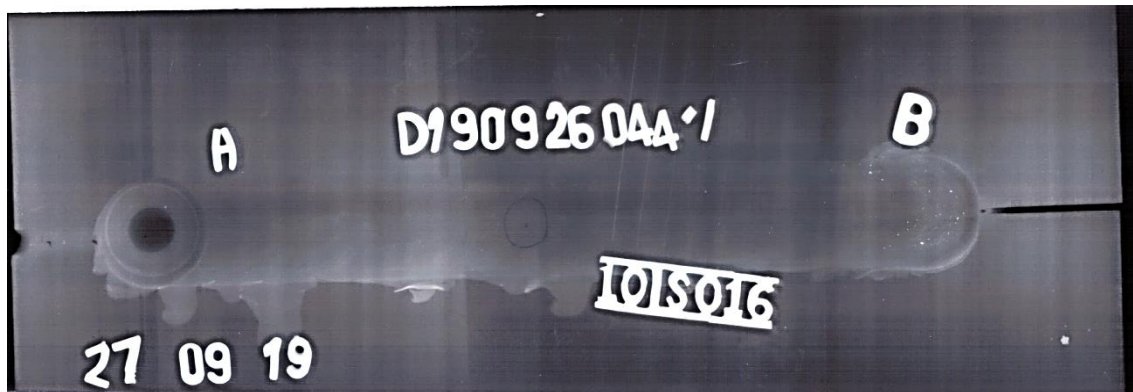


Figure 4.39 X-ray radiography of processed plate.

Also, the experts of the laboratory in which the processed plate was radiographed, passed the plates. The detailed result of the radiography has been shown in Table 4.7.

Table 4.7 Results of the radiographic testing.

Sample	Results	Acceptability
A	Some flash	Acceptable
B	Some flash	Acceptable
C	No defect	Acceptable
D	Some flash	Acceptable
E	Some flash	Acceptable
F	No defect	Acceptable

It was observed from the results given in the above table that all the processed plates possess acceptable quality.

4.2.4 Metallography

The micrographs obtained in different regions of the processed plates were closely examined and have been described in the following sections. Since the grains and the microstructural feature were readily visible under the optical microscope, most of the microscopy was restricted to optical microscopy. However, for the purpose of grain size measurement of different regions, scanning electron microscopy was also carried out.

4.2.4.1 Microstructures of different regions

The micrographs shown in Figure 4.40 (b) shows the different regions of the PR. The different regions like PR, thermo mechanically affected zone (TMAZ) and heat affected zone in the friction stir processing operation [HAZ (FSP)] were clearly visible after polishing and etching and could be distinguished in the scanned figure of the

sample. The regions have been marked and labeled in the figure. The typical microstructures in those regions have also been presented in the Figure 4.40.

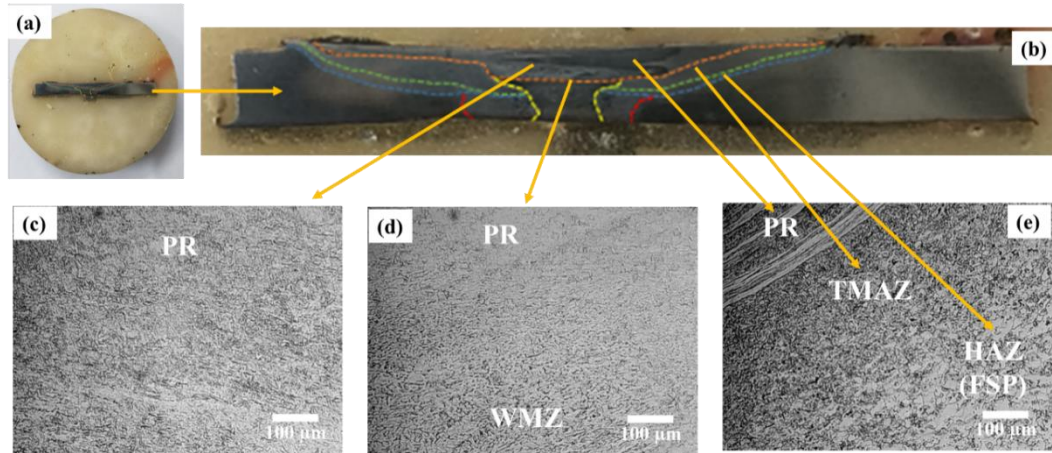


Figure 4.40 (a) Metallographic sample, (b) Macrostructure of processed plate, (c) Microstructure of PR, (d) Microstructure at the interface of PR and WMZ, and (e) microstructure showing PR, TMAZ and HAZ (FSP).

From Figure 4.40, it can be clearly seen that the PR possess much finer grains than the other regions such as WMZ, HAZ (FSP), TMAZ and BMZ. The microstructural evolution in the different regions can be explained based on the theory of dynamic recovery and dynamic recrystallization.

Dynamic recovery

When the material is deformed, the density of point defects and dislocation increases. These imperfections (defects) possess high strain energy. When the heat is applied to the deformed material, the material tends to reduce this excess strain energy by rearrangement or annihilation of these imperfections, particularly dislocations. This process is known as the recovery process. This process occurs more readily when the material possesses more amount of excess energy, i.e. heavily deformed. Excess strain energy is the driving force for the recovery process. This process depends upon the stacking fault energy (SFE) of the materials to be deformed. In high SFE material, the

recovery process is easy; that is why, dislocations arrange themselves into subgrains that are surrounded by low angle grain boundaries. In this process, high angle grain boundaries don't migrate, instead of that low angle grain boundaries migrate. When the recovery process is occurred during deformation, as in the case of FSP operation in which deformation and heat are applied simultaneously to the material, that type of recovery process is known as dynamic recovery.

Dynamic recrystallization

The formation of new strain free grains by the migration of high angle grain boundaries in a deformed material is known as recrystallization. The driving force for recrystallization is the excess strain energy produced due to the deformation process. When recrystallization occurs during the deformation, that type of recrystallization is known as dynamic recrystallization. In dynamic recrystallization, the high angle grain boundaries migrate, while in the dynamic recovery process, low angle grain boundaries migrate.

Depending upon the manner in which the nucleation of grains occurred, dynamic recrystallization can be classified into two main categories:

- i. Discontinuous dynamic recrystallization
- ii. Continuous dynamic recrystallization

i. Discontinuous dynamic recrystallization

In this type of dynamic recrystallization, the nucleation and growth stages of new grains are easily distinguishable. It is generally found in the low stacking fault energy materials (Cu, Ni or austenitic stainless steel). In the materials having low SFE, the cross slip of dislocations is not easy; that is why, rearrangement and annihilation of the dislocations become slow, which means dynamic recovery occurs slowly than the rate of formation of dislocations. In such conditions, the dislocations are accumulated. The

density of dislocations are continuously increasing, and after some time, it attains the critical density of dislocations, then nucleation occurs on the grain boundaries. Grain growth of nuclei occurred by the migration of grain boundaries at the expense of pre-existing grains. Discontinuous dynamic recrystallization is generally evolved in necklace structures of grains. Nucleation of new grains occurred along grain boundaries. These new grains act as nucleation sites for further grains, and thus, the pre-existing grains are consumed by the new grains. Thus producing extremely fine grains as compared to the size of the pre-existing grain.

ii. Continuous dynamic recrystallization

In continuous dynamic recrystallization, the nucleation and grain growth stages are not distinguishable. This is generally occurred in high SFE materials (Al, ferritic stainless steel). In this type of material, the dynamic recovery rate is more than the formation of dislocations. Due to easier cross slip, the dislocation form cells, which involve the low angle grain boundaries. During the hot deformation process, boundary misorientations increase and formation of high angle grain boundary occurs, and formation of new grain happened, which are much finer than the pre-existing grains.

Since the ferritic stainless steel possesses higher SFE, continuous dynamic recrystallization is assumed to happen in the PR during the FSP operation of arc welded plate.

Microstructure evolution

As shown in the macrograph, the sample possesses various regions such as PR, TMAZ, HAZ corresponding to FSP, HAZ corresponding to the welded plate, WMZ and BMZ.

In the FSP operation of the welded plate, all regions of the welded plate, i.e. HAZ corresponding to the welded plate, WMZ and BMZ, have been processed up to a thickness of 1.0 mm.

To determine the phases present in the PR, TMAZ and HAZ (FSP), standard phase diagrams cannot be used because, during operation, the shoulder and the tool pin stirs the material of different zones of welded plates having different phases and different chemical compositions. The final nugget zone is actually composed of a portion of HAZ and the weld metal. Therefore, the final composition of the nugget is somewhere in between the composition of the HAZ (which is the same as the base material) and the weld metal (composed of filler material diluted with the base material). Since it has been well established that during FSW, there is good mixing of material in the nugget, it can be safely assumed that the composition of the nugget is uniform throughout.

The TMAZ and the HAZ (FSP) would be maintaining the same chemical composition as the base material as they have been a part of unaffected base material after GMAW, and FSP is not expected to change the chemical composition.

Thus, each region obtained after FSP may consist of austenite, martensite, ferrite and precipitates of carbides, and nitrides.

4.2.4.2 X-ray diffraction analysis

The presence of different phases formed in the PR has been investigated by XRD analysis, as shown in Figure 4.41. The scanning has been carried out in the range of 10° to 90° with the scanning speed of $10^\circ/\text{min}$. Peaks of different intensities were analysed by X'Pert High Score Plus software.

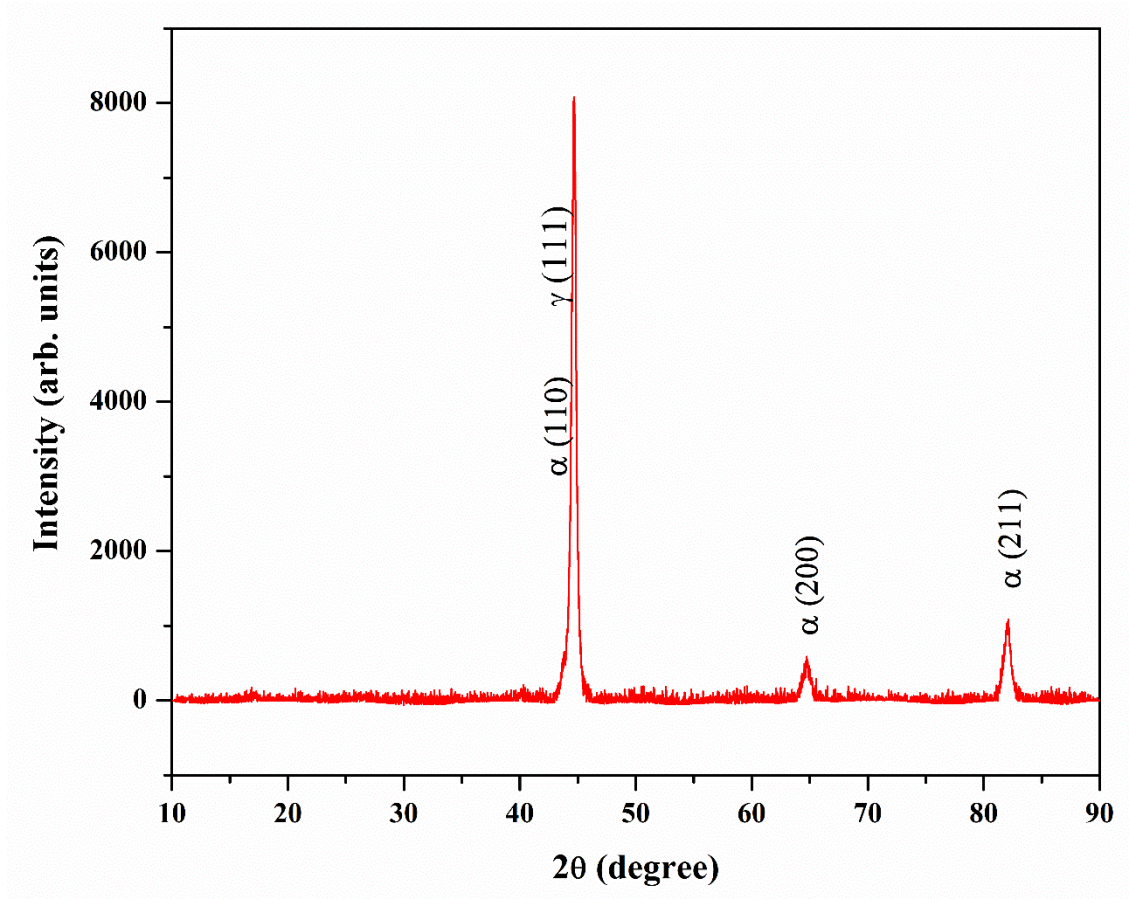


Figure 4.41 XRD analysis of the processed plate.

From the above figure, major peaks of alpha ferrite are found at 44.68°, 65.03° and 82.34° and are matching with the ICSD file number 98-005-3451. While major peaks of austenite are found at 44.68° and 50.57° and are matching with the results of SS304L of Lee et al. [215] and Raeissi et al. [216].

It can be seen from the figure that ferrite and austenite are the main phases present in the PR.

The peaks of carbide phases such as iron carbide, iron chromium carbide and chromium carbide are not appearing in the XRD graph of the processed region, however these peaks were found in the XRD graph of the weldmetal region as shown in Figure 4.14. Due to high heat input during GMAW welding and the melting and solidification process involved, carbides form and were also observed in this work (Figure 4.10).

During the friction stir processing, the plate experiences moderate heating followed by cooling and intensive plastic deformation, which act as the driving force for the thermally induced dissolution and strain induced dissolution of carbides. The volume fraction of the carbides therefore decreases after FSP. Consequently, the peaks corresponding the carbides could not be detected when XRD was performed on samples after FSP in Figure 4.41.

4.2.4.3 Effect of process parameters on the grain size of the processed region

It has been shown previously and can also be seen from Figure 4.42, that processed region (PR) has finer grains than the other regions while HAZ (FSP) possess coarser grains. The variation in the grain size of different regions is due to the variation in the temperature and deformation experienced by different regions. PR is that region which is has been subjected to maximum stirring and temperature during FSP. Due to this, the processed nugget region developed refined grains because of dynamic recrystallization. TMAZ is the region that is affected by both the heat as well as deformation but not under the direct contact of the tool. The temperature, deformation and time are also not sufficient to cause dynamic recrystallization. The grains can be seen to be elongated in the direction of stirring. The HAZ (FSP) region is that region in FSP samples that has been subjected to heating followed by cooling. The plastic deformation of the material has not taken place in this region.

The grain size in the nugget of the PR depends not only on the temperature, but also on the strain rate. The process parameters, most notably, the RS, SD and PS, affect both the strain rate and the maximum temperature generated. The grain size has been measured using standard methods in different regions of the processed plate. SEM images have been taken for better clarity and measurements have been carried out on these SEM images, as shown in Figure 4.42.

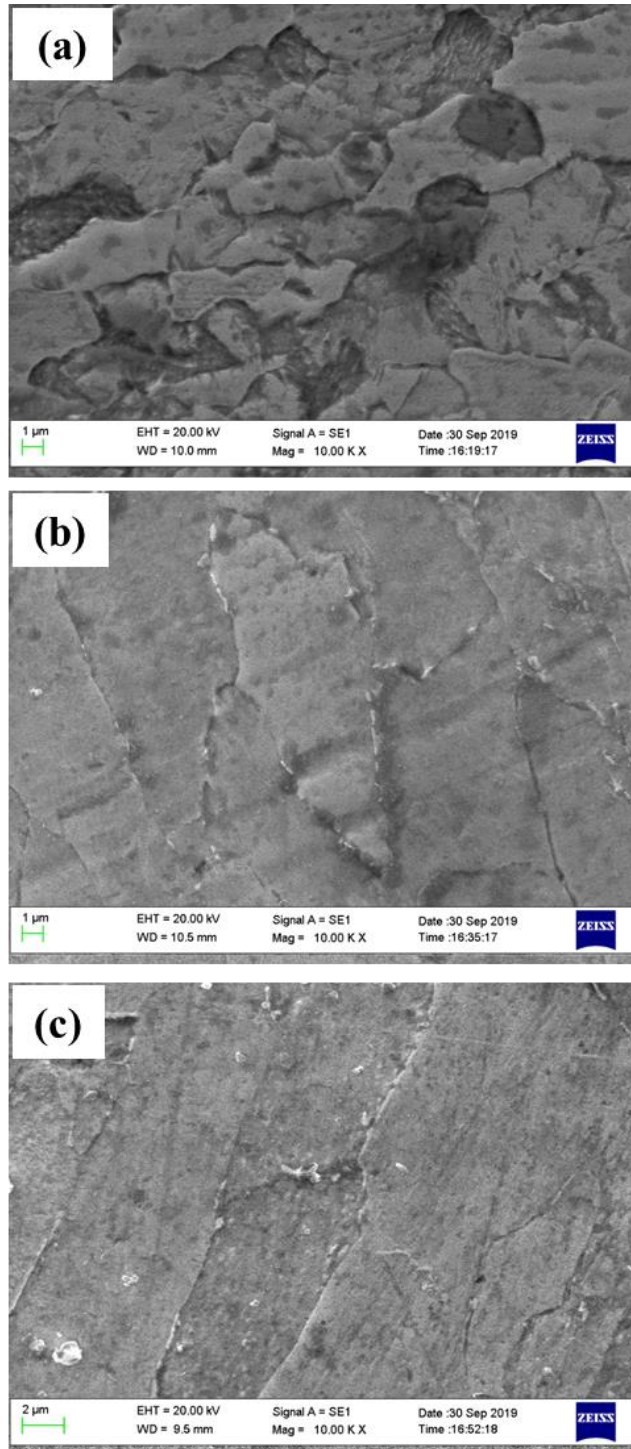


Figure 4.42 Microstructure of different regions of friction stir processed plate taken by scanning electron microscope: (a) PR, (b) TMAZ and (c) HAZ (FSP).

Various process parameters affect the grain size of different regions. The variations obtained in the grain size in different regions of the processed plates obtained at different values of tool RS/PS have been shown in Figure 4.43.

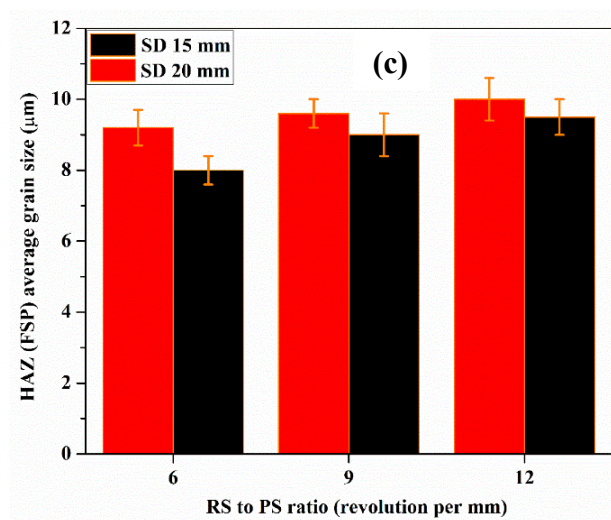
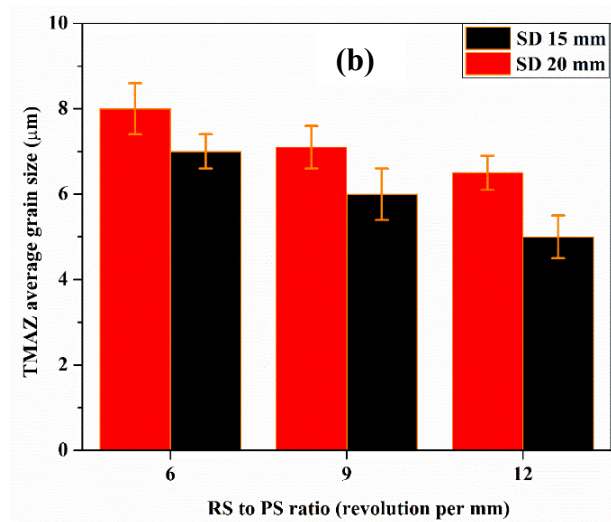
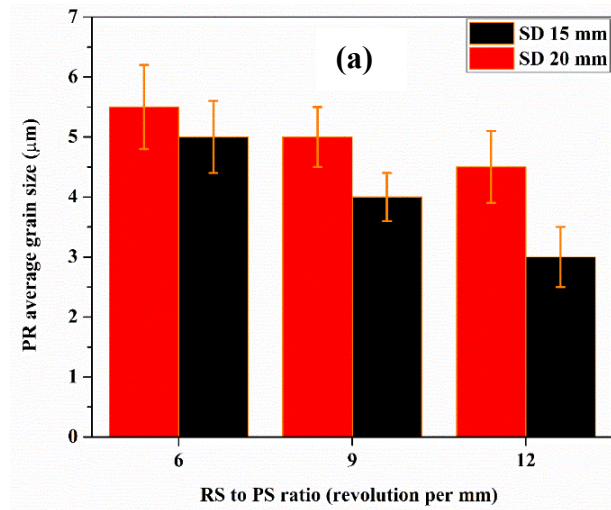


Figure 4.43 Grain size of different zones of friction stir processed plate: (a) PR, (b) TMAZ and (c) HAZ (FSP).

It can be seen from the figure that on increasing the value of (RS / PS) for a particular SD, the grain size of the PR as well as TMAZ decreases, while the grain size of HAZ increases. It was also observed that on increasing the SD for a particular combination of process parameters (RS to PS ratio), the grain size increases. The reason for this variation in the grain size of different regions with different process parameters has been discussed based on the theory of maximum temperature generated, the strain rate prevailing during processing and the Zener Holloman parameter.

Maximum temperature in the processed region

All the process parameters such as SD, RS and PS affect the maximum temperature obtained by the material during FSP operation. For constant SD, the effect of RS and PS on the maximum temperature obtained by the material during FSP operation can be shown by equation (4.7) [217].

$$\frac{T_{max}}{T_{melt}} = k \left[\frac{60 * RS^2}{PS * 10^4} \right]^\alpha \quad (4.7)$$

Where,

T_{max} = Maximum temperature generated during FSP operation in the PR

T_{melt} = Melting temperature of the alloy in °C

$k = 0.7$; $\alpha = 0.005$ both are constant

This equation can also be shown in another form

$$\frac{T_{max}}{T_{melt}} = k \left[\left(\frac{RS}{PS} \right) \left(\frac{60 * RS}{10^4} \right) \right]^\alpha \quad (4.8)$$

From the above equation (4.8), two conclusions can be drawn. First is that for a constant value of (RS/PS), T_{max} will be proportional to the RS. Second is that on increasing RS and decreasing PS, T_{max} will increase. Therefore, the T_{max} corresponding to (RS/PS) will be higher when (RS/PS) value is higher. As a result, (RS/PS) value of

12, 9 and 6 for a constant SD possessed corresponding T_{max} in decreasing order. It was also found that on increasing SD, T_{max} was also increased.

Strain rate obtained in the PR

Various parameters affect the strain rate of the PR, and it is given by equation (4.9) [151].

$$\dot{\epsilon} = \frac{R_m * 2\pi r_e}{L_e} \quad (4.9)$$

Where, - $\dot{\epsilon}$ represents the strain rate

- R_m represents the average material flow rate, which is assumed to be half of the RS

- r_e represents the effective radius of the dynamic recrystallization zone, which is about $\pi/4$ of the shoulder radius, and

- L_e represents the depth of the dynamic recrystallization zone, which is about $\pi/4$ of the plunge depth.

From the above equation, it was found that for a constant plunge depth, strain rate is directly proportional to the SD and RS.

Zener – Holloman parameter

Various authors have found that a parameter named as Zener–Holloman parameter given in equation (4.10) can be used to determine the effect of strain rate and temperature on the grain size.

$$Z = \dot{\epsilon} \exp\left(\frac{Q}{RT}\right) \quad (4.10)$$

Where,

$\dot{\epsilon}$ is the strain rate,

Q is the activation energy for deformation,

R is the ideal gas constant and

T is the temperature in the PR.

Grain size and Zener – Holloman parameter are inversely proportional to each other, i.e. higher the value of Z, finer is the grain size.

From the above equation, it can be found that temperature and strain rate show contrast behaviour to determine the grain size of the PR.

Grain size of the processed region

For a particular SD, on increasing the value of (RS/PS), the temperature of the PR increases (From equation (4.8)) which decreases the value of Z that tends to increase the grain size of the PR and strain rate $\dot{\epsilon}$ get increased on increasing RS (From equation (4.9)), which increases the value of Z that tends to reduce the grain size of the PR. The dominating factor out of the temperature and strain rate will decide the grain size. From Figure 4.43, it was observed that on increasing the value of (RS/PS) for a particular SD, the grain size of the PR decreases. It was due to the dominance of the strain rate effect over the temperature effect.

Keeping all the process parameters constant, on increasing the SD, the temperature of the PR increases due to the increase in the contact area that decreases the Z value, which tends to increase the grain size of the PR and strain rate $\dot{\epsilon}$ get increased on increasing SD (from equation (4.10)) which increases the value of Z that tends to reduce the grain size of the PR. From Figure 4.43, it was observed that on increasing the value of SD for a particular combination of the process parameters, the grain size of the PR increases. It was due to the dominance of the temperature effect over the strain rate effect.

Grain size of the thermo mechanically affected zone

Since thermo mechanically affected zone (TMAZ) is that region that is affected by both the heat as well as deformation, same as in the PR but to a lower extent, therefore

TMAZ shows similar behaviour of the variation of grain size with the process parameters.

Grain size of the heat affected zone in the friction stir processed plate

From Figure 4.43, it was observed that on increasing the value of (RS/PS) for a particular SD, the grain size of the heat affected zone in the friction stir processed plate (HAZ (FSP)) increases. It was also observed that on increasing the value of SD for a particular combination of the process parameters, the HAZ (FSP) grain size also increases.

The HAZ (FSP) grains are only affected by the heat, as no deformation takes place in this region. In other words, the variation of grain size of this region depends only on the temperature, on the strain rate. The temperature of the PR increases by increasing the value of (RS/PS) for a given SD as well as by increasing the SD for a given combination of process parameters. In both the conditions, on increasing the temperature of the PR, the temperature of the HAZ (FSP) also increases correspondingly. On increasing the temperature of the HAZ (FSP), the cooling rate becomes slower, which helps in grain growth in the HAZ (FSP).

4.2.5 Microhardness testing

The hardness testing of various regions of the processed plate was carried out on the transverse section of the metallographic sample from the advancing side to the retreating side. The comparative hardness profile of the processed and welded plate is shown in Figure 4.44. The red colored curve shows the hardness of the transverse section of the plate welded using GMAW, and the black curve shows the hardness of the same cross section after FSP of the welded plate.

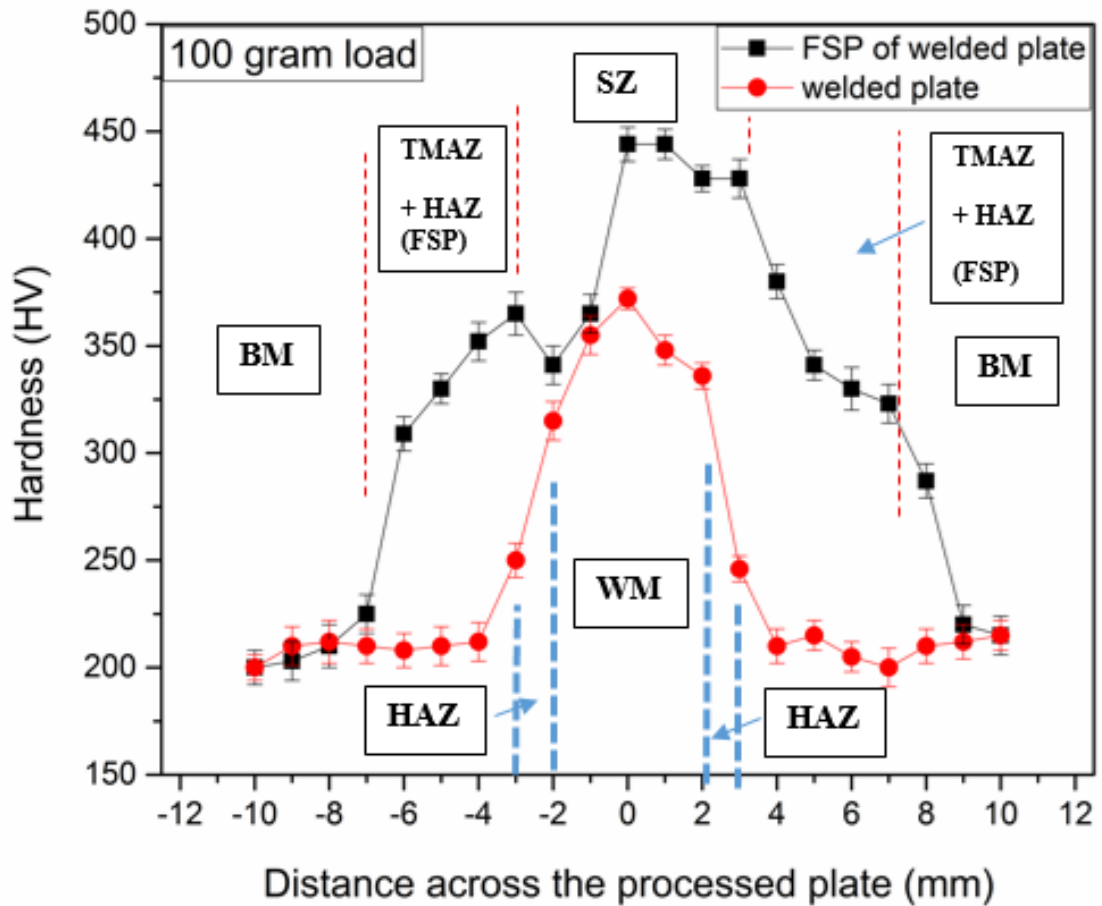


Figure 4.44 Comparative hardness profile of different regions of friction stir processed plate and gas metal arc welded plate.

It can be seen from Figure 4.44 that on applying the FSP operation on the welded plate, the hardness of all the regions of the welded plate, particularly HAZ, has been increased. It was due to the refining of the coarser grains of the HAZ and WMZ by the FSP operation. As the grains are finer, the movement of dislocations becomes difficult and thus, hardness increases.

The effect of SD and (RS/PS) on the hardness of different regions of the processed plate has been shown in Figure 4.45.

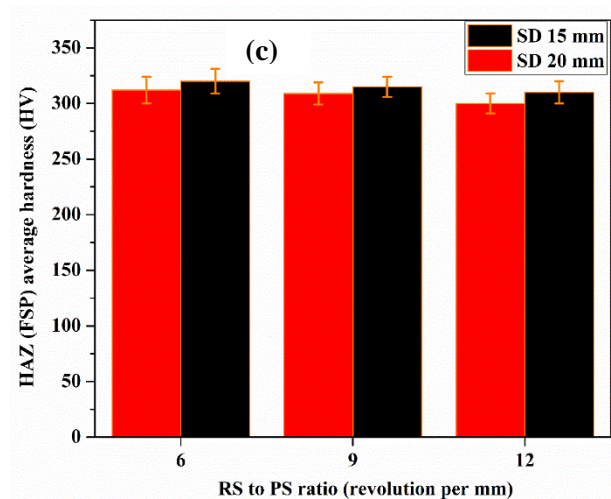
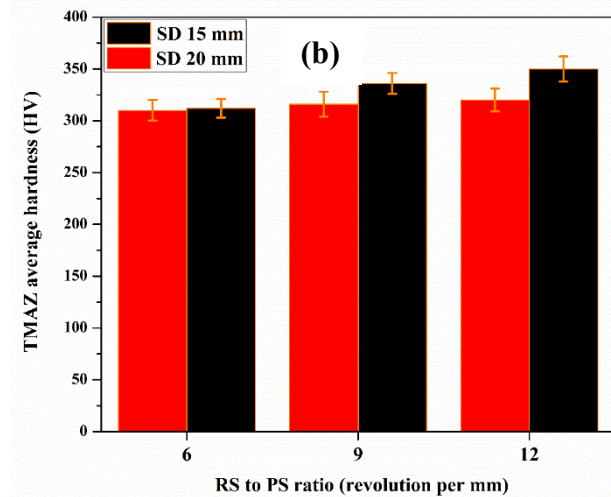
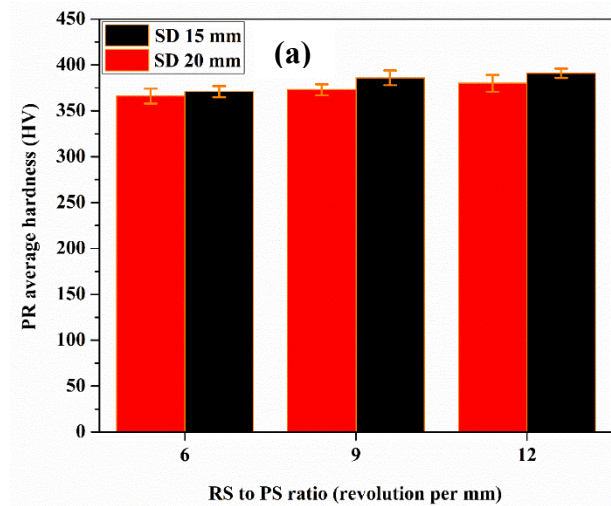


Figure 4.45 Hardness of different zones of friction stir processed plate: (a) PR, (b) TMAZ and (c) HAZ (FSP).

From Figure 4.45 (a) and (b), it can be observed that hardness of PR and TMAZ increases on increasing the value of (RS/PS) and decreasing the SD, while the hardness of HAZ (FSP) as shown in Figure 4.45 (c), decreases on increasing the value of (RS/PS) and SD.

Since the hardness is directly influenced by the grain size; therefore, coarser grains possess lower hardness, and finer grains possess higher hardness. As observed from Figure 4.43 (a) and (b), the grain size of the PR and TMAZ decreases by increasing the value of (RS/PS) and decreasing SD. Therefore, the hardness of PR and TMAZ increases on increasing the value of (RS/PS) and decreasing the value of SD. Sample A possesses the maximum value of hardness of PR and TMAZ due to the combination of higher value of (RS/PS) and smaller value of SD. Also, for the HAZ (FSP), the grain size increases on increasing the value of (RS/PS) and SD. Therefore, the hardness was decreased by increasing the value of (RS/PS) and SD.

4.2.6 Tensile testing

On performing FSP operation on the welded plate, the mechanical properties of the welded plate changed due to the grain refinement of the interested region of the welded plate. To determine the tensile properties, tensile testing has been carried out. Two types of tensile specimen were prepared; one is the transverse section tensile sample which is used to find the weakest region of the processed plate and another is the reduced section tensile sample which is used to find the tensile properties of the PR.

4.2.6.1 Transverse tensile testing

On performing transverse tensile testing, the transverse tensile test specimen fractured in the unaffected BMZ. It is contrary to what was happening during the transverse tensile testing of the GMAW welded specimen, which all fractured in the HAZ. The FSP operation modified the top 1.0 mm of the HAZ obtained during GMAW

welding. On applying FSP operation on the welded plate, the strength of the HAZ of welded plate increased due to the phenomenon of dynamic recrystallization, which refined the grains. Even though, the FSP has been carried out for only up to 1.0 mm thickness, but still, the increase in strength of the HAZ along with other regions was so significant that overall the strength in PR exceeded the strength of base material, and the fracture took place in the BMZ, instead of the HAZ.

Since the fracture occurred in the BMZ, it only tells the tensile properties of the BMZ. The tensile properties of the transverse tensile testing samples were nearly the same as the base material's tensile properties. The ultimate tensile strength of the samples was found in the range of 533 MPa to 562 MPa, whereas yield strength was in the range of 406 MPa to 431 MPa. The percentage elongation was varying in the range of 30 to 37.

4.2.6.2 Reduced section tensile testing

During the transverse tensile testing, the BMZ has been found as the weakest region. But to quantify the strength of the region where FSP has been carried out after GMA welding reduced section tensile testing has been carried out. All samples were reduced in the region that was friction stir processed and thus made to fracture in the PR. Therefore, the tensile properties obtained by this testing reflects the tensile properties of the PR. The obtained tensile properties of the PR are given in Table 4.8.

Table 4.8 Tensile properties of the processed region

Sample	Ultimate tensile strength (MPa)	Yield strength (MPa)	% Elongation
Base metal	583	450	25
A	750	556	16
B	726	542	16
C	645	521	18
D	697	530	17
E	660	525	18
F	630	512	19

It can be seen from the above table that ultimate tensile strength, yield strength and the percentage elongation changes after FSP. The ultimate tensile increased and reached in the range of 630 MPa to 750 MPa, while the yield strength increased to lie between 512 MPa to 556 MPa. However, the percentage elongation decreased and lied between 16 to 19.

Sample A possess the highest value of ultimate tensile strength and yield strength. This high strength was achieved because sample A possessed finer grain size of the PR than the others. It is well known that finer grains lead to increase in strength. However, the percentage elongation of sample A possessed the lowest value. It occurred due to more strain hardening possessed by the PR grains of this sample during tensile testing. Thus it can be concluded from this testing that FSP increases the strength of the welded plate.

4.2.7 Charpy impact testing

To find out the improvement in the toughness of the WMZ and HAZ of the welded plate on carrying out the FSP upon them, Charpy impact testing was performed. The impact toughness of the base metal is already known. Also, the impact toughness of the WMZ and HAZ of the welded plate S7 has been found and already reported in section 4.1.14. However, the values of impact toughness of the base metal as well as WMZ and HAZ of the welded plate S7 are again given in Table 4.9. The impact toughness of both types of samples taken out from the processed plates was found, and the results of the impact testing are shown in Table 4.10. The impact toughness of the processed plate in which the notch is present at the centre of the PR is represented by I_1 and in which the notch is present in the PR at the corresponding location of the HAZ of the welded plate is represented by I_2 . Charpy specimens after impact testing are shown in Figure 4.46.



Figure 4.46 Charpy impact toughness test specimen after testing.

Table 4.9 Charpy impact toughness of different regions of sample S7.

Sample	Charpy impact toughness (J)
Base metal	29
S7 WMZ	37
S7 HAZ	26

Table 4.10 Charpy impact toughness of processed plates.

Sample	I ₁	I ₂
A	50	31
B	49	30.5
C	47	29.5
D	48	30
E	47.2	29
F	46	28

From the above tables, it can be seen that the impact toughness I_1 of all samples is always greater than the impact toughness of the WMZ, and also, the impact toughness I_2 of all samples is always greater than the impact toughness of the HAZ.

It is already discussed in section 4.1.14 that the grain size greatly influences the impact toughness. Both of them (I_1 and I_2) are inversely proportional to each other. Since the grain boundaries act as hurdles in the movement of dislocations that are produced due to the plastic deformation of the material during impact testing, energy is consumed to cross these hurdles for the propagation of the dislocations. Therefore, as the grain size is reduced, more energy is required to cross these hurdles (grain boundaries). Thus the toughness is increased on refining the grain size. A welded, as well as processed plate, consist of different regions having different grain sizes; therefore, the toughness of each region will be different according to their grain size.

The more value of impact toughness I_1 and I_2 of all processed samples in comparison to the impact toughness of the WMZ and HAZ of the welded plate S7, respectively is due to grain refinement of these regions (WMZ and HAZ) by FSP operation.

The variation of I_1 and I_2 with the SD as well as RS to PS ratio are shown in Figure 4.47 and Figure 4.48, respectively.

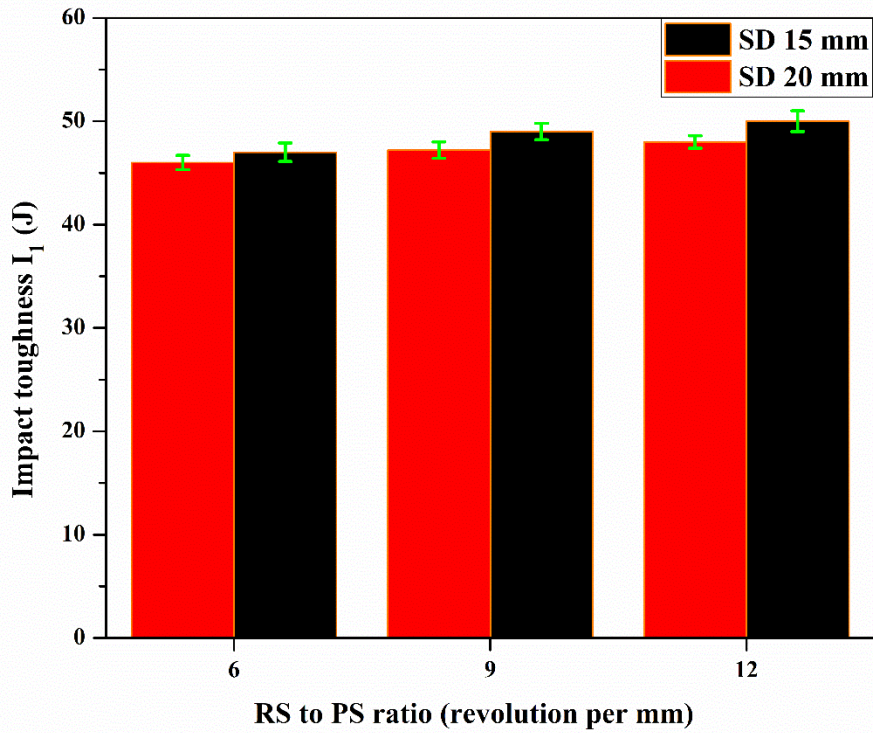


Figure 4.47 Variation of impact toughness I_1 with the RS to PS ratio.

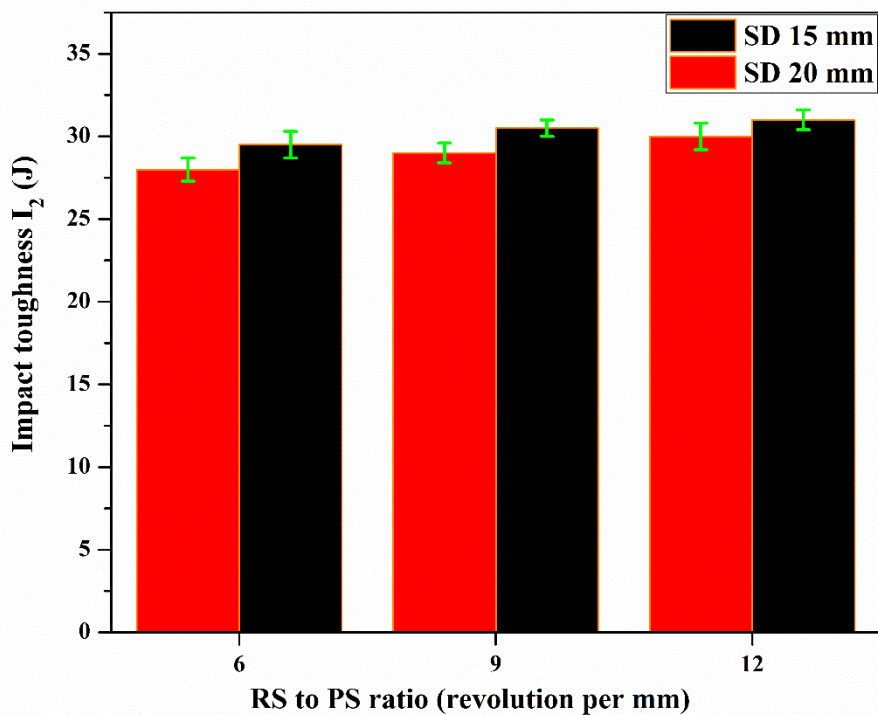


Figure 4.48 Variation of impact toughness I_2 with the RS to PS ratio.

From the above both figures, it was observed that at a particular value of SD, either 20 mm or 15 mm, on increasing the RS to PS ratio, the value of impact toughness I_1 and I_2 are increasing. This type of variation in I_1 and I_2 are due to the decrease in the grain size of the stir zone of the processed plates on increasing the ratio of the RS to PS, since the toughness is inversely proportional to each other as described earlier.

It was also observed from Figure 4.47 and Figure 4.48 that for any value of the RS to PS ratio, larger SD (20 mm) possessed lower value of impact toughness I_1 and I_2 than the value of impact toughness associated with the smaller diameter (15 mm). It occurred because larger SD (20 mm) possessed coarser grains than the smaller diameter (15 mm), as shown in Figure 4.43.

4.2.8 Residual stress measurement of the processed plate

The variation of the longitudinal residual stress at different locations of the processed plate sample A along the width of the plate is shown in Figure 4.49.

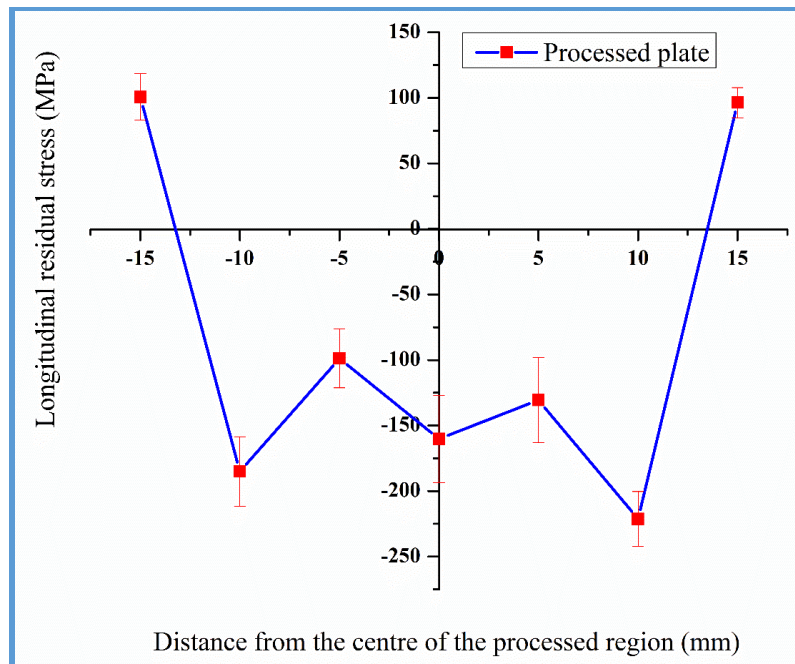


Figure 4.49 Longitudinal residual stress measurements in the processed plate.

The above figure shows that the BMZ possesses tensile residual stress, and PR is under the compressive residual stresses. The magnitude of the compressive residual stresses is more than the compressive residual stress that exist in the welded plate (i.e. in the HAZ of the welded plate). At all locations of the PR, the residual stress is of compressive nature, therefore the area of the compressive residual stress becomes more than the welded plate.

During the FSP operation, the heat within the base material to be processed is generated by different sources, such as frictional heating and plastic deformation. This heat tends to expand the material, but the plates are rigidly tightened by the clamping arrangements; therefore, its expansion is greatly hindered by these clamping arrangements, which set compressive residual stresses in the PR. Also, the residual stress is produced due to non-uniform plastic deformation in the processed plates during FSP operation. During this operation, a large amount of load is applied on the plate by the FSP tool; therefore, the plate undergoes intense plastic deformation along with the elastic deformation. As the FSP tool traverses further from a point, the load exerted by the FSP tool on that point is removed, then the plate tries to recover the elastic part of the deformation, but is restricted from full recovery due to the adjacent plastically deformed material. That creates compressive residual stresses in the PR of the processed plates.

The diameter of the shoulder is more than the total width of the WMZ and HAZ, and since the location of the FSP tool is just at the centre of the WMZ of the welded plate, therefore the WMZ and HAZ comes under the area of the PR.

In the welded plate, the WMZ is under the tensile residual stress, but in the processed plate, these WMZ comes under the PR; therefore, the tensile residual stress of the WMZ is converted into the compressive residual stress. The HAZ of the welded plate

already have compressive residual stress, but in the processed plate, this region come under the PR, which have compressive residual stresses.

4.2.9 Micro-magnetic characterisation of processed plates

The MBN and MHL testing has been performed by using MBN analyser. In this testing, the focus was on the PR in the processed plate and different zones in the welded plate so that the comparative study of variation in the magnetic properties at constant MFI and magnetizing frequency can be done.

4.2.9.1 Magnetic hysteresis loop testing

The micro-magnetic testing using the MHL technique has been performed at different zones (BMZ, HAZ and WMZ) of the welded plate S7 and PR of sample A at constant values of MFI of 800 Oe and magnetising frequency of 0.05 Hz.

A comparative study of hysteresis response such as AMFD, coreloss, average permeability, coercivity and remanence between the welded plate and processed plate has been done.

(a) Comparative study of average permeability of various zones

As it is already discussed that the permeability refers to the ease of magnetisation on applying the external magnetic field.

Average permeability of various zones on the welded plate before processing and the PR on the processed plate (sample A) at the magnetising frequency of 0.05 Hz and MFI of 800 Oe has been shown in Figure 4.50.

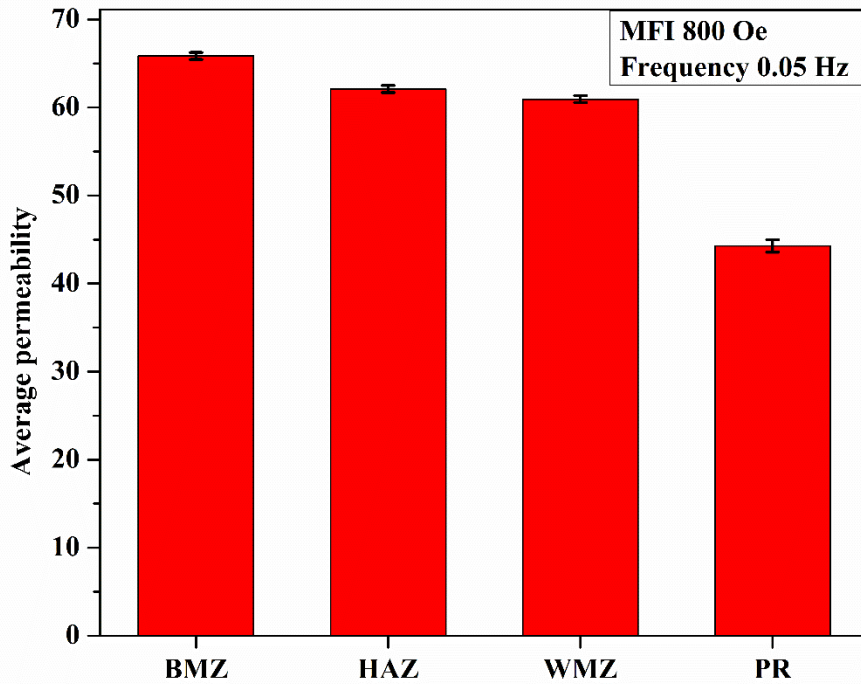


Figure 4.50 Average permeability of various zones.

It was observed from Figure 4.50 that the BMZ possessed a higher value of average permeability, whereas the PR possessed a lower value. As described earlier that the magnetisation process does not entirely dependent on the grain size but also depends upon the process parameters and the inner structure of the grains, such as distribution of precipitates, phases, etc. If the process parameters are kept constant, then the magnetisation depends upon the grain size and inner structure of the grains. It was also found in the earlier discussion that it is not necessary to possess higher magnetisation in the coarser grains because eddy current is also produced due to the motion of domain walls which tends to restrict the motion of domain walls (according to Lenz's law) and hence tends to reduce the magnetisation. Therefore, the amount of magnetisation is the result of competition between these two factors. The grain size of HAZ is larger followed by BMZ, WMZ and PR. The combination of eddy current with the grain size results in the higher permeability of the BMZ followed by HAZ, WMZ and PR.

(b) Comparative study of average maximum flux density of various zones

The definition of AMFD has already been described, but in short, it is the average of the magnetic flux density corresponding to the maximum value of the applied magnetic field in both directions, i.e. positive as well as negative.

AMFD of various zones on the welded plate before processing and the PR on the processed plate (sample A) at the magnetising frequency of 0.05 Hz and MFI of 800 Oe has been shown in Figure 4.51.

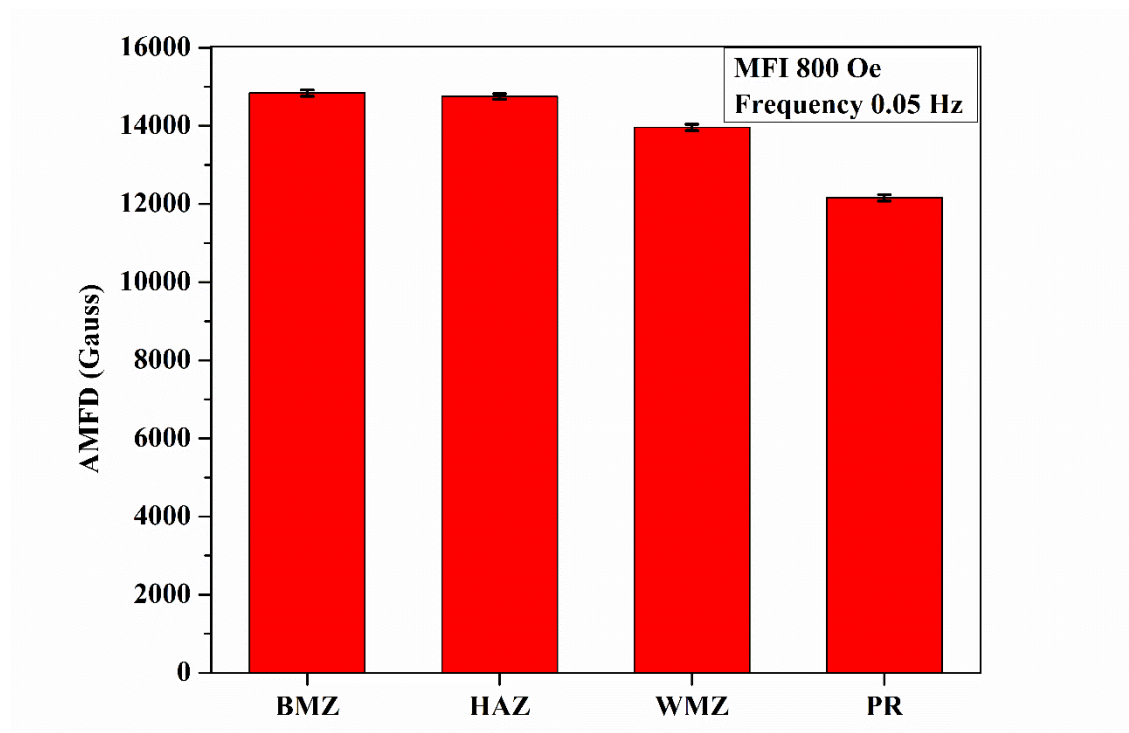


Figure 4.51 AMFD of various zones.

It was observed from Figure 4.51 that the AMFD is possessed in increasing order by PR, WMZ, HAZ and BMZ at a constant value of process parameters. Also, the value of average permeability of BMZ is higher, followed by HAZ, WMZ and PR. Since the permeability refers to the ease of magnetisation, therefore higher permeability results in higher magnetisation on applying the external magnetic field and thus higher value of

AMFD, whereas lower permeability results in lower magnetisation and thus lower value of AMFD. Therefore, the value of AMFD of each zone is directly related to the value of average permeability. Since the BMZ possessed a higher value of average permeability followed by HAZ, PR and WMZ, therefore the BMZ possessed a higher value of AMFD followed by HAZ, WMZ and PR.

(c) Comparative study of remanence of various zones

The remanent magnetisation on removing the external magnetic field from the maximum value to zero is known as remanence.

The remanence value of each zone at constant process parameters is shown in Figure 4.52.

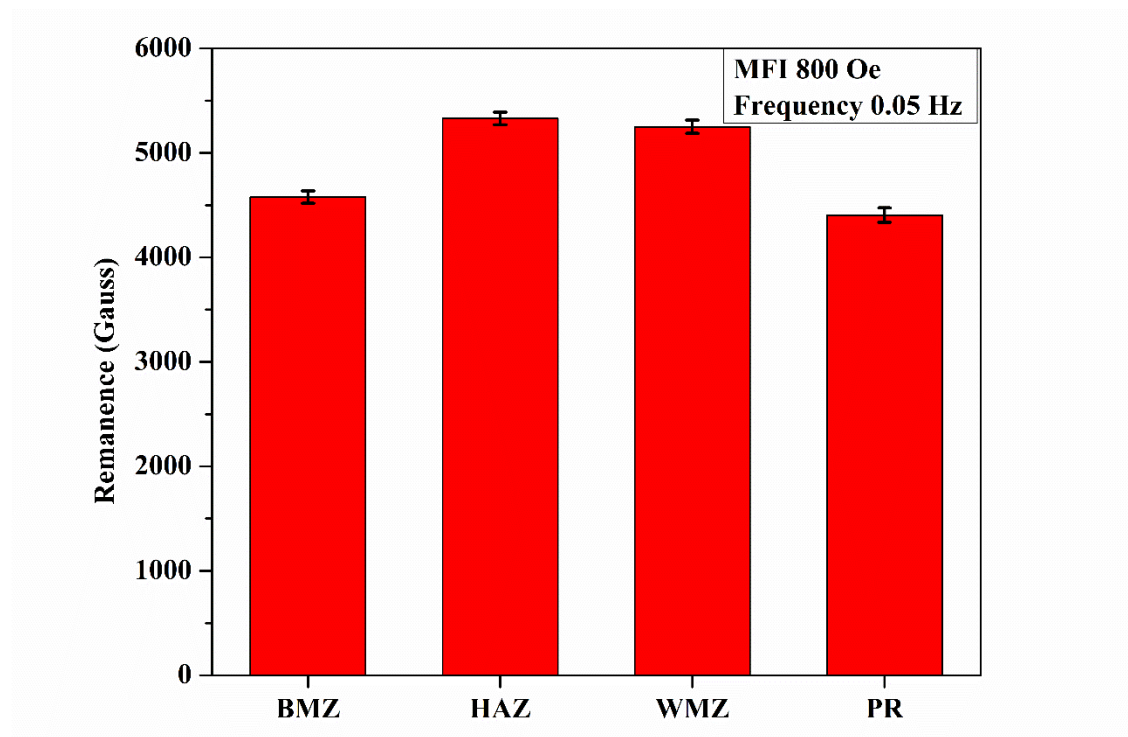


Figure 4.52 Remanence of various zones.

Figure 4.52 shows that the HAZ possessed a higher value of remanence followed by WMZ, BMZ and PR. It is already described that the remanence depends upon the value of AMFD as well as permeability. On the one hand, higher average permeability

results in a higher value of AMFD, but on the other hand, when the applied magnetic field is decreased in a hysteresis loop from its maximum value, then the magnetisation is decreased at a much faster rate with a higher value of average permeability which results into the lower value of remanence. Higher the value of AMFD tends to increase the remanence. The HAZ and WMZ possessed a lower value of AMFD than the BMZ, which tend to cause the lower remanence of HAZ and WMZ than the BMZ, but the difference in their AMFD values is not much therefore the effect of AMFD values of HAZ and WMZ on the remanence is very less. However, the difference in the values of average permeability between BMZ and WMZ, BMZ and HAZ is significant; therefore, the remanence values of WMZ and HAZ is higher than the BMZ due to the lower value of average permeability of WMZ and HAZ than the BMZ. The remanence of the PR is lower than the other regions because it possessed much lower AMFD values than the other regions.

(d) Comparative study of coercivity of various zones

The magnitude of the magnetic field applied in the negative direction to bring the remanence to zero is known as coercivity.

The coercivity of each zone at constant process parameters is shown in Figure 4.53.

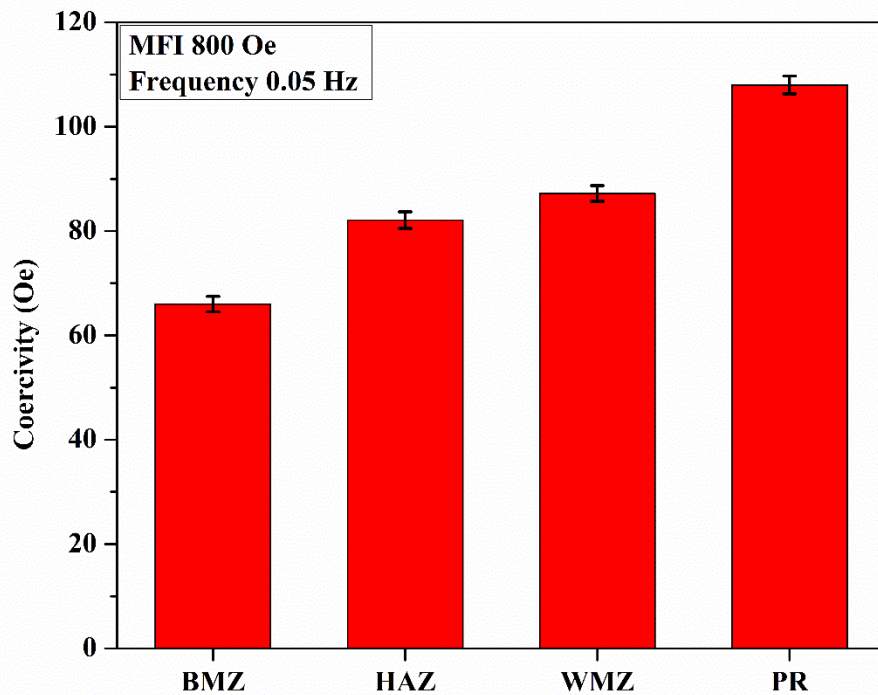


Figure 4.53 Coercivity of various zones.

It was observed from Figure 4.53 that the maximum value of coercivity is possessed by PR followed by WMZ, HAZ and BMZ. It is already described that the coercivity depends upon the remanence as well as pinning sites in the form of grain boundaries. The finer grains possessed more grain boundaries which tend to restrict the demagnetisation process, and thus tends to increase the coercivity. The PR possessed finer grains than the other zones, which cause more coercivity than the other zones; however, their remanence is lower than the other regions. Similarly, the coercivity of WMZ is higher than the other regions, except PR, due to the finer grains. The grain size of the HAZ is higher than the other regions; therefore, lesser pinning sites in the form of grain boundaries act as an obstacle to the motion of domain walls which tends to reduce the coercivity, but the value of coercivity also depends upon the remanence. HAZ possessed the highest value of remanence, which tended to increase the coercivity and it also possessed coarser grains, which tend to decrease coercivity. The competition

between these two factors results the value of coercivity higher than the coercivity of BMZ.

(e) Comparative study of coreloss of various zones

The coreloss has been described earlier in detail. These losses are due to the generation of eddy current during the jumping and motion of domain walls and on applying the external magnetic field to the conductor as well as energy loss to cross the pinning sites. The area of the hysteresis loop is equal to the coreloss. The coreloss of each zone at constant process parameters is shown in Figure 4.54.

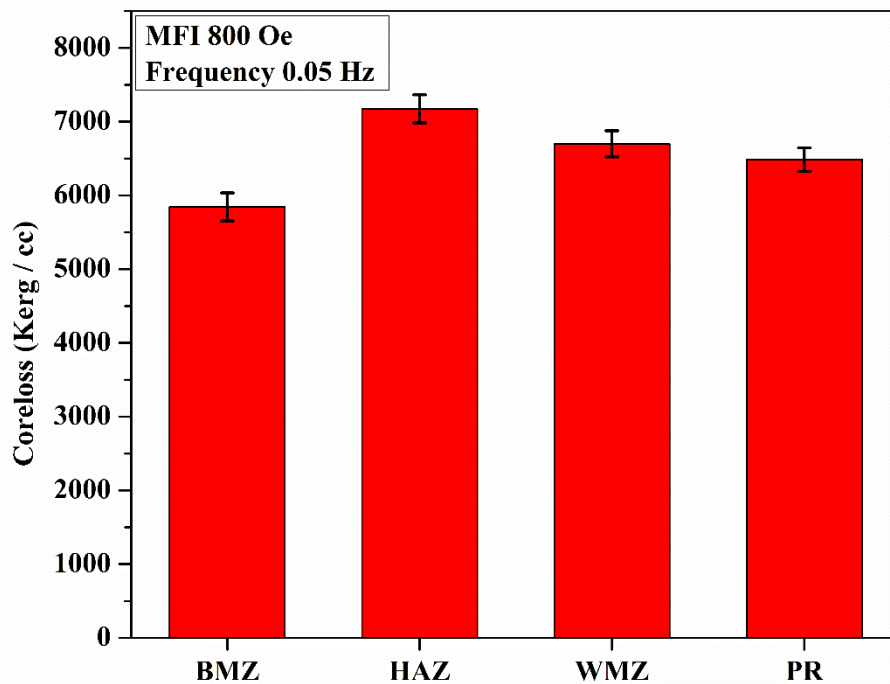


Figure 4.54 Coreloss of various zones.

From Figure 4.54, it was observed that the HAZ possessed higher coreloss followed by WMZ, PR and BMZ. The different coreloss values by different zones are decided by the combined effect of eddy current and pinning sites. Shortly, the more the area of the loop, the more will be coreloss. The coreloss of the HAZ is more than the other zones, which reflects the more area of hysteresis loop possessed by the HAZ.

4.2.9.2 Magnetic Barkhausen noise analysis

Magnetic Barkhausen noise (MBN) analysis of different zones has been carried out at the constant process parameters of MFI of 800 Oe and magnetising frequency of 10 Hz. RMS value of induced voltages and number of pulses are used as a characteristic feature to study this analysis.

(a) Comparative study of the number of pulses of various zones

The number of pulses of different zones at the constant process parameters of MFI of 800 Oe and magnetising frequency of 10 Hz is shown in Figure 4.55.

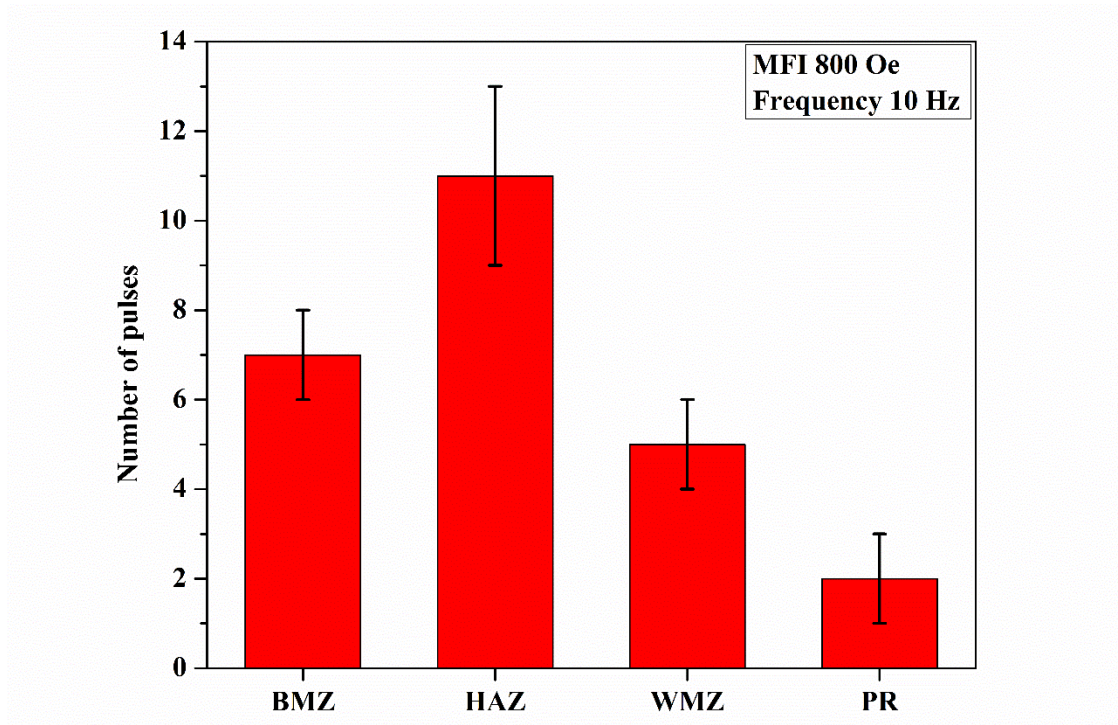


Figure 4.55 Number of pulses of various zones.

From Figure 4.55, it was found that the HAZ possessed a higher value of the number of pulses followed by BMZ, WMZ and PR. The number of pulses in the MBN analysis results from the jumping of domain walls between its local minima. More the restriction in the path of motion and hence jumping of domain walls tend to reduce the number of pulses. Since the grain boundaries act as hurdle points, therefore, the zone

which possessed finer grains will produce more hurdles which tend to reduce the number of pulses. Since the grain size of HAZ is higher followed by BMZ, WMZ and PR, therefore, the number of pulses follows the same trend.

(b) Comparative study of root mean square value of various zones

The RMS value of induced voltages of different zones at the constant process parameters of MFI of 800 Oe and magnetising frequency of 10 Hz is shown in Figure 4.56.

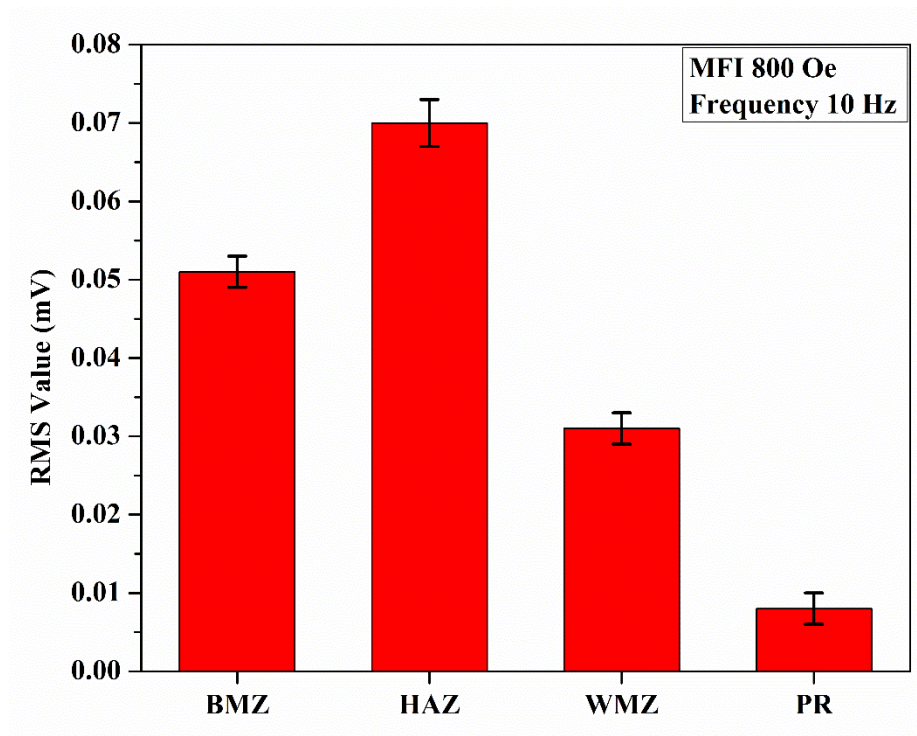


Figure 4.56 RMS value of various zones.

It was observed from Figure 4.56 that the HAZ possessed a higher value of RMS followed by BMZ, WMZ and PR. As it is already described that the MBN response is the result of jumping of domain walls through the pinning sites, which are mainly in the form of grain boundaries. Finer the grain size result in more grain boundaries which means more pinning sites to the motion of domain walls. More hindrance to the motion

of domain walls by the grain boundaries tends to reduce the induced voltages in terms of RMS value.

The grain size of HAZ is larger followed by BMZ, WMZ and PR; therefore, the RMS value of induced voltages follows the same trend because the RMS value is strongly dependent on the grain size and related to each other as described above.